TESIS DE LA UNIVERSIDAD DE ZARAGOZA

2015

79

Carlos Ernesto Rizzo Bobbio

Propagation, Localization and Navigation in Tunnel-like Environments

Departamento

Informática e Ingeniería de Sistemas

Director/es

Villarroel Salcedo, José Luis
Lera García, Francisco

ISSN 2254-7606

Prensas de la Universidad Universidad Zaragoza

ISSN 2254-7606

Universidad Zaragoza
1542

Tesis Doctoral

PROPAGATION, LOCALIZATION AND NAVIGATION IN TUNNEL-LIKE ENVIRONMENTS

Autor

Carlos Ernesto Rizzo Bobbio

Director/es

Villarroel Salcedo, José Luis
Lera García, Francisco

UNIVERSIDAD DE ZARAGOZA

Informática e Ingeniería de Sistemas

2015

Universidad Zaragoza
1542

Tesis Doctoral

Propagation, Localization and Navigation in Tunnel-like environments

Autor

Carlos Ernesto Rizzo Bobbio

Director/es

José Luis Villarroel Salcedo
Francisco Lera García

Informática e Ingeniería de Sistemas / Escuela de Ingeniería y Arquitectura

2015

Universidad Zaragoza

Instituto Universitario de Investigación en Ingeniería de Aragón
Universidad Zaragoza

PHD THESIS

Propagation, Localization and Navigation in Tunnel-like Environments

CARLOS ERNESTO RIZZO BOBBIO

Advisors

José Luis Villarroel Salcedo

Francisco Lera García

Robotics, Perception and Real Time Group (RoPeRT)

Instituto de Investigación en Ingeniería de Aragón (I3A)

Escuela de Ingeniería y Arquitectura (EINA)

Universidad de Zaragoza (UZ)

May 2015

Propagation, Localization and Navigation in Tunnel-like Environments

by

Carlos Ernesto Rizzo Bobbio

Submitted to *Departamento de Informática e Ingeniería de Sistemas* in partial fulfillment of the requirements for the degree of

Doctor of Philosophy

at

Universidad de Zaragoza

May 2015

Advisors	
José Luis Villarroel Salcedo	Universidad de Zaragoza, Spain
Francisco Lera García	Universidad de Zaragoza, Spain

Composition of the Thesis Commitee	
Aníbal Ollero Baturone	Universidad de Sevilla, Spain
Luis Montano Gella	Universidad de Zaragoza, Spain
Luis Almeida	Universidade do Porto, Portugal
Alberto Sanfeliu Cortés	Universitat Politècnica de Catalunya, Spain
Rachid Alami	Laboratoire d'analyse et d'architecture des systèmes, France

International Reviewers	
Jonathan Fink	U.S. Army Research Laboratory, USA
Stephanie Gil	Massachusetts Institute of Technology, USA
Ramviyas Parasuraman	KTH Royal Institute of Technology, Sweden

To my parents Chelo and Tony,
to my brother Gabriel and my sister Carolina,
and to my wife Eugenia.

Acknowledgements

The authors acknowledge *Dirección del Túnel de Somport* and *Unidad de Carreteras de Huesca, Ministerio de Fomento*, for their support in the countless experiments in the Somport tunnel facilities. We also thank Felix Andreu from *Confederación Hidrográfica del Ebro* for his help in the Santa Ana dam, and *Minera Santa Marta S.A.* together with the *SAMCA group* for allowing us to work in the Santa Marta mine. The support of Jennifer Wozencraft and Thomas Hood of the US Army Corps of Engineers in the Allatoona dam is also acknowledged.

Personally, I would like to thank my advisors, José Luis Villaroel and Francisco Lera, who guided me through the whole thesis. From them, I had the privilege of getting the best of the theoretical and practical worlds in both communications and robotics. They are more than academic supervisors to me, but are also personal advisors and tapas, beer, and wine sharers.

I would also like to thank the whole RoPeRT group, who have been a family to me during these 4 years of PhD. Special thanks to professors Carlos Sagüés, Luis Montano and José Antonio Cuchí, and my labmates Danilo Tardioli, Domenico Sicignano, Luis Riazuelo and Pablo Urcola, who have been important contributors to this thesis.

Many thanks to professor Vijay Kumar for receiving me at the GRASP Lab for 8 months and for making me part of their family. I deeply thank him for his brilliant insights and for providing me with feedback on many ideas. I also thank Tolga Ozaslan and Yash Mulgaonkar for their technical support and discussions in regards to the experiments in the Allatoona dam. I am also grateful to the GRASP Lab family, where I

made special friendships that I would like to last forever.

I also want to thank my former institution, the Mechatronics Group at *Universidad Simón Bolívar*, especially professors Gerardo Fernandez and Juan Carlos Grieco, who introduced me to the world of mechatronics and kept track of me during my whole PhD.

Many thanks to Johnathan Fink, Stephanie Gil, Ramviyas Parasuraman and Jeffrey Twigg for being the international reviewers, whose helpful comments and fruitful discussions helped me to improve this thesis. Special thanks also to Sarah Tang for her huge effort helping to proofread this manuscript.

Thanks to the support of my special friends Tony, Diego, Juan, Cestari, Hamana, Denisse, Emily, Cecilia, Leonardo, Danilo, Domenico, Henry, Yasir, Mickey and Sarah.

Finally, I would like to thank my parents Chelo and Antonio, my brother Gabriel and my sister Carolina, and my wife Eugenia, who have always being there for me and have been the greatest personal support in the most stressful situations. Mom, you accompanied me during most of this thesis and only God knows why you had to leave us. I am deeply grateful for the life you gave me and for the quality time we spent together. I am sure we will see each other again. I dedicate this thesis to you.

Funding

This thesis has been funded by grant FPI BES-2010-038377 within project TESSEO: TEams of robots for Service and Security missiOns (ref. DPI2009-08126, Spanish Government), and project TELOMAN: TEams of robots for LOgistics, MAintenance and eNvironment monitoring (ref.DPI2012-32100, Spanish Government).

The financial support of DGA (Aragon Gov.), FSE (Fondo Social Europeo) is acknowledged. The authors also thank partial funding from grant no. W911NF-08-2-0004, of the US Army Research Laboratory.

Resumen

La robótica de servicio, entendida como aquella destinada al uso de uno o varios robots con fines de, por ejemplo, vigilancia, rescate e inspecciones, ha ido tomando cada vez más relevancia en los últimos años. Debido a los grandes avances en las distintas áreas de la robótica, los robots han sido capaces de ejecutar satisfactoriamente tareas que resultan peligrosas o incluso imposibles para los humanos, en diversos entornos. Entre ellos, los entornos confinados como túneles, minas y tuberías, han atraído la atención en aplicaciones relacionadas con transporte ferroviario, redes vehiculares, búsqueda y rescate, y vigilancia, tanto en el ámbito civil como militar.

En muchas tareas, la utilización de varios robots resulta más provechoso que utilizar sólo uno. Para cooperar, los robots deben intercambiar información sobre el entorno y su propio estado, por lo que la comunicación entre ellos resulta crucial. Debido a la imposibilidad de utilizar redes cableadas entre robots móviles, se despliegan redes inalámbricas.

Para determinar la calidad de señal entre dos robots, inicialmente se utilizaban modelos de propagación basados únicamente en la distancia entre ellos. Sin embargo, estas predicciones sólo resultan útiles en exteriores y sin la presencia de obstáculos, que sólo componen una pequeña parte de los escenarios de la robótica de servicio. Mas aún, la naturaleza altamente multi-trayecto de la propagación electromagnética en túneles hace que éstos actúen como guías de onda para cierto rango de frecuencias, extendiendo considerablemente el alcance de comunicación en comparación con entornos exteriores. Sin embargo, la señal se ve afectada con profundos desvanecimientos (llamados *fadings* en inglés). Esto los convierte en un reto para la robótica que considera la comunicación entre robots como fundamental.

Además, la naturaleza hostil de estos entornos, así como también la falta de características visuales y estructurales, dificultan la localización en estos escenarios, cuestión que resulta fundamental para ejecutar con éxito una tarea con un robot. Los métodos de localización utilizados en interiores, como aquellos basados en SLAM visual, resultan imprecisos por la falta de características distintivas para cámaras o lásers, mientras que los sensores utilizados en exteriores, como el GPS, no funcionan dentro de túneles o tuberías.

En esta tesis abordamos problemas fundamentales para la robótica con el fin de proporcionar herramientas necesarias para la exploración con robots en entornos tipo túnel,

manteniendo la conectividad de la red de comunicaciones formada por varios robots y una estación base. Para ello, primeramente caracterizamos, en términos de propagación, los dos escenarios tipo túnel más comunes: un túnel de hormigón y una tubería metálica. Hacemos énfasis en el fenómeno de los *fadings*, ya que son el problema más importante a considerar para mantener la comunicación. Posteriormente presentamos una estrategia de navegación para desplegar un equipo de robots en un túnel, lidiando con los *fadings* para mantener la conectividad de la red formada por los robots. Esta estrategia ha sido validada a través de numerosos experimentos realizados en un túnel real, el túnel de Somport. Luego, abordamos el problema de la localización, proponiendo e implementando una técnica que permite estimar la posición de un robot dentro de una tubería, basada en la periodicidad de los *fadings*. El método es validado a través de experimentos reales en tuberías de pequeña y grandes dimensiones. Finalmente, proponemos esquemas de diversidad espacial, de forma que se facilita la navegación mientras se mejora la localización.

Abstract

Deploying a team of robots for search and rescue, inspection, or surveillance, has increasingly gained attention in the last years. As a result of the advances in several areas of robotics, robots have been able to successfully execute tasks that are hazardous or even impossible for humans in a variety of scenarios, such as outdoors, indoors, or even underground. Among these scenarios, tunnel-like environments (such as tunnels, mines, or pipes) have attracted attention for train applications, vehicular networks, search and rescue, and even service and surveillance missions in both military and civilian contexts.

In most of the tasks, utilizing a multi-robot team yields better results than a single-robot system, as it makes the system more robust while reducing the time required to complete tasks. In order to cooperate, robots must exchange information about their current state and the surrounding environment, making communication between them a crucial task. However, due to the mobile nature of robots used for exploration, a wired architecture is not possible nor convenient. Instead, a wireless network is often deployed.

Wireless propagation in tunnel-like environments, characterized for the presence of strong fading phenomena, differs from regular indoor and outdoor scenarios, posing multiple challenges for communication-aware robotics. In addition, accurate localization is a problem in environments such as tunnels or pipes. These environments generally lack distinctive visual and/or structural features and are longer than they are wide in shape. Standard indoor localization techniques do not perform well in pipelines or tunnels given the lack of exploitable features, while outdoor techniques (GPS in particular) do not work in these scenarios.

In this thesis, we address basic robotics-related problems in order to provide some tools necessary for robotics exploration in tunnel-like scenarios under connectivity constraints. In the first part, we characterize, in terms of propagation, two of the most common tunnel-like environments: a pipe and a tunnel. We emphasize the spatial-fadings phenomena, as it is one of the most relevant issues to deal with, in a communications context. Secondly, we present a navigation strategy to deploy a team of robots for tunnel exploration, in particular maintaining network connectivity in the presence of these fadings. Several experiments conducted in a tunnel allow us to validate the connectivity maintenance of the system. Next, we address the localization problem and propose a technique that uses the periodicity of the fadings to estimate the position of the robots

from the base station. The method is validated in small-scale and large-scale pipes. Finally, we propose spatial diversity schemes in order to ease the navigation while improving the localization.

List of Figures

List of Tables

Acronyms

BER Bit Error Rate.

EM Electromagnetic.

FEM Finite Element Method.

GPS Global Positioning System.

IMU Inertial Measurement Unit.

IR Infrared.

ISM Industrial, Scientific and Medical.

LNG Liquefied Natural Gas.

LoS Line of sight.

LQM Link Quality Matrix.

MIMO Multiple Input Multiple Output.

PDR Packet Delivery Ratio.

RF Radio Frequency.

RSS Received Signal Strength.

RSSI Received Signal Strength Indicator.

SLAM Simultaneous Localization and Mapping.

SNR Signal-to-noise Ratio.

TE Transverse Electric.

TEM Transverse Electromagnetic.

TM Transverse Magnetic.

WLAN Wireless Local Area Network.

Contents

Chapter 1

Introduction

1.1 Introduction

Using ground or aerial robots for search and rescue, inspection, or surveillance operations has increasingly gained importance in the last years. As a result of the advances in several areas of robotics, such as vision, navigation, coordination and control, localization and mapping, robots have been able to successfully execute tasks that are hazardous or even impossible for humans. For example, [Michael 12] shows a team of ground and aerial robots used for collaborative mapping of an earthquake-damaged building after the 2011 Tohoku earthquake, and in [Walker 09], the authors describe a project that uses a robot for surveillance of underground galleries against smugglers at national borders.

To perform some tasks, utilizing a multi-robot team yields better results than a single-robot system, as it makes the system more robust while reducing the time required to complete tasks. In order to cooperate, robots must exchange information about their current state and the surrounding environment, making communication between them a crucial task. However, due to the mobile nature of robots used for exploration, a wired architecture is not possible nor convenient. Instead, a wireless network is often deployed. This is composed of the robots, and in most cases, a base station used for data gathering and visualization, and depending on the system architecture and degree of autonomy, sending commands.

In this context, understanding how the signal propagates in the environment is necessary for maintaining the network connectivity, planning the robot deployment, restricting the robots'

movements, and taking advantage of the areas where the quality of the links can be increased while avoiding the zones where the links can be broken, leaving one or more robots inoperative. A huge effort has been made in terms of mathematical modeling and field work in order to predict radio-wave propagation in different types of scenarios, such as indoor, outdoor, urban, or even underground. Among these scenarios, tunnels have attracted attention for train applications, vehicular networks, and even service and surveillance missions in both military and civilian contexts [Cerasoli 04, Kjeldsen 06, Masson 11, Bernado 11, Boksiner 12].

Wireless propagation in these environments differs from regular outdoor or indoor scenarios. In tunnels, the communication range can be greatly extended in comparison to free space, but the signal is affected by strong fading phenomena. In addition, due to their hostile nature and usual lack of visual and structural features, accurate localization inside tunnels is a challenging task. In this thesis, we perform an in-depth analysis of radio propagation in tunnel-like environments (such as tunnels, mines, or pipelines) to address the single and multi-robot navigation problem under connectivity constraints. We also provide solutions to localize within these scenarios, taking advantage of specific propagation characteristics.

Propagation

Wireless propagation in tunnel environments is described as strongly multipath. If the wavelength of the signal is much smaller than the cross-section dimensions, the tunnel acts as an oversized dielectric waveguide. In this case, the attenuation per unit length is low enough to allow communication over a range of several kilometers. Metallic pipes, such as those used in dam penstocks, gasoducts, or air conditioning/heating installations, also behave as cylindrical waveguides for Radio Frequency (RF) signals above certain frequencies.

However, in both scenarios the signal is affected by strong *fading* phenomena. In this thesis, we refer to fadings in a spatial domain (as a consequence of the constructive and destructive interference caused by the multipath effect), in contrast with the case of the small-scale fadings, which are understood as temporal variations of the channel. Fig. 1.1 shows an example of the measured received power after displacing a receiver 4 km from the transmitter inside a tunnel, highlighting the presence of fadings.

The analysis of the propagation of electromagnetic waves inside tunnels with arbitrary cross

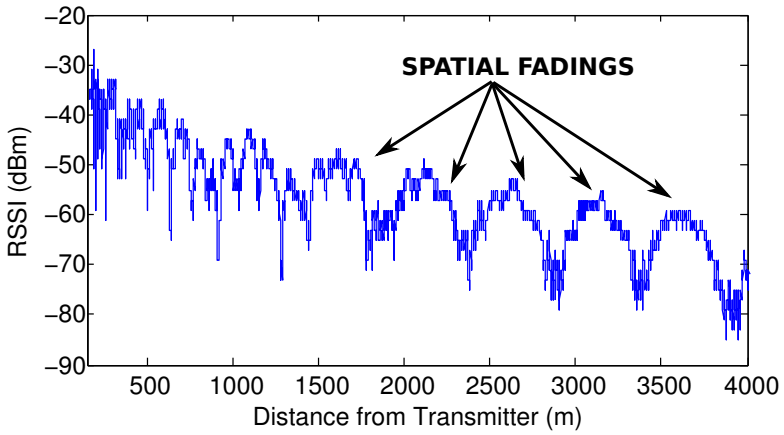

Figure 1.1: Measured Received Power at 2.4 GHz. The transmitter was kept fixed close to the entrance of the tunnel and the receiver was displaced along 4 km from the transmitter.

sections is not analytically feasible. Even for simple geometries, such as rectangular or circular cross sections, no exact closed form solutions are available. As in many scenarios, propagation in tunnels has been statistically analyzed (see [Lienard 98]). The most common approaches to obtain approximate solutions are the Modal Theory and the Geometrical Optics Theory. In Modal Theory, tunnels are modeled as oversized imperfect waveguides with rectangular or circular geometries. The received field is the sum of the fields consisting of a fundamental mode and a number of higher order modes [Mahmoud 74b, Emslie 75, Chiba 78, Dudley 07]. Geometrical Optics Theory models radio signals as rays and considers the tunnel walls as reflecting planes. Propagation is achieved via a direct path and all possible reflected paths. The techniques proposed are Ray Launching and Ray Tracing [Mahmoud 74a, Schaubach 92, Seidel 92, Honcharenko 92, Chen 96]. Still, many characteristics remain unsolved, such as the structure of the above mentioned fadings in three-dimensional space, which is necessary for exploring tunnels while maintaining network connectivity.

Navigation

In the literature, different approaches to address the connectivity problem in multi-robot exploration missions in urban scenarios have been adopted. In [Hsieh 08], a system to maintain connectivity of a robot team is described. A signal map is first constructed and used to plan the exploration in urban environments. A chain multi-hop network is created by the robots, which

have to move forward and backward to maintain the signal strength above a minimum acceptable level. In [Fink 10], different methods are proposed for modeling and mapping radio signal strength using robots. A maximum likelihood estimation of the source location is provided and a robot-motion control-law is applied to localize the source. A similar approach is described in [Wadhwa 11a], where the authors improve the characterization of the spatial variations of the Received Signal Strength (RSS) over space using Ray Tracing. They propose an adaptive algorithm which uses short and long term RSS averages to estimate both the traveling direction towards the source and how to proceed along the chosen direction. In [Gil 13], the authors propose and implement an adaptive solution that positions a team of robot routers to provide communication coverage to an independent set of client robots, without previous knowledge of the clients' positions nor the environment. Instead of stochastically sampling the environment or using propagation models, the authors incorporate the concept of directionality, mapping the signal strength it receives along each spatial direction. The controller then uses this profile to find directions of movement that yield better communication quality. The system is able to position the robotic routers to satisfy the robotic client demands, while adapting to changes in the environment and fluctuations in the wireless channels.

However, there is little to no literature addressing the robot communication problem in tunnel-like environments. In [Walker 09], the authors describe a project involving a robot for surveillance of underground galleries against smugglers at national borders. The problem of communication loss is mentioned, but no solutions are proposed. In [Peasgood 06], a work about multi-robot path planning in tunnel-like scenarios is presented. Only simulation results are shown, and the multi-robot communication problem is not addressed. In [Zhuang 08], a robot for inspecting tunnels, capturing images, and registering the concentration of some poisonous gases is developed. All of these cited works focus on single robots, on their mechanical aspects, on mapping, and on specific applications, without considering the connectivity problem. As a result of specific propagation phenomena in these environments, special techniques must be adopted in order to ensure reliable communication between the robots.

Localization

Accurate localization is challenging in environments such as tunnels or pipes. These environments generally lack distinctive visual and/or structural features and are longer than they are wide in shape. Standard indoor localization techniques (e.g. visual SLAM) do not perform well in pipelines or tunnels because of the lack of exploitable features, while outdoor techniques (GPS in particular) do not work in these scenarios.

Specifically, visual odometry algorithms, such as those presented in [Hansen 11, Lee 09, Lee 11], can only work if there are identifiable surface features or irregularities such as rust. A similar problem arises with Simultaneous Localization and Mapping (SLAM) algorithms, which need to find and match features in order to reduce the localization uncertainty. As a result, if the environment is smooth and lacks either visual or texture features for cameras and lasers, as is the case of most tunnels and penstock pipes in hydro electric power stations, the localization uncertainty continuously increases and cannot easily be reduced.

Other methods rely on wheel odometry systems for localization, but pipes tend to be slippery due to their circular geometry, humidity, and the presence of fluids and mold. Hence, the robot wheels tend to slide, accumulating errors and thus making this method unreliable for position estimation. Furthermore, wheel odometers are not suitable for certain types of robots such as aerial vehicles.

As an alternative to the above mentioned systems, localization methods based on RF signals have been developed. The goal of these is to estimate the target (e.g. robot) position through RF signal measurements after conveniently deploying a set of WiFi Access Points or taking advantage of an existing infrastructure.

Different approaches have been proposed. For instance, [Serrano 04, Lee 07] use wireless signal strength propagation models over which the robot estimates its position, but due to the complex interactions of WiFi signals and the necessity of a detailed description of the environment (objects, materials), data-driven signal map based methods have been found more suitable [Rolfe 07, Biswas 10, Howard 03, Ladd 02]. The first stage of these methods is to build a map of the received signal power [Ocaña 07]. However, this is time consuming job and not always possible, as in the case of an emergency or unforeseen situation.

1.2 Approach

The main objective of this thesis is to solve the robotic-related issues needed to develop a system capable of exploring tunnel-like environments for search and rescue, service, or surveillance, in particular addressing the connectivity constraints. We address the problem in three steps: propagation studies, navigation, and localization, all of which are supported by strong experimental evidence.

In the first part, we characterize two of the most common tunnel-like environments with different geometries, in terms of wireless propagation: a cylindric metallic pipe and a dielectric horseshoe-shape tunnel. As previously stated, although fadings are mentioned in the literature, there is still much to investigate in order to implement a complete robotic system capable of exploring the area while maintaining connectivity with a team of robots and base station. By performing several measuring campaigns in the previously mentioned scenarios and adopting the Modal Theory [Emslie 75] from a theoretical point of view , we provide the setups to produce easily-recognizable periodic fadings and describe its structure in three dimensions, to subsequently use it for navigation and localization.

Next, we address the problem of navigation inside a tunnel under connectivity constraints. Taking into account the previous studies, we propose a general algorithm that considers the derived characteristics of propagation in tunnels to plan the deployment of a team of robots and is also able to react based on real-time measurements. The algorithm is tuned and tested through simulations and experiments.

Lastly, we address the problem of localization in these featureless environments. In this case, a pipe is chosen instead of a tunnel as it has less features. We derive a technique for localization based on the periodicity of the fadings previously studied. This technique can be used to estimate the position of a robot inside these scenarios or to correct the accumulated errors by methods such as visual/wheel odometry. Finally, we take into account the structure of the fadings to ease the navigation while improving the localization, proposing spatial diversity schemes to improve the connectivity.

Although wireless protocols are used in this thesis, an in-depth analysis about the problems related to its performance, routing schemes, and so on is out of the scope of this work.

1.3 Thesis Timeline: Telling the Story

The developmet of this thesis took place in a four year period between June 2011 and June 2015. For an easier and more straightforward comprehension, the structure of the thesis does not match the chronological order in which the events happened. In this section, we recount the chronological order of our work to clarify any confusion.

Our research group has a special interest in developing technologies for hostile environments, such as tunnels or mines. Previous to the development of this thesis, several experiments involving communications were performed by our research group in the Somport tunnel, a 7 km straight tunnel located in Canfranc, Spain. Among these experiments, the deployment of a wireless network composed of several access points to provide coverage to an inspection car along the tunnel deserves special attention. It was experimentally shown that propagation in the tunnel differed from other scenarios, as a higher received power was perceived in certain zones farther from the transmitter.

One of the main goals proposed for this thesis was to lay the foundations for autonomous robotic exploration of a tunnel while maintaining the connectivity with a base station, simulating an emergency situation where human operators are not allowed to enter the tunnel and a team of robots is deployed instead. Clearly, a deeper analysis about propagation in this tunnel needed to be done.

Two robotic tools were developed to analyze propagation: a Pioneer P3AT robot with communication modules and a human-driven instrumented all-terrain vehicle. As an initial experiment, we explored the effects of changing the transmitter position by recording the received power along the tunnel (maintaining the same receiver cross-section position) for different transmitter positions. In all the configurations, the presence of strong fadings was noticed, but under one of them in particular, well-defined periodic fadings appeared. Motivated by this phenomena, we documented the experimental setup and repeated the experiment on different days, obtaining the same results. After a literature review, we found some publications referring to the presence of these periodic fadings, but no analysis of how to produce them nor their structure along the tunnel cross-section.

As another variable of study, we changed the receiver position under the transmitter configuration that produced the periodic fadings, this time obtaining different fadings for some receiver

positions. It was clear that the fadings were a function of the cross section positions of both the transmitter and receiver, but we did not find previous work in the literature nor did we have enough equipment to study the fadings along the cross-section.

After determining that along the same path the fadings were repeatable, we developed a navigation technique to deal with these fadings in order to maintain the connectivity in the network formed by the robots and with a base station. In this case, the fadings were modeled with a periodic mathematic function, obtained by means of fitting the experimental data.

After acquiring and incorporating a large number of RF receivers to the all-terrain vehicle, we performed an in-depth analysis of the transversal structure of these fadings. From a theoretical point of view, we adopted the Modal Theory, which allowed us to analyze the field distribution of the interacting modes and associate the transversal fading structure to it.

In the meantime, a six month research stay was performed at the GRASP Laboratory at the University of Pennsylvania, under the advisory of Dr. Vijay Kumar. Although the initial goal of the stay was to study ways to create coverage maps using quadrotors, we evaluated a possible contribution in a project using quadrotors to perform inspections of dam pipes. Motivated by problems when using visual odometry to estimate the position of the quadrotor inside the pipe and the appearance of periodic fadings in the Somport tunnel, we developed the idea of taking advantage of this periodicity to localize. No similar work was found in the literature, so we faced the challenge of adapting what we obtained in tunnels to metallic pipes. As first results, periodic fadings were obtained under some configurations in the Allatoona dam penstock pipe in Georgia, USA.

After the research stay, we acquired a small steel pipe, which allowed us to explore different setups to study propagation inside these scenarios. Later on, we had the opportunity to perform experiments in the large-scale drainpipe of the Santa Ana dam in Castillonroy, Spain. Note that a huge planning effort and large crew of people was required to perform experiments in this kind of facilities. Furthermore, as these facilities were in operational state (as the case of both dams), a service outage had to take place, which involved security procedures, training, emptying the pipes, on top of the money and man-hours required.

The experiments in the pipes allowed us to explore different setups to produce periodic fadings. Based on this data, a localization methodology that takes advantage of the periodicity of the fadings was developed and tested in both small-scale and large-scale pipes. Motivated by

the transversal structure of the fadings in the tunnel, a cross-section analysis was performed in the large-scale Santa Ana dam pipe, which allowed us to improve the localization resolution of the proposed method.

Finally, we started to adapt the developed method for tunnels, where some propagation phenomena make the method more challenging to implement. A first set of experiments were performed to estimate the position of an odometry-less robot, specifically a hexrotor, inside the tunnel.

1.4 Thesis Structure and Contributions

This thesis presents several contributions to the fields of communications and robotics, organized in the different chapters as follows:

First, in **Chapter 2**, we introduce the basics of wireless propagation in waveguides and analyze the case of circular metallic waveguides, emphasizing the fading phenomena. By means of evaluating the interacting modes' electric field distributions, we propose the most appropriate transmitter-receiver setups in order to produce easily recognizable and well-defined periodic fadings structures [Rizzo 14a]. Subsequently, we study the behavior of the fadings in the transversal dimension (cross-section). That is, we study the effects of the cross-section position over the fadings depth and relative phase. To the best of our knowledge, neither of the above mentioned issues have been addressed in the literature.

Next, in **Chapter 3**, we present the results of an in-depth analysis of propagation in tunnels, also emphasizing the fading phenomena. Although the presence of the longitudinal fadings is stated in the literature, we go further and corroborate the spatial and temporal repeatability of these fadings, an issue disregarded before and relevant for this work [Rizzo 12]. As in the previous case, by analyzing the interacting modes' field distributions, we study different transmitter-receiver configurations to obtain well-defined fadings structures, as well as analyze the large-scale structure of the fadings along the tunnel cross-section, an issue not addressed in the literature [Rizzo 13b]. We also introduce the use of the wavelet as a powerful tool for analyzing propagation in these environments, allowing us to observe the main propagation characteristics of these environments within one graph [Rizzo 13c]. From the theoretical point of view, an approach that has been widely used in the literature to obtain approximate expressions

of the field inside a tunnel with arbitrary cross-section is to model it as the equivalent rectangular or circular waveguide that best reproduces the experimental measurements. In this context, we validate this method with the FEM. This has not been done before as, since the very beginning of propagation studies in tunnels, this method has been considered extremely time consuming and memory demanding. Nevertheless, we prove that in the case of uniform tunnels, the problem translates into a 2D problem and the general characteristics can be simulated quickly with computers with common processing power nowadays.

The above mentioned contributions in **Chapter 2** and **Chapter 3** are the result of extensive measuring campaigns carried out in a four year period in different locations, among which deserve special attention: the Somport tunnel (Canfranc, Spain), the Santa Marta mine (Toledo, Spain), the Santa Ana drainpipe (Castillonroy, Spain), and the Allatoona dam penstock pipe (Georgia, USA), as well as several indoor and outdoor propagation studies carried out at the University of Zaragoza (Zaragoza, Spain) and the University of Pennsylvania (Philadelphia, Pennsylvania, USA).

Based on the previous propagation studies, in **Chapter 4**, we propose and implement a navigation technique in order to explore a tunnel with a team of robots while maintaining the connectivity with a base station located at the entrance of the tunnel at all moments [Rizzo 13a]. The algorithm has been evaluated through simulations and real experiments in the Somport tunnel. To the best of our knowledge, multi-robot deployment exploiting the signal transmission characteristics in real and large tunnel-like environments has not been addressed in the literature. Furthermore, a 2D navigation approach is proposed, where a single robot exploits the transversal structure of the fadings to improve the communication with the base station [Rizzo 14c]. Although these techniques have been tuned and particularized to the case of the propagation parameters of the Somport tunnel, they can be adapted to any tunnel-like fading environment.

In **Chapter 5**, we exploit the waveguide effect and the previously proposed setups to obtain periodic fadings, to develop a localization methodology designed for tunnel-like environments, where common localization algorithms perform erratically as a result of the lack of visual and structural features and the GPS-denied nature. The robot counts the number of maxima and minima encountered and estimates its position from the transmitter or base station. The method has been tested experimentally with ground robots in a small-scale pipe and in a real large-scale drainpipe [Rizzo 14a]. Subsequently, we propose an extension of the method for tunnels,

suggesting how to address propagation-related issues characteristic of these scenarios, such as localization in the messy near sector [Rizzo 14b]. A localization technique that offers an alternative to standard techniques by means of exploiting the periodic fadings has not been proposed in the literature. We also propose large-scale spatial diversity schemes to facilitate the navigation while improving the localization and communications. To the best of our knowledge, spatial diversity techniques have been studied only on a small scale. Nevertheless, in tunnel scenarios, the transversal structure of the fadings deserves special attention that cannot be ignored when designing such techniques. Moreover, we highlight the importance not only of the separation between antennas, but its cross-section position.

Finally, **Chapter 6** sets out the conclusions, lessons learned, and proposes future work that needs to be done.

In summary, although fadings in these confined environments are unavoidable and are usually considered a serious problem for communication purposes, we show an interesting way of addressing this issue by appropriately generating and detecting somewhat 'ad-hoc', known-geometry periodic fading structures, demonstrating how to navigate to deal with these fadings to maintain the network connectivity, and how to benefit from their periodicity to localize in these challenging featureless environments.

1.4.1 Publications

The novelty and originality of the approaches presented in this thesis are supported by the following peer-reviewed international robotics and communications journals, conferences and workshops (organized by reverse chronological order).
Currently under review

- [Rizzo 15a] Carlos Rizzo, Francisco Lera, and Jose Luis Villarroel. Spatial Diversity Fadings Analysis inside Pipes towards Localization. In *IEEE Transactions on Vehicular Technology*, Apr 2015, under review.

- [Rizzo 15b] Carlos Rizzo, Francisco Lera, and Jose Luis Villarroel. On the validation and limitations of the Rectangular Waveguide Approximation using the Finite Element Method towards Localization inside Tunnels. In *IEEE Vehicular Technology Conference (VTC Fall)*, 2015, under review.

- [Rizzo 15c] Carlos Rizzo, Francisco Lera, and Jose Luis Villarroel. Three-dimensional Fadings Structure Analysis in Straight Tunnels towards Localization and Navigation. In *IEEE Transactions on Vehicular Technology*, Feb 2015, under review.

Already published

- [Rizzo 14b] Carlos Rizzo, Francisco Lera, and Jose Luis Villarroel. A methodology for localization in tunnels based on periodic RF signal fadings. In *2014 IEEE Military Communications Conference (MILCOM)*. Baltimore, (USA), pages 317–324, Oct 2014.

- [Rizzo 14a] Carlos Rizzo, Vijay Kumar, Francisco Lera, and Jose Luis Villarroel. RF odometry for localization in pipes based on periodic signal fadings. In *2014 IEEE/RSJ International Conference on Intelligent Robots and Systems (IROS)*. Chicago, Illinois (USA), Sep 2014.

- [Rizzo 14c] C. Rizzo, D. Sicignano, F. Lera, and J. Villarroel. Promoting RF signal fadings: a solution for localization and navigation in tunnel-like featureless environments. In *Robotics: Science and Systems. Workshop on Communication-aware Robotics: New Tools for Multi-Robot Networks, Autonomous Vehicles, and Localization*. Berkely, California (USA), Jul 2014.

- [Rizzo 13a] Carlos Rizzo, Danilo Tardioli, Domenico Sicignano, Luis Riazuelo, Jose Luis Villarroel, and Luis Montano. Signal based deployment planning for robot teams in tunnel-like fading environments. *The International Journal of Robotics Research*, vol. 32, no. 12, pages 1381–1397, 2013.

- [Rizzo 13b] Carlos Rizzo, Francisco Lera, and Jose Luis Villarroel. Transversal fading analysis in straight tunnels at 2.4 GHz. In *13th International Conference on ITS Telecommunications (ITST)*, Tampere (Finland), pages 313–318, Nov 2013.

- [Rizzo 13c] Carlos Rizzo, Francisco Lera, and Jose Luis Villarroel. UHF and SHF fading analysis using wavelets in tunnel environments. In *IEEE 78th Vehicular Technology Conference (VTC Fall)*, Las Vegas, Nevada (USA), pages 1–6, Sept 2013.

- [Rizzo 12] Carlos Rizzo, Jose Luis Villarroel, and Danilo Tardioli. Spatial diversity based coverage map build- ing in complex tunnel environments. In *International Conference*

on Wireless Communications in Unusual and Confined Areas (ICWCUCA), Clermont-Ferrand (France), pages 1 –7, aug. 2012. Best Presentation Award.

Chapter 2

Propagation in Pipes

Wireless propagation in tunnel-like environments differs from propagation in regular outdoor and indoor scenarios. In this Chapter, we first introduce the fundamentals of Electromagnetic (EM) propagation, followed by a theoretical analysis of the specific case of propagation in metallic cylindric waveguides. Next, we present the results of extensive measurement campaigns carried out in a laboratory small-scale test pipe and a real large-scale drainpipe, emphasizing the spatial fading phenomena. We explore different transmitter-receiver setups in order to produce periodic fadings and analyze their structure along the longitudinal and cross-section dimensions of the pipe. Later on, this information will be used for navigation (Chapter 4) and localization (Chapter 5).

2.1 Electromagnetic Waveguide Propagation Foundations

In this section we introduce the basics of EM propagation relevant for this work. For a more detailed description, a good online resource can be found in [Orfanidis 14].

In free space, an RF source, such as an antenna, produces spherical waves that have a non-isotropic spatial distribution, corresponding to the radiation pattern of the antenna. Far enough from the emitter, the waves can be considered as locally plane Transverse Electromagnetic (TEM) propagating along the radial directions (for such uniform amplitude waves, the Maxwell equations impose that the respective electric and magnetic fields are in phase, perpendicular

to the propagation direction and also perpendicular one to each other). The radiated power is spread over a surface that grows as r^2, and thus the power density decays as $\frac{1}{r^2}$ in the best case. Unavoidable losses and impedance mismatch in real circuits, plus multipath, atmospheric attenuation, diffraction and other phenomena further decrease the power density available in a radio frequency link.

If, however, an emitting antenna is inside an air filled pipe or tunnel-like infinitely long cavity (that we will assume with uniform, but otherwise arbitrary, cross section), the spherical wavefronts will be multiply scattered by the surrounding walls. The superposition of all these scattered waves is itself a wave that propagates in one dimension – along z, the tunnel length - with a quasi-standing wave pattern in the transversal dimensions. One can think of this as throwing a rubber ball in a long corridor, which ends up traveling along it while bouncing in the walls, floor and ceiling.

For ideal lossless scattering in the surrounding walls, the time-averaged power of the propagated wave should be constant, not subject to the $\frac{1}{r^2}$ decay of free space propagation, and thus an infinite range is expected. In any real situation, however, losses arise from scattering due to the finite conductivity of the metallic walls, or in the case of dielectric guiding, to the power leakage through them. All this suggests that the electromagnetic field of a guided wave can be described as a one dimensional, attenuated, possibly non-uniform traveling wave for which we can use an expression similar to, but more involved than, the one used for plane waves. The electric and magnetic fields are given by:

$$E(x,y,z) = E_0(x,y)e^{-jk_g z} \tag{2.1}$$

and

$$H(x,y,z) = H_0(x,y)e^{-jk_g z} \tag{2.2}$$

where k_g is the so called wavenumber in the waveguide. Notice that this wave is not necessarily TEM, as the field amplitudes are not uniform but dependent on the transversal (x,y) coordinates. In free space, and in practice in air, the wavenumber follows the expression:

$$k_0 = \frac{2\pi}{\lambda_0} \tag{2.3}$$

with

$$\lambda_0 = \frac{c}{f} \tag{2.4}$$

where c is the free space speed of light and f is the operating frequency. For lossy media, the guided wave wavelength λ_g, phase velocity, and the wavenumber are in general different from the free space ones. If losses are present, wavenumbers become complex, $k_g = k_r - jk_i$. In many communications textbooks and in the literature, it is common to use the so called propagation constant, $\gamma = jk_g = \alpha + j\beta$, instead of the complex wavenumber. Its real part, α, is the attenuation constant (Np/m) and its imaginary part, $\beta = \frac{2\pi}{\lambda_g}$, is the phase constant (rad/m).

To better understand the different possible solutions and simplify its management, the fields are split into their longitudinal components, along z, and their transversal ones, in the xy plane.

$$E(x,y,z) = E_t(x,y,z) + E_z(x,y,z) = e(x,y)e^{-jk_g z} + e_z(x,y)e^{-jk_g z} \tag{2.5}$$

$$H(x,y,z) = H_t(x,y,z) + H_z(x,y,z) = h(x,y)e^{-jk_g z} + h_z(x,y)e^{-jk_g z} \tag{2.6}$$

Analogously, defining the transversal plane propagation constant as $k_c^2 = k_0^2 - k_g^2$, the Helmholtz equations for the electric and magnetic fields in the air region inside the tunnel or pipe are each split in two - one for the transversal and another for the longitudinal component. Only the two equations for the longitudinal components need to be solved.

$$\nabla_t^2 e_z + k_c^2 e_z = 0 \tag{2.7}$$

$$\nabla_t^2 h_z + k_c^2 h_z = 0 \tag{2.8}$$

It turns out that the boundary conditions (cross section geometry and nature of the walls) for each waveguide type force k_c^2 to take on certain values, which can be positive, negative, or zero, and characterize the set of particular solutions of a given problem, called **modes**. For example, in an air surrounded dielectric waveguide k_c^2 is positive inside the guide and negative outside it; in a hollow conducting waveguide k_c^2 takes on certain quantized positive values; in a TEM line, k_c^2 is zero.

Each mode has its own wavelength, attenuation constant, and wave impedance. The solutions for the longitudinal-transversal components of the fields are called themselves **modes**, and are usually indexed according to the standing wave patterns they represent and to the polarization of the associated fields.

The modes are usually classified according to the longitudinal fields present as:

- TEM (Transverse Electromagnetic) modes: when e_z and h_z are both null.
- TE (Transverse Electric) modes: when e_z is null and h_z is not null.
- TM (Transverse Magnetic) modes: when e_z is not null and h_z is null.
- Hybrid modes: when e_z and h_z are both not null. These are further classified in EH or HE modes depending on whether the components of E or H make the larger contribution to the transverse field.

TEM modes are characteristic of free space far field propagation and are also present in transmission lines (coaxial and other two-conductor cables). In metallic waveguides – rectangular or cylindrical – exact solutions for perfect conductor walls exist and very accurate approximate solutions can be found for real cases. Transverse Electric (TE) and Transverse Magnetic (TM) modes are possible, each one with a cutoff frequency that depends on the cross section geometry and size, below which the mode does not propagate. The mode with the lowest cutoff frequency is called the dominant mode. For communications purposes, metallic waveguides are used mostly in the so called monomodal regime, choosing an operating frequency that allows only the dominant mode to propagate.

For rectangular waveguides, the equations are solved in Cartesian coordinates. The dominant mode is the TE_{10} mode. For cylindrical waveguides, the equations are solved in cylindrical coordinates, and the dominant mode is the TE_{11}. We will show more details later on.

For air-filled rectangular dielectric waveguides (tunnels), there is not an exact analytic solution available. We will see later that there exist good approximate solutions valid for frequencies high enough to have corresponding free space wavelengths much smaller than the cross section dimensions. Only hybrid EH modes are possible and there is strictly speaking not a cutoff frequency. Its overall shape is quite close to the shape of the modes that will characterize a

metallic waveguide of the same size, corresponding to much lower frequencies. In fact, all possible modes can propagate, but higher order ones attenuate faster and thus, only a few remain detectable after some distance from the emitting antenna. The losses are a consequence of power transmission through the wall boundary, and subsequent dissipation inside. Higher order modes need more reflections to advance a given longitudinal distance and thus have higher attenuation rates. It is worth noting that scattering in any obstacles that breaks the uniformity of the waveguide cross section, adds an extra dissipation mechanism to the propagation of lower order modes.

The electric and magnetic fields produced inside a waveguide by an excitation source – in this thesis, a thin linear antenna – can be expressed as a linear combination of all the possible modes supported by the guide. To calculate the power coupled to each mode from the excitation source, a standard microwave procedure as described in Chapter 4 of [Pozar 05] can be followed. For example, using the subscript n to index the modes, the electric field of a forward traveling wave would be:

$$E = \sum_n A_n^+ (e_n + \hat{z} e_{zn}) e^{-jk_{gn}z} \tag{2.9}$$

For metallic waveguides and also for air-filled oversized dielectric waveguides, the tangential fields are vanishingly small at the guide walls and then:

$$A_n^+ = -\frac{1}{P_n} \int_L (e_n - \hat{z} e_{zn}) e^{jk_{gn}z} I(r') dl \tag{2.10}$$

$$P_n = 2 \int_{S_0} (e_n \times h_n^*) \hat{z} ds \tag{2.11}$$

Here, the line integral is calculated with the differential dl vector along the antenna length L, z is the longitudinal antenna position inside the guide, $I(r')$ is the usually not uniform current distribution on the linear antenna and Pn is a normalization constant proportional to the power flow of the n^{th} mode, obtained as a surface integral evaluated on the guide cross section S_0.

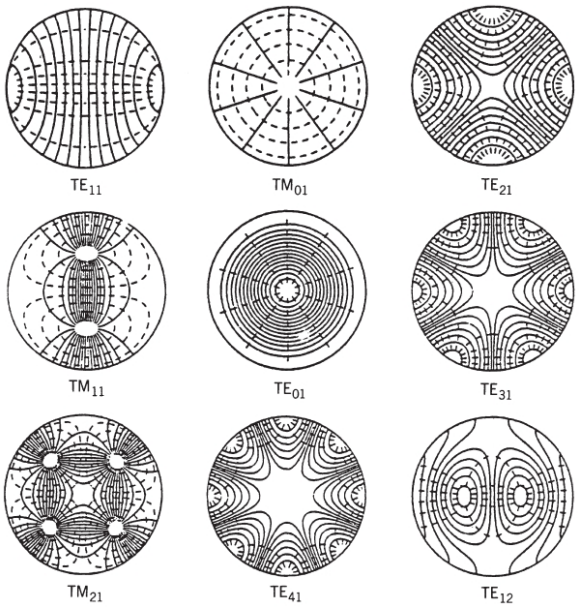

Figure 2.1: Field structure for the first nine propagating modes in a circular waveguide. The solid lines represent the electric field, and the dashed lines the magnetic field. The source is a vertically oriented dipole slightly offset from the tunnel center.

2.2 Theoretical Analysis: Propagation in Cylindrical Waveguides

A circular cross section metallic pipe behaves as a cylindrical waveguide for RF signals. Electromagnetic wave propagation inside the guide is strongly frequency dependent. This is a classical problem. Detailed insight can be found in Chapter 9 of [Balanis 89]. In the following paragraphs, we summarize the characteristics of waveguide propagation most relevant for this work.

The electromagnetic fields inside a cylindrical waveguide are best described in cylindrical coordinates (r, ϕ, z) to take advantage of the geometrical symmetry. Applying the electromagnetic boundary conditions at the metallic wall, many different solutions for the field configurations can be obtained. These are customarily called modes, and are classified as TE or TM. These modes are further indexed with two integer subscripts ($m = 0, 1, 2, 3..., n = 1, 2, 3...$) that account for the mode structure across the r and ϕ dimensions. Each TE_{mn} or TM_{mn} mode describes a geometrical arrangement of the electromagnetic fields in the guide cross section (see Fig. 2.1, taken from [Lee 85]). For each mode, there is a geometry dependent cutoff frequency,

f_c. RF fields of frequency f can propagate along the guide only in modes with $f > f_c$. For an air filled cylindrical pipe of radius a:

$$f_{c\,mn}^{TM} = \chi_{mn}\frac{c}{2\pi a} \tag{2.12}$$

$$f_{c\,mn}^{TE} = \chi'_{mn}\frac{c}{2\pi a} \tag{2.13}$$

where c is the free space speed of light, χ_{mn} is the n^{th} zero of the Bessel function J_m of the first kind and χ'_{mn} is the n^{th} zero of J'_m, the derivative of the Bessel function J_m of the first kind. The mode with the lowest cutoff frequency is called the dominant mode and is the TE_{11} with $\chi'_{11} = 1.8412$. The next three cutoff frequencies correspond to TM_{01} with $\chi_{mn} = 2.4049$, to TE_{21} with $\chi'_{21} = 3.0542$ and to the degenerate TE_{01} and TM_{11} modes with χ'_{01}=$\chi_{11} = 3.8318$.

In free space λ, the wavelength of an RF wave of frequency f is governed by Eq. 2.4. In waveguides, the situation is more complex and for a given frequency $f > f_c$, each propagating mode has its own wavelength:

$$\lambda_g = \frac{\lambda}{\sqrt{1-\left(\frac{f_c}{f}\right)^2}} = \frac{c}{f\sqrt{1-\left(\frac{f_c}{f}\right)^2}} \tag{2.14}$$

An RF source at a given frequency f (an antenna, for example) inside a pipe generates a complex RF field that is a superposition of many different modes with different amplitudes. The energy coupled to each mode depends on the source characteristics (antenna length, polarization, radiation pattern) and on its source position and orientation inside the waveguide. The modes with $f < f_c$ do not propagate and are negligible at a distance in the order of λ from the source. The modes with $f > f_c$ propagate along the waveguide with an attenuation that is also frequency dependent (see [Balanis 89] for the corresponding expressions).

For communication purposes, cylindrical waveguides operate usually in single mode: the frequency is selected with a value that allows only one propagating mode, the dominant one. Only one wavelength is present inside the guide and the RF field is reasonably simple.

If the operating frequency allows the propagation of two modes, each with its own wavelength, the situation becomes more complex. When a wave - with wavelength λ_g - travels a

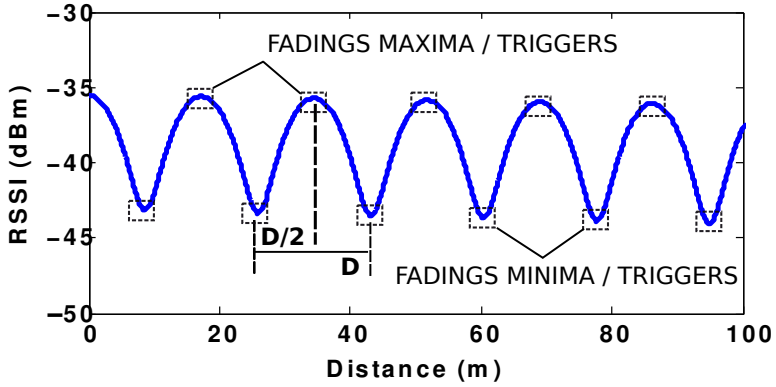

Figure 2.2: Simulation of bimodal propagation (f=65 MHz) in a 4-meter diameter pipe. D denotes the spatial period of the fadings.

positive distance d it accumulates a phase delay:

$$\varphi = 2\pi \frac{d}{\lambda_g} \tag{2.15}$$

If two modes with different wavelengths are present, the phase delay accumulated by each one will be different for a given travel distance d. The superposition of the modes will take place with different relative phases in different positions inside the guide, producing constructive interference if both modes are in phase and destructive interference if the relative phase differs in π. This gives rise to a periodic fading structure on the RF power inside the waveguide. The period of this fading structure D is the distance that creates a relative phase of 2π among the two considered modes. If λ_{g1} and λ_{g2} are the two mode wavelengths, then:

$$D = \frac{\lambda_{g1}\lambda_{g2}}{|\lambda_{g1} - \lambda_{g2}|} \tag{2.16}$$

When more than two propagating modes are present, every possible pair will create a fading structure with its own characteristic spatial period, giving rise to an increasingly complex signal. The total RF field will be the superposition of all of them.

Fig. 2.2 shows a simulation of a 65 MHz signal propagating in a 4 m diameter steel pipe. The interaction between the first two modes, TE_{11} and TM_{01}, creates 17.3 m of period fadings. The fadings' maxima and minima will be used as triggers for localization in Chapter 5. For the moment, we are interested in creating periodic fadings, with their spatial periods as short as

possible.

2.3 Test Scenario and Experimental Setup

2.3.1 Small-scale Test Pipe

First, the theoretical aspects of propagation were tested in a controlled environment, specifically in a small-scale test pipe inside a laboratory. This is a stainless steel pipe with an internal diameter of 0.125 m, 0.002 m thick, and 6 m in length.

To analyze the propagation behavior, an RF transmitter (Agilent model E4432B) and a portable spectrum analyzer (RF Explorer model 3G) were used. The transmitter antenna was longitudinally fixed at 0.5 m from one of the pipe ends, and its cross-section position and orientation will be specified according to the experiment. The receiver was placed on a moving platform, a small motorized robot capable of moving forward and backward inside the pipe. To fit inside the pipe, all antennas were 0.03 meter-long dipoles with a $2dBi$ gain. A Hokuyo laser distance sensor was placed at the other end of the pipe (opposite to the transmitter location), pointing at the moving platform, in order to obtain the position estimation. Both the laser sensor and the moving receiver were connected to a computer running ROS (Robots Operating System [Quigley 09]) over Linux operating system (Ubuntu 12.04), allowing us to synchronize the data and maintain the same timestamp. The whole setup is shown in Fig. 2.3 . A summary of the tools used for propagation studies in this thesis can be found in Appendix A.

2.3.2 Large-scale Scenario: Santa Ana Dam Drainpipe

The real scenario was a 4 m internal diameter and 300 m long carbon steel pipe, used as a drainpipe for the Santa Ana dam in Castillonroy, Spain (Fig. 2.4). As the operating frequency range differs in comparison to the small-scale pipe, two telescopic antennas were used instead. A human-driven platform acted as the moving receiver and an ad-hoc system based on landmarks provided the position estimation. A summary of the experimental scenarios used in this thesis, together with details of the experiments performed, can be found in Appendix B.

Figure 2.3: Laboratory experimental setup. From upper left, clockwise: the small-scale pipe, the receiver robot, the transmitter platform, and the the laser sensor for position estimation.

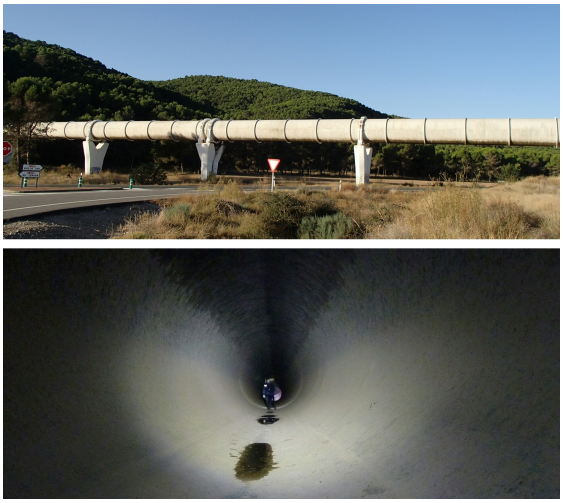

Figure 2.4: Large-scale scenario. Drainpipe (4-m diameter, 300-m length) at the Santa Ana dam (Castillonroy, Spain).

2.4 Longitudinal Fadings Analysis

In order to analyze propagation, several experiments were performed under different configurations. In particular, the effects of the transmitting frequency, as well as the transmitter-receiver antenna position and orientation were explored. The frequencies were chosen to allow up to five propagating modes. The proposed antenna configuration took into account both the geometry of the propagation modes and the practical implementation aspect (Fig. 2.5). Hereinafter, the first

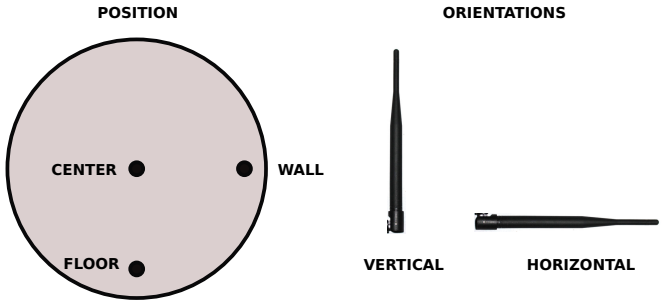

Figure 2.5: Pipe front view. Antenna positions and orientations

Table 2.1: Cutoff frequencies for the first five propagating modes

	Mode 1	**Mode 2**	**Mode 3**	**Mode 4 / 5**
Small-sclae pipe (GHz)	1.40	1.83	2.33	2.92
Large-scale pipe (MHz)	43.95	57.41	72.91	91.47

letter refers to the antenna position in the cross section (C, W, F for Center, Wall, or Floor) and the second letter to the antenna orientation (V, H for Vertical or Horizontal respectively).

For future reference, Table 2.1 shows the cutoff frequencies for the first five modes for the small-scale and large-scale pipes (Eq. (2.2) and Eq. (2.2)), while Fig. 2.6 shows the fadings period for a wide range of frequencies, caused by the pairwise interactions between the first three propagating modes (Eq. 2.2).

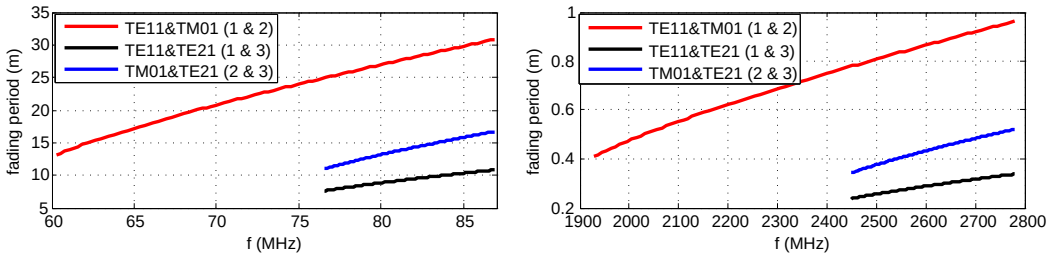

(a) Large-scale pipe (b) Small-scale pipe

Figure 2.6: Fading periods caused by the pairwise interactions between the first three propagation modes.

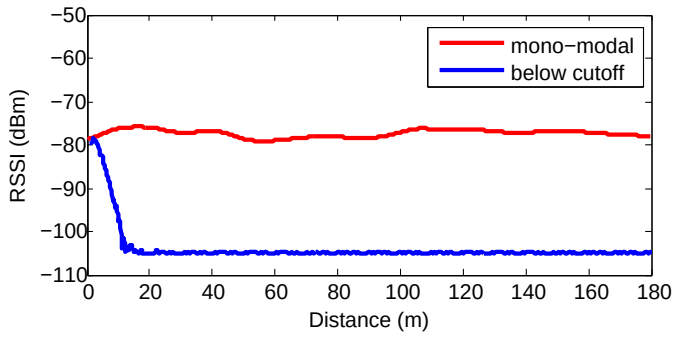

Figure 2.7: Propagation below the cutoff frequency and mono-modal propagation in the large-scale pipe.

2.4.1 Propagation Below the First Mode Cutoff Frequency and Mono-modal Propagation

Below the first mode cutoff frequency, the expected behavior of the signal is a rapid attenuation, as the pipe does not act as a waveguide for these frequencies. On the other hand, the mono-modal propagation is achieved by selecting a frequency above the first mode cutoff frequency, but below the second one. This setup is commonly used to transmit signals for communication, as it avoids interference with higher order modes. The selected frequencies for both cases were chosen as 40 MHz and 51 MHz for the large-scale pipe, as stated in Table 2.1. Both transmitting and receiving antennas were placed in the Center of the pipe, with a Vertical orientation (C-V), and the received power was measured along 180 m. Results are shown in Fig. 2.7.

As can be seen, below the cutoff frequency, the signal completely attenuates after just one wavelength distance. Therefore, this setup is useful for neither communication nor to create periodic fadings. On the other hand, the mono-modal propagation shows a signal with no interference and low attenuation along the pipe. Although useful for communications, as our goal is to produce periodic and well-defined fadings, this setup is not useful either.

2.4.2 Bimodal Propagation

In bimodal propagation, interference from the first two modes (TE_{11} and TM_{01}) is provoked. The chosen frequencies for the small-scale and large-scale pipes were 2.29 GHz and 71 MHz (located between the second and third modes cutoff frequencies), which yield theoretical fading

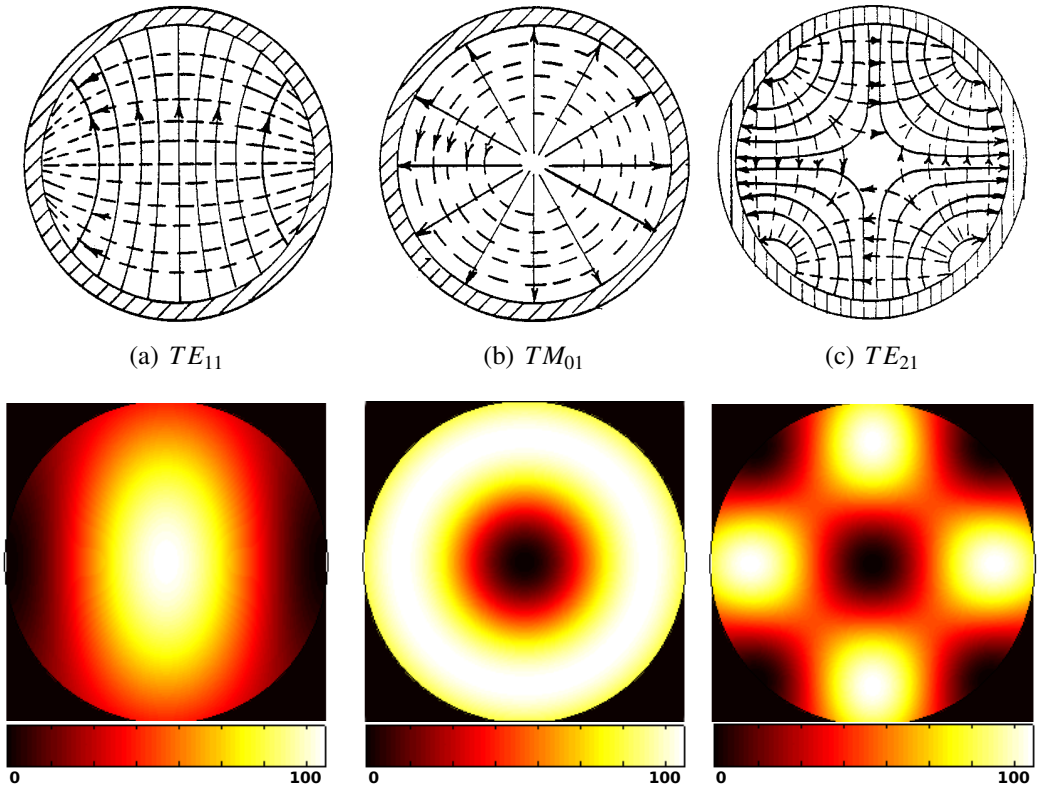

(a) TE_{11} (b) TM_{01} (c) TE_{21}

(d) TE_{11} (e) TM_{01} (f) TE_{21}

Figure 2.8: Field structure (the solid lines represent the electric field, and the dashed lines the magnetic field) and normalized power (arbitrary units) for the first three propagating modes inside a metallic cylindrical waveguide. The source is a vertically oriented dipole slightly offset from the tunnel center.

periods of 0.68 m and 21.5 m, respectively.

For the antenna setup, the modal field and power distribution were used to enhance the modes' excitation and detection. In this particular case, Fig. 2.8(a) shows vertically oriented electric field lines for the first mode and a power maximum, both around the pipe center. For the second mode, Fig. 2.8(b) shows a radial symmetry with a power minimum in the pipe center. On this basis, both the transmitting and receiving antennas were placed slightly vertically offset from the tunnel center, with a vertical orientation.

Fig. 2.9(a) and Fig. 2.9(b) show the measured received power for the case of bimodal propagation (as well as trimodal propagation addressed in the next Section) for both pipes.

The experimental mean value for the fading periods along the studied distances are 0.69 m

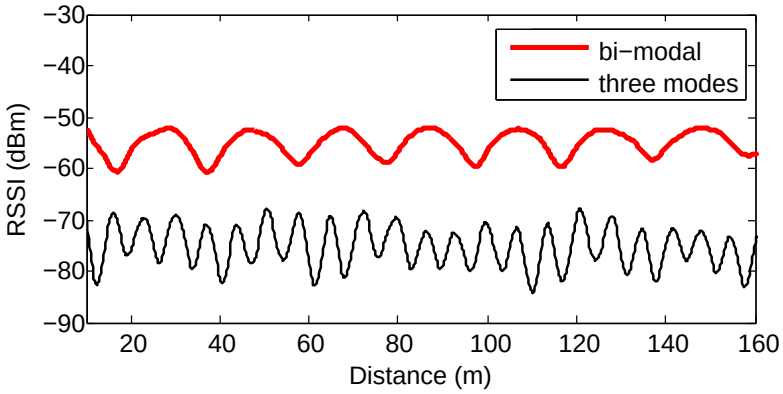

(a) Large-scale pipe

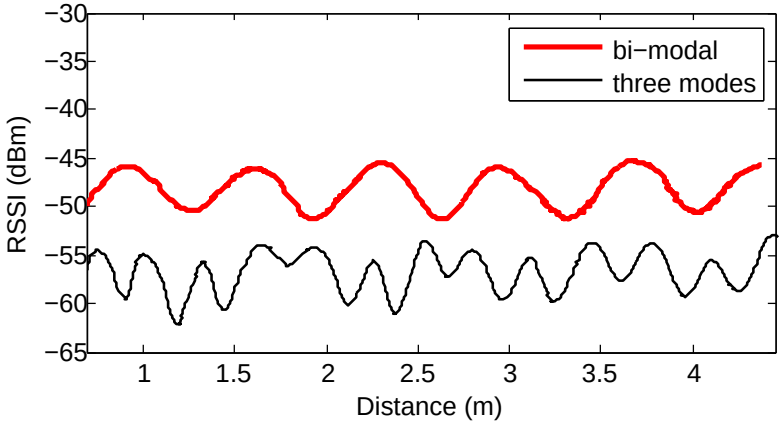

(b) Small-scale pipe

Figure 2.9: Measured received power for bimodal and trimodal propagation in the large-scale and small-scale pipe. Signals are offset in the vertical axis for clarity.

and 21 m for the the small-scale and large-scale pipe, respectively, yielding differences of 1.4% and 2.3% with respect to the theoretical values.

On the other hand, Fig. 2.10 denotes the importance of the antenna setup, contrasting the previous setup with a C-V for the transmitter and a W-V for the receiver. Fadings are clearer using the first configuration, C-V for both transmitter and receiver.

In all the cases, the signals have being filtered with a butterworth low-pass filter with a cutoff frequency above the respective frequency of the expected fadings periods. Nevertheless, for practical applications, moving average filters yield good results. As will be evidenced in Section 2.4.5, the metallic pipe shield avoids external interference, making the received signal low in noise. Fig. 2.11 shows the raw signal and the filtered signal after applying a moving

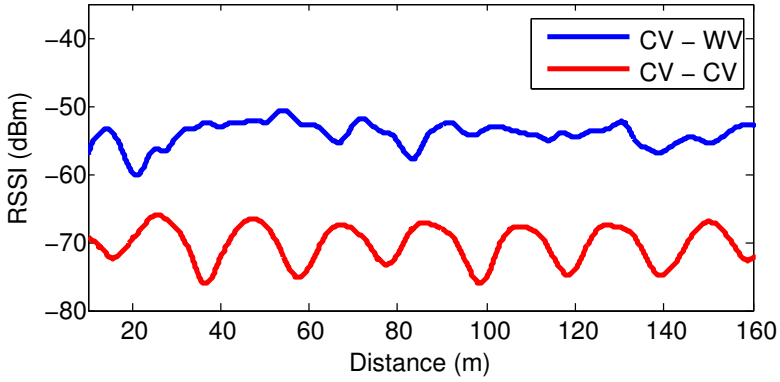

Figure 2.10: Received signal power for two different antenna configuration, for bimodal propagation. The signals are offset in the vertical axis for clarity.

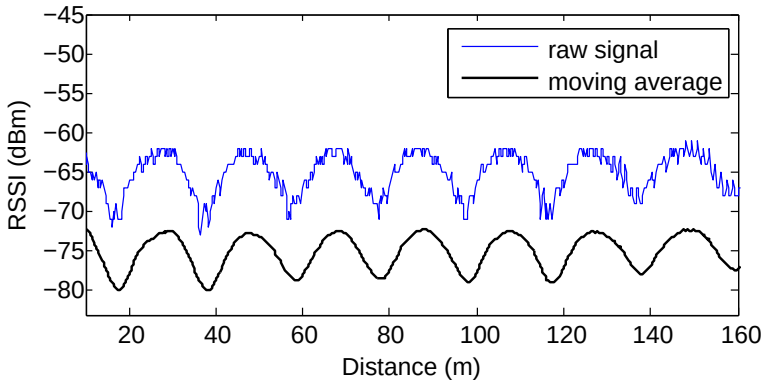

Figure 2.11: Raw signal and moving average filtered signal for bimodal propagation in the Large-scale pipe. The signals are offset in the vertical axis for clarity.

average with a window size of 10 samples (being the receiver sampling frequency 16 Hz), for the case of bimodal propagation in the large-scale pipe. This represents a feasible solution for online calculations and practical applications.

2.4.3 Trimodal Propagation

It can be observed from Eq. (2.2) and Fig. 2.6 that the interaction between the first and third modes produce shorter period fadings compared to the previous case. As will be discussed in Chapter 5, shorter period fadings are more useful for localization.

Selecting a frequency to allow propagation of the first and third modes also involves propagating the second one. Hence, the alternative is to take advantage of the modes' geometries to

choose an emitter-receiver configuration with enhanced sensitivity for the first and third interference mode, while being less sensitive to the interference between the first and second mode.

Fig. 2.8(c) shows a cross geometry for the electric field and power distribution for the third mode, with maxima almost at the extremes of this shape. In order to reduce the power coupled to the second mode (which is geometrically radial), the transmitter antenna was placed slightly vertically offset from the tunnel center, with a horizontal orientation. By adopting this configuration, the antenna is perpendicular to the electric field of the second mode and thus the power coupling to this mode is minimized. The receiver was placed in the same cross-section position, vertically oriented, although a horizontal orientation would have reduced the detection of the second mode even more.

Fig. 2.9 shows the measured received power along both pipes, and corroborates the shorter period fadings and the insignificant influence of the second mode. The values obtained for the fading periods are 0.295 m and 6.9 m for the small-scale and large-scale pipe, yielding differences of 1.72% and 1.5% with respect to the theoretical values.

2.4.4 Multimodal Propagation

Table 2.1 shows the same cutoff frequency for the degenerate fourth and fifth modes, producing a collective propagation of the first five modes when the operating frequency is slightly above the fourth mode's cutoff frequency. Given the geometrical configuration of these modes (see Fig. 2.1), it is not trivial to choose a transmitter-receiver setup in order to excite and detect selectively some of them. Besides, as each pair of modes is responsible for creating a periodic fading structure, the number of possible combinations will increase as $C_{m,2}$, where m is the number of propagating modes.

As an example, the measured received power for the case of five modes propagating in the small-scale pipe is shown in Fig. 2.12. Notice that multiple fadings with different periods take place. Hence, propagating more than three modes involves more complex received-signal patterns with irregular periods.

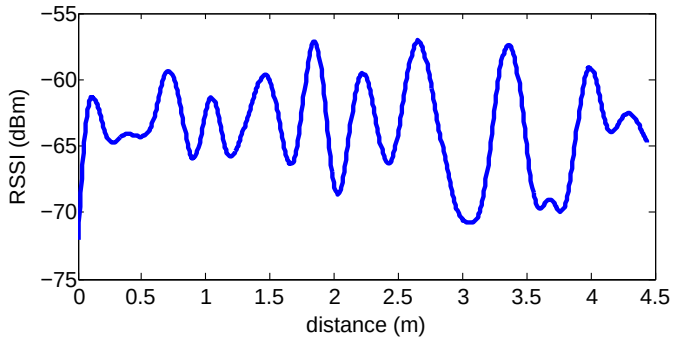

Figure 2.12: Measured received power for the case of five modes propagating in the small-scale pipe.

2.4.5 Stationarity of the Signal

It is also important to measure the noise level or the variations of the signal inside the pipe under stationary conditions. To this end, the receiver was left steady for a five minute period inside the small-scale pipe. The results show that the received signal strength variation was below the receivers sensitivity, which is 1 dBm in this case. This can be explained by the fact that inside the pipe, the metallic walls act as a nearly perfect shield ('Faraday cage') for RF fields coming from the exterior. A small amount couples to the interior through the openings, and thus this is a nearly noise-free environment. Only internal noise sources are relevant. Hence, the received signal can be considered stable and low in noise.

2.4.6 Repeatability of the Signal

If the final use is for localization and navigation, it is also important to test the repeatability of the fadings. After choosing the trimodal propagation, the receiver was displaced along the same distance inside the small-scale pipe, under the same transmitter-receiver configuration, in three different occasions. The results of the measured received power is shown in Fig. 2.13, where it is corroborated that the period and shape of the fadings are maintained, indicating that the behavior is repeatable in the time domain.

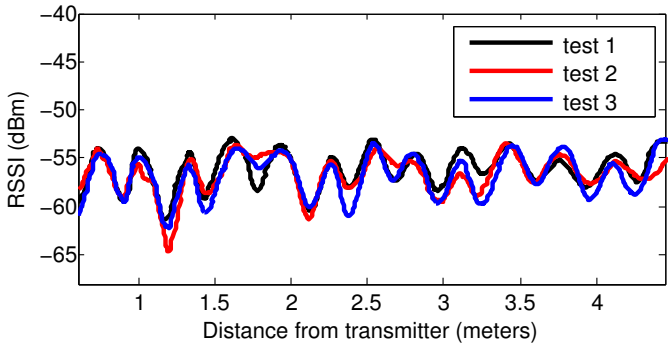

Figure 2.13: Repeatability of the signal inside the laboratory pipe.

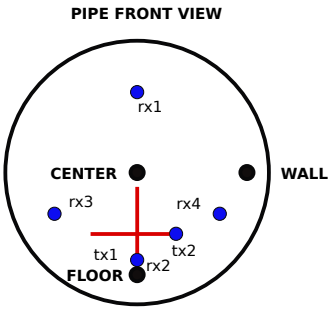

Figure 2.14: Transmitter-receiver positions for different cross-section fadings analysis.

2.5 Transversal Fadings Analysis

After studying the received fadings in the longitudinal dimension, in particular the cases of bimodal and trimodal propagation, and the transmitter-receiver setup that enhances the excitation and detection of the modes of interest for both cases, we performed the transversal fadings structure analysis. That is, we studied the effects of the cross-section position on the received power and relative phase of the fadings. By analyzing the electric field distribution of the first three modes (Fig. 2.8), two cases of study become relevant: virtually dividing the pipe with respect to the center horizontally (upper vs lower half) and vertically (right vs left half). Notice that, as will be discussed later, because of the circular symmetry of the pipe, if the configuration of the transmitter and receivers is arbitrarily rotated, the resulting electric field distribution will be rotated as well.

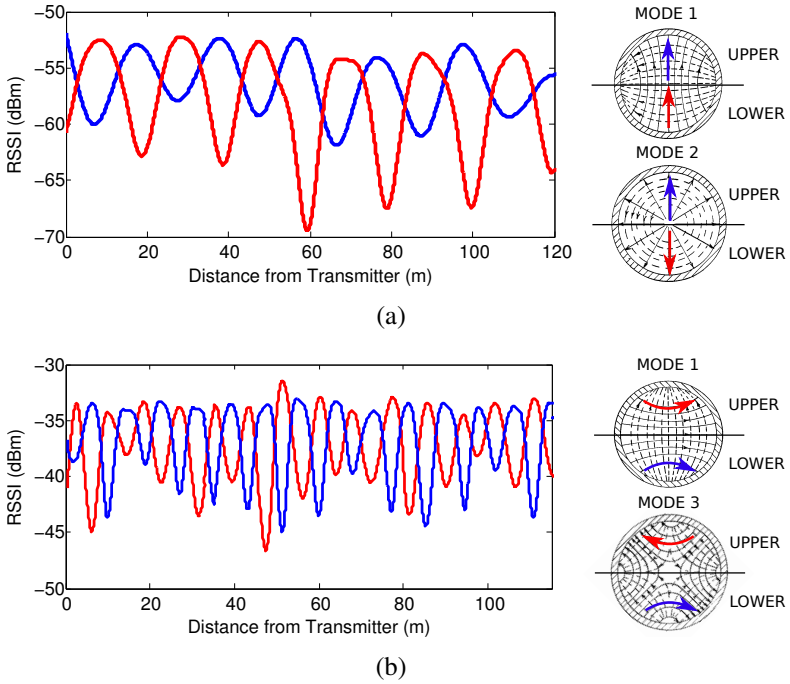

Figure 2.15: Received signal power in the upper and lower half, together with the electric field distribution for (a): bimodal propagation (b) trimodal propagation. The blue arrows represent constructive interference, while the red arrows destructive interference.

2.5.1 Horizontal Division: Upper vs Lower Half

2.5.1.1 Bimodal Propagation

Fig. 2.15(a) illustrates that whenever constructive interference appears in the upper half of the pipe (represented with blue arrows, indicating that the electric field goes in the same direction in both modes), destructive interference appears in the lower half (red arrows, indicating that the electric field goes in opposite directions), and vice-versa. To test these effects over the fadings, the experiments were conducted in the large-scale pipe.

The transmitter antenna was placed vertically at position *tx1* (Fig. 2.14), emitting at a frequency of 70 MHz, and the two receivers used (one for each sector) at positions *rx1* and *rx2*. Results after measuring the received signal power along 120 m are shown in Fig. 2.15(a), where there is clearly a 180 degree relative phase difference between the fadings corresponding to each sector (i.e. a maximum in one fading matching a minimum in the other fading).

2.5.1.2 Trimodal Propagation

In this case, the transmitter was placed at position *tx2* (f=78 MHz) and horizontally oriented, as previously discussed, to minimize the coupling to the second mode. A receiver was placed in each sector, at positions *rx1* and *rx2*. By orienting the transmitter antenna horizontally, the modal coupling of the first mode differences from that of the previous vertical case (Fig. 2.15(a)). Here, the electric field lines are horizontal instead of vertical. The same reasoning applies to the modal coupling of the third mode.

Following the same convention, Fig. 2.15(b) represents the constructive and destructive interference for the interaction between the first and third modes. It can be seen, as in the previous case, that in the upper half of the tunnel, destructive interference takes place when constructive interference occurs in the lower half, and vice-versa.

Results of the measured signal power in each sector are shown in Fig. 2.15(b), where it can be seen that there is a 180 degree relative phase difference between both halves. This time, as previously studied, the fadings period is shorter compared to the case of bimodal propagation.

2.5.2 Vertical Division: Left vs Right Half

2.5.2.1 Bimodal Propagation

In the case of virtually dividing the pipe vertically, from Fig. 2.16(a) it can be seen that whenever constructive or destructive interference takes place in the right half, the same occurs in the left.

The transmitter antenna was placed vertically at position *tx1* (Fig. 2.14), emitting at a frequency of 70 MHz, and the two receivers were oriented horizontally at positions *rx3* and *rx4*, following the radial structure of the second mode. Results of the measured power by each receiver are shown in Fig. 2.16(a), where it is noticed quite good match between both signals, showing no relative phase difference between both sectors.

2.5.2.2 Trimodal Propagation

As in the previous case of trimodal propagation, the transmitter was horizontally placed at position *tx2* (f=78 MHz) and the receivers at positions *rx3* and *rx4*.

Like the case for bimodal propagation, Fig.2.16(b) illustrates that the first and third modes

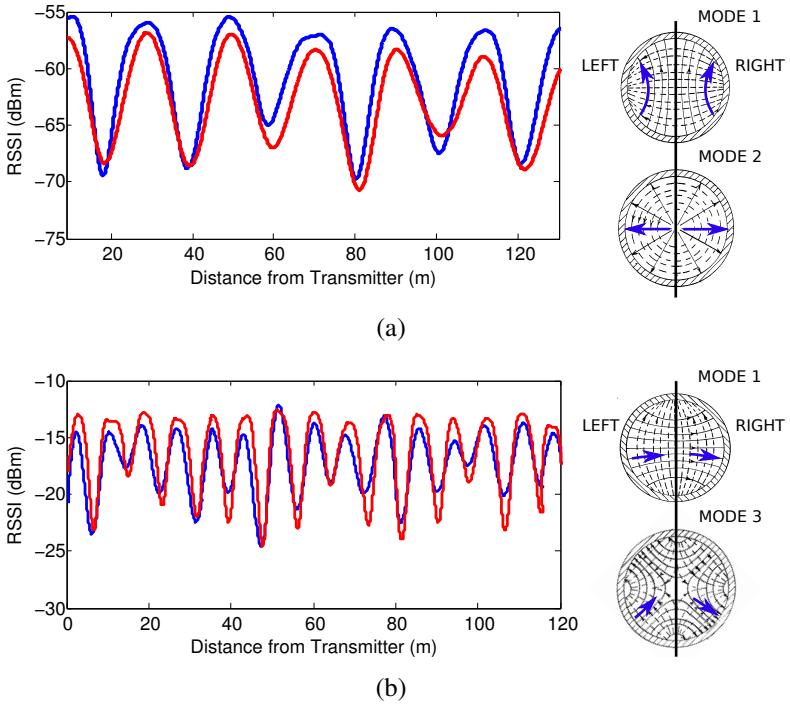

Figure 2.16: Received signal power in the left and right half, together with the electric field distribution for (a): bimodal propagation (b) trimodal propagation. The blue arrows represent constructive interference.

interact constructively at the same time in both halves. The same occurs for destructive interference. The results for the received signal power in each of these sectors are shown in Fig. 2.16(b). Again, no relative phase difference is noticed between both halves, and the period is shorter than the case of bimodal propagation.

Due to the circular symmetry of the pipe, if the transmitter setup is rotated the previous interpretation is rotated as well. For instance, if the transmitter is placed horizontally at the floor operating at a frequency to provoke trimodal propagation, there is a phase difference of 180 degrees between the lower and upper half, and the same phase between the left and right half (Fig. 2.17(a)). If the transmitter is placed vertically close to the wall (Fig. 2.17(c)), equivalent to a 90 degree rotation with respect to the previous configuration, the phase difference of 180 degree happens between the left and right half, instead of between the upper and lower half. The phase difference will be exploited in Chapter 5 to improve the resolution of the localization algorithm. Therefore, one can choose the appropriate setup depending on the desired resulting fading structure.

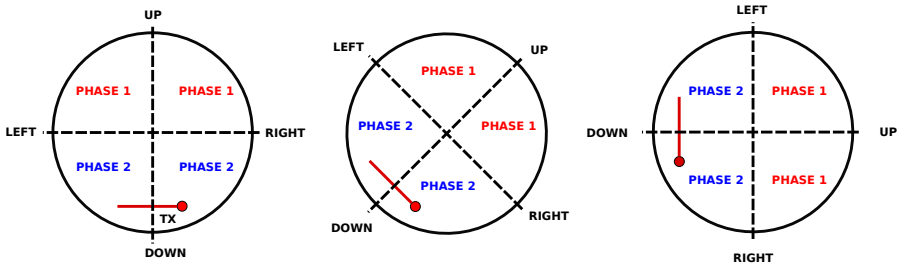

(a) 0° (b) 45° (c) 90°

Figure 2.17: Effects of rotating the antenna setup on the cross-section fadings structure. The phase difference between *phase 1* and *phase 2* is 180 degrees.

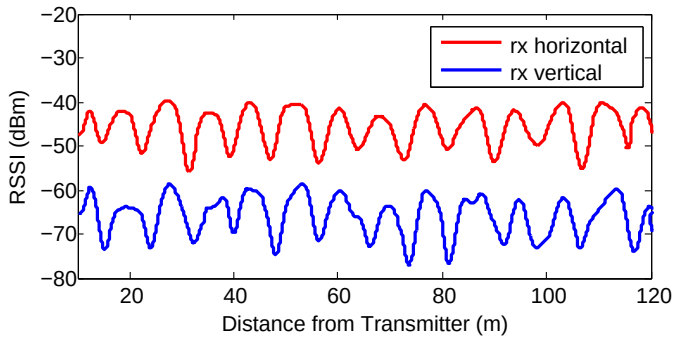

Figure 2.18: Effects of antenna polarization over the fadings' relative phase.

2.5.3 Influence of the Antenna Polarization over the Phase Difference

To study the effect of the antenna polarization over the phase difference, an experiment was performed with the two calibrated receivers in the same cross-section position (*rx1*), one horizontally oriented and one vertically oriented. The transmitter's antenna was horizontally oriented at position *tx2* at a frequency of 78 MHz to provoke trimodal propagation. Results of the received signal power are shown in Fig. 2.18, where it is seen that there is no relative phase shift. Nevertheless, the power measured by each receiver differs by 25 dB. With this transmitter setup, the electric field lines of the first mode are horizontal, and hence the power coupled with an horizontal antenna (red signal in Fig. 2.18) is maximized, while a vertical antenna is perpendicular to the electric field lines and minimizes the coupling (blue signal in Fig. 2.18).

2.6 Summary

In this section, we carried out a theoretical analysis to derive the expressions for RF propagation in metallic pipes, with emphasis on the fading phenomena. Experimentally, these concepts were tested in a laboratory small-scale pipe and a real scenario, a large-scale drainpipe used in the Santa Ana dam, in Spain.

By tuning the operating frequency, as well as the transmitter and receiver antenna cross-section positions and orientations, we obtained the adequate setups to produce well defined fadings. Results show that the most useful configurations propagate two or three modes, where the period is shorter in the latter case. In both cases, the geometry of the interacting modes, as well as the power distribution, were used to improve the modal excitation and detection, allowing us to select the antenna position and orientation that enhances the power coupled to a given mode. Moreover, propagating three modes allowed for minimization of the influence of the second mode, as its detection is undesirable under this configuration.

In addition, an analysis of the electric field arrangement of the interacting modes allowed to study the spatial structure of the fadings (i.e. the effects of the receiver position over the received signal fadings). In this context, the pipe was virtually split in two sectors horizontally (upper and lower half) and vertically (left and right half). Depending on the setup, the received fadings presented a relative phase difference of about 180 degrees compared to the other sector. Due to the cylindrical geometry, the problem and interpretation are rotated by means of rotating the transmitting setup. Furthermore, the fadings proved to be repeatable in the time domain, and the received signal was low in noise inside the pipe.

Finally, propagating more than three modes yield signals that were more complex because of the mutual interaction among all the modes involved.

Chapter 3

Propagation in Tunnels

Tunnels represent strong multipath environments for communications. Like in pipes, wireless propagation in tunnels differ from regular indoor and outdoor scenarios. If the wavelength of the propagating signal is much smaller than the cross-section dimensions, tunnels behave as oversized waveguides, extending the communication range but affecting the signal with strong fadings. In this Chapter, we first analyze the case of propagation in dielectric tunnels. Then, we present the results of extensive measuring campaigns carried out at the Somport tunnel, in Spain. Particularly, we explore the transmitter-receiver setups to produce periodic fadings and analyze these fadings in the longitudinal, transversal, and vertical dimensions of the tunnel. We also introduce the Wavelet as a powerful tool for analyzing fading phenomena in tunnels. In the literature, tunnels are modeled as rectangular or circular waveguides. We validate and explore the limitations of this approach using the Finite Element Method. Finally, we compare the case of propagation in tunnels with the previous case of propagation in metallic pipes.

3.1 Introduction

Wireless communication systems have become increasingly important as they represent, most of the time, a faster, more economical, and sometimes the only option to deploy a network (e.g. communications between mobile agents). As the prediction of radio coverage levels is required to develop communication systems and to optimize their deployment, ensuring availability and robustness of the radio links, a huge effort has been made in terms of mathematical modeling

and propagation measuring campaigns in different types of scenarios, from indoor, outdoor, urban, to even underground. Among these scenarios, tunnels have attracted attention for train applications, vehicular networks, and even service and surveillance missions in both military and civilian contexts [Cerasoli 04, Kjeldsen 06, Masson 11, Bernado 11, Boksiner 12].

To provide radio coverage in long tunnels (railway, road or mines), two main methods are used: the leaky feeder, based on the use of radiating cables, and systems based on the natural propagation of radio-waves inside the tunnel. Owing to the high cost of leaky-feeder installations and the fact that they are susceptible to failures in disasters, the natural propagation system is preferred in many applications.

Wireless propagation in these environments is described as strongly multipath, and if the wavelength of the signal is much smaller than the tunnel cross section, tunnels act as an oversized dielectric waveguide. In this case, the attenuation per unit length is low enough to allow communications over a range of up to several kilometers. However, the signal is affected by strong *fading* phenomena, as has been studied by many authors.

The analysis of the propagation of electromagnetic waves inside a tunnel with arbitrary cross section is not analytically feasible. Even for simple geometries, such as rectangular or circular cross section, no exact closed form solutions are available. The obtain approximate solutions, the most common approaches are the Modal Theory and the Geometrical Optics Theory. In Modal Theory, tunnels are modeled as oversized imperfect waveguides with rectangular or circular geometry. The received field is the sum of the fields consisting of a fundamental mode and a number of higher order modes [Mahmoud 74b, Emslie 75, Chiba 78, Dudley 07]. The Geometrical Optics Theory models radio signals as rays and considers the tunnel walls as reflecting planes. Propagation is achieved via a direct path and all possible reflected paths. The techniques proposed are Ray Launching and Ray Tracing [Mahmoud 74a, Schaubach 92, Seidel 92, Honcharenko 92, Chen 96].

Propagation in tunnels has also been statistically analyzed. In [Lienard 98], fadings are classified in short-term (also referred to as *fast-fadings*) and long-term (*slow-fadings*), and three regions are established where fadings behave differently along a tunnel: 0-50 m, 50-500 m, and beyond 500 m from the emitter. A complete survey about radio propagation modeling in these scenarios is presented in [Hrovat 14].

Areas of special interest are the influence of the operating frequency, the antenna charac-

teristics, and the tunnel cross section geometry and its longitudinal uniformity. As an example, [Sun 10] presents a complete analysis of propagation in tunnels and mines, focusing on the effects of the operating frequency and antenna polarization. Masson [Masson 09b] studies the influence of the tunnel geometry, and [Gentile 12] considers the case of tunnels with varying cross section.

In the literature, the presence of strong fadings is highlighted, but only those that take place in the longitudinal dimension have received attention [Emslie 75, Laakmann 76, Dudley 07]. However, the signal also suffers from strong fadings in the cross-sectional dimension of the tunnel, where they have only been analyzed statistically and on a small scale. Most of the studies focus on channel capacity. In [Kyritsi 02], the authors demonstrate that the latter increases with the number of modes excited by each transmitting element. In [Valdesueiro 10], the authors perform Multiple Input Multiple Output (MIMO) channel measurements in a tunnel varying the antenna separation, concluding that the theoretical maximum capacity is slightly increased with the antenna spacing. Lienard et al.[Lienard 06, Molina-Garcia-Pardo 08c, Molina-Garcia-Pardo 08b, Molina-Garcia-Pardo 08a, Molina-Garcia-Pardo 09b, Lienard 14] have performed extensive measuring campaigns to study the channel capacity as a function of the antenna correlation, claiming that the capacity increases as the correlation decreases, and that good performances of MIMO techniques can be obtained under the condition of small correlation between paths relating each transmitting and receiving antennas. In [Masson 12], the authors highlight that channel correlation at reception decreases when increasing the antenna spacing, while [Nasr 06] denotes that the correlation strongly increases as the transmitter-receiver separation does so.

In all this cited work, the studies were performed in a zone around 0 to 500 meters from the transmitter, in the presence of multiple propagation modes. Nevertheless, to the best of our knowledge, there are no studies focused on determining the structure of the transversal fadings far away from the transmitter.

As fadings greatly affect the connectivity between mobile agents, particularly robots, special techniques must be adopted in order to ensure a secure communication. Following this motivation, in this Chapter we aim to study in detail the fadings structure along the longitudinal, transversal, and vertical dimensions of the tunnel.

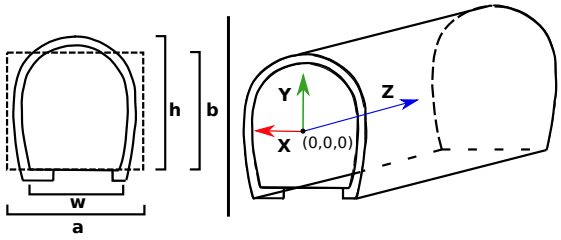

Figure 3.1: Equivalent rectangular waveguide and tunnel Coordinate System.

3.2 Theoretical Analysis

In this work, we have adopted the Modal Theory approach, using the approximate expressions for the electromagnetic field modes and the corresponding propagation constants obtained by [Laakmann 76] for rectangular hollow dielectric waveguides, which are valid for high enough frequencies (i.e. with free space wavelength much smaller than the tunnel cross section dimensions). These solutions are called hybrid modes because both the electric and the magnetic fields have non-null longitudinal component, although both are much smaller than the transversal ones.

We model the Somport tunnel (a horseshoe-shaped straight tunnel used as our testbed) as a rectangular dielectric waveguide of equivalent dimensions a x b. A Cartesian system is placed at the tunnel center (Fig. 3.1). The plane $z = 0$ contains the transmitting antenna (tx), that in our case will be a vertically oriented dipole. Further inside the tunnel ($z > 0$), vertically oriented dipoles will be the receiving antennas (rx).

The electromagnetic field excited by an antenna inside a tunnel can be described as a superposition of different propagating modes associated with the guiding characteristics of the tunnel. The power coupled to each mode depends on the antenna type and polarization, as well as on its orientation and position inside the tunnel.

We model an emitting antenna radiating P_{tx} total power at a frequency f as an ideal vertical half wave dipole with its center located at coordinates $(x_{tx}, y_{tx}, z_{tx} = 0)$. We assume a sinusoidal filament current distribution along its length:

$$I_{tx}(y) = I_0 \cos[k_0(y - y_{tx})] \tag{3.1}$$

with

$$I_0 = \sqrt{\frac{2P_{tx}}{73}} \tag{3.2}$$

and

$$k_0 = \frac{2\pi}{\lambda} \tag{3.3}$$

$$\lambda = \frac{c}{f} \tag{3.4}$$

where c is the free space velocity of electromagnetic waves and f is the operating frequency. For this antenna orientation, only the coupling to the EH^y_{mn} modes of the rectangular tunnel is relevant (where m represents the number of half-waves along the x axis and n the number of half-waves along the y axis). To estimate this coupling, we have followed a procedure similar to the one outlined in Appendix G of [Emslie 75] for the EH^x_{11} mode, which we have extended to any EH^y_{mn} mode with the technique described in Chapter 4 of [Pozar 05] for rectangular metallic waveguides. This is indeed an approximation. The tunnel acts as an oversized dielectric waveguide and thus the tangential electric field on the walls is not null, as it would be in the case of metallic waveguides. But for frequencies high enough to get free space wavelengths much smaller than the tunnel size, the tangential fields for the relevant propagating modes are small enough at the tunnel walls so that the metallic waveguide boundary conditions are satisfied to a good enough approximation, giving the same mode shapes as the corresponding modes with the same mn indexes in tunnel size metallic waveguides [Emslie 75]. There is a significant difference, though: as the free space wavelength is much smaller than the tunnel size, the wave impedance of the modes in the tunnel is quite close that in free space, $\eta_0 \approx 377\Omega$. Then, following [Pozar 05], we calculate A^+_{mn}, the amplitude of the EH^y_{mn} mode traveling in $+z$ direction as:

$$A^+_{mn} = \frac{\eta_0}{ab} \int_{y'=y_{tx}-\lambda_0/2}^{y'=y_{tx}+\lambda_0/2} e_{mn}(x_{tx}, y') I_{tx}(y') dy' \tag{3.5}$$

where e_{mn} is the modal electric field (see Eq. (3.10)). To compute the power coupled to a vertical receiving antenna located at coordinates (x, y, z), we will need the y-directed electric field at this position, that is:

$$E_y^+ = \sum_{m,n} A_{mn}^+ e_{mn}(x,y) e^{-\gamma_{mn} z} \tag{3.6}$$

where γ_{mn} is the EH_{mn}^y mode propagation constant, as derived in [Laakmann 76]. The sum should extend over all the possible modes, although in practice only a few ones are relevant. Once propagating, every mode decays exponentially with an attenuation constant α_{mn}. It is shown in [Dudley 07] that this constant is well approximated for frequencies with wavelengths much smaller than the tunnel dimensions as:

$$\alpha_{mn} \simeq \frac{1}{2}\left(\frac{c}{f}\right)^2 \left[\frac{m^2}{a^3}\frac{1}{\sqrt{\varepsilon_r - 1}} + \frac{n^2}{b^3}\frac{\varepsilon_r}{\sqrt{\varepsilon_r - 1}}\right] \tag{3.7}$$

where ε_r is the relative permittivity. Hence, the attenuation is higher for low frequencies, and higher order modes attenuate faster than lower order ones.

Each mode propagates with its own wavelength λ_{mn} (close but not equal to the free space one). From Eq. (54) in [Dudley 07], this can be written as:

$$\lambda_{mn} = \frac{\lambda}{1 - \frac{1}{2}\left(\frac{m\lambda}{2a}\right)^2 - \frac{1}{2}\left(\frac{n\lambda}{2b}\right)^2} \tag{3.8}$$

As explained for the case of pipes, when two modes with different wavelengths are present, their interaction gives rise to a periodic fading structure on the RF power inside the waveguide. The period of this fading structure D is the distance that creates a relative phase of 2π among the two considered modes (see Eq. 2.16). For the case of tunnels, from Eq. (3.8), this is:

$$D = \frac{8}{\frac{c}{f}\left|\frac{m_2^2 - m_1^2}{a^2} + \frac{n_2^2 - n_1^2}{b^2}\right|} \tag{3.9}$$

As the transmitter-receiver setup used in this work benefits the excitation and detection of the EH_{m1}^y modes (i.e. vertically polarized antennas), notice that only the width of the waveguide determines the period of the fadings.

If more than two propagating modes are present, each possible couple of wavelengths will create its own periodic fading structure. The total electromagnetic field will be the superposition of all of them.

In the tunnel cross section, for a given z, the electric field of the y-polarized hybrid modes is given by [Laakmann 76]:

$$\begin{aligned} e_{mn}(x,y) = &\left\{ \cos\left(\frac{m\pi}{2a}x+\phi_x\right) - \sin\left[\frac{i}{ka\sqrt{\varepsilon-1}}\left(\frac{m\pi}{2a}x\right)\right]\sin\left(\frac{m\pi}{2a}x+\phi_x\right)\right\} \\ &\left\{ \sin\left(\frac{n\pi}{2b}y+\phi_y\right) + \sin\left[\frac{i\varepsilon}{kb\sqrt{\varepsilon-1}}\left(\frac{n\pi}{2b}y\right)\right]\cos\left(\frac{n\pi}{2b}y+\phi_y\right)\right\} \end{aligned} \tag{3.10}$$

with

$$\phi_x = \frac{1+(-1)^m\pi}{4}; \phi_y = \frac{1+(-1)^n\pi}{4} \tag{3.11}$$

$$k = \frac{2\pi}{\lambda} \tag{3.12}$$

$$\varepsilon = \varepsilon_r - \frac{i\sigma\varepsilon_0}{2\pi f} \tag{3.13}$$

This field distribution will be used subsequently in order to both excite the modes of interest and to analyze the received signal power.

3.3 Test Scenario and Experimental Setup

3.3.1 The Somport Tunnel

The Somport tunnel was selected as the location to carry out the experiments. This is an old out-of-service railway tunnel representative of long straight tunnels common in transport or mine applications. The 7.7 km long railway tunnel connects Spain with France through the central Pyrenees. It has a horseshoe-shape cross section, approximately 5 m high and 4.65 m wide. The tunnel is straight but suffers a change in slope at approximately 4 km from the Spanish entrance (Fig. 3.2(a)). The walls are limestone with short sections covered with a thin concrete layer. The tunnel also has small emergency shelters every 25 m, which are 1 m wide, 1.5 m high, and 0.6 m in depth. It also has 17 lateral galleries, each more than 100 m long and of the same height as the tunnel (Fig. 3.2(b)).

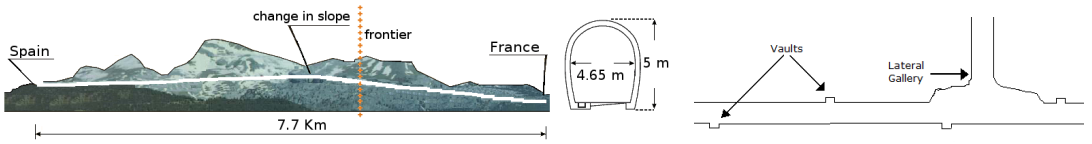

(a) The Somport tunnel

(b) Upper view: lateral shelters and galleries

Figure 3.2: Testbed

3.3.2 Measurement Setup

To study the RF signal propagation in the tunnel, a Continuous Wave Signal Generator was used as the transmitter (Agilent model E4432B), and an array of portable spectrum analyzers as receivers (RF Explorer model 3G). The transmitter antenna was placed on a non-conductive tripod, and its position inside the tunnel will depend on the experiment.

The selected frequencies are 433, 868, 1800 and 2400 MHz, for radio, cellular and WiFi practical applications. Also, as most of them are part of the Industrial, Scientific and Medical (ISM) radio bands, transceivers for these frequencies are commercially available for relatively low cost, making them suitable for many practical applications. For each frequency, all antennas used were vertically oriented dipoles with a $4dB_i$ gain for 433 MHz, $2.15dB_i$ for 868 MHz, $2dB_i$ for 1800 MHz, and $4dB_i$ for 2400 MHz. The receivers streamed the data to a computer running ROS (Robot Operating System [Quigley 09]) over Ubuntu 12.04.

At 2.4 GHz, TP-LINK tl-wn7200nd wireless adapters with Ralink chipset were additionally used, with the transmitter broadcasting frames every 5 ms at a power of 20 dBm. The receiver array was composed of twelve TP-LINK wireless adapters, placed at a height of 2 m from the soil, on the moving platform. The antennas are separated 0.125 m apart, the wavelength of the signal at the working frequency. As in [Molina-Garcia-Pardo 09a], we fixed the spacing between two successive elements to be greater than one half of the wavelength to minimize the coupling between antennas. The whole setup can be seen in Fig. 3.3.

To synchronize the received signals data with the position in the tunnel, an all terrain vehicle was used as the mobile platform. It is equipped with two 0.5 degree resolution encoders and a Scanning Laser Range Finder (Fig. 3.3). The all-terrain vehicle localizes itself in the tunnel with a localization algorithm on a previously built map [Lazaro 10], allowing to maintain the

(a) Transmitter (b) Receiver setup: receivers, odometer, laser

Figure 3.3: Measurement Setup

same position reference for all the experiments. The periodic emergency shelters every 25 m, characteristic of our testbed, play an important role in the localization and synchronization, allowing us to correct the odometric cumulative error after being detected by the laser.

3.4 Experimental Fading Analysis

In this section we present the experimental results of an extensive measurement campaign carried out at the Somport tunnel and compare them with classical studies from the literature, evaluating the validity of the rectangular dielectric waveguide approximation for this tunnel, followed by an analysis of the received signals' fadings in the longitudinal, transversal, and vertical dimension, with emphasis on creating noticeable periodic fadings.

3.4.1 Longitudinal Fadings

3.4.1.1 Near and Far Sectors

A first experiment was performed to analyze the characteristics of radio wave propagation in the Somport tunnel. As in many examples from the literature, for practical purposes, the transmitter was placed inside the tunnel and close to the wall, specifically at 100 m from the entrance, 2 m above the ground, and 1.5 m apart from the right wall. One moving-receiver's antenna was

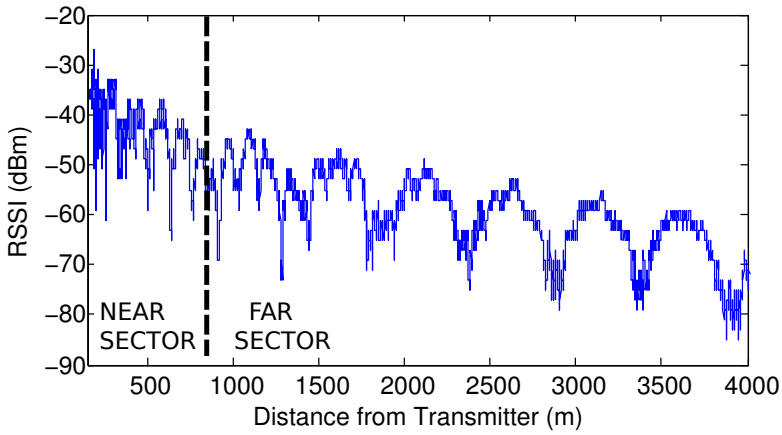

Figure 3.4: Measured Received Power at 2.4 GHz. The transmitter was kept fixed and the receiver was displaced along 4 km from the transmitter. The vertical dashed line denotes the limit between the near and the far sector.

placed at the same cross-section position, and it was displaced from the transmitter up to 4 km, maintaining the line-of-sight between them. The signal was sampled with a spatial period of 0.1 m. The result is shown in Fig. 3.4.

As can be observed, two main sectors can be identified in the tunnel according to the signal behavior. The border between the sectors is at a point around 750 m from the emitter. The *near sector* is characterized for rapid fluctuations of the signal or *fast fadings*, where the distance path loss dominate. Once the higher order modes (which have higher attenuation rate) are mitigated with the distance, the lower modes survive, giving rise to the *far sector* where the *slow fadings* dominate [Delogne 91].

3.4.1.2 Fast Fadings and Slow Fadings

To analyze the *fast fadings* and *slow fadings* in greater detail, we followed the methodology presented in [Lienard 98]. First, the distance path loss (calculated by regression) is subtracted from the raw signal power since it is not related with fadings. Then, to mitigate *fast fadings* and highlight the *slow fadings* contributions, a 100λ window size moving average is applied [Lienard 98, Masson 09a]. Fig. 3.5 shows the resulting signal and the corresponding periodogram for the far sector. The periodogram shows that the main oscillation has a spatial frequency of 2 cycles per kilometer, that is, a period of about 500 m.

To subsequently analyze the *fast fadings*, the distance path-loss and the *slow fadings* were

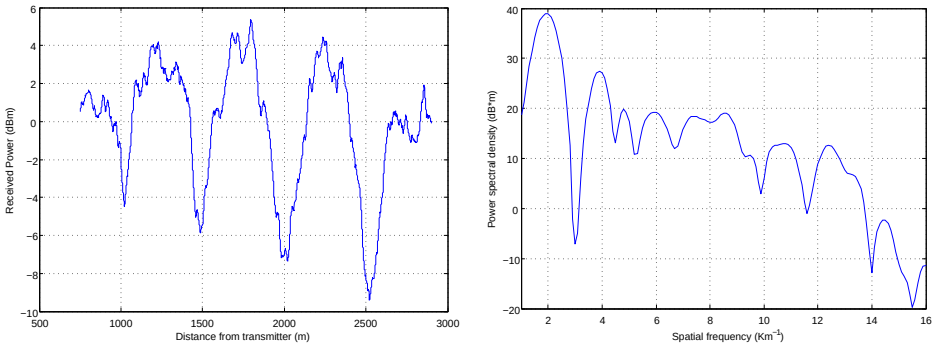

(a) Signal Power (b) Periodogram

Figure 3.5: Slow-fadings in the far sector of the tunnel

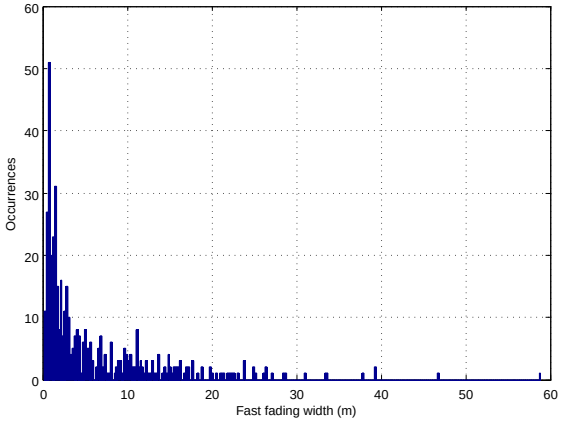

Figure 3.6: Fast-fadings width histogram

subtracted from the raw signal power. The maximum width of these fast-fadings has been measured as the distance between two alternate zero crossings, and 94% of them have a width less than 20 meters (shown in a Histogram in Fig. 3.6).

The stated qualitative behavior of the tunnel (presence of *near* and *far sectors*, as well as *fast* and *slow fadings*, periodicity, etc.) can be extrapolated to other tunnels. For example, in the results presented in [Mariage 94, Dudley 07, Sun 10], although no analyses were performed, the cited behaviors can be clearly observed. However, the value of the parameters depends on the frequency and on the tunnel characteristics.

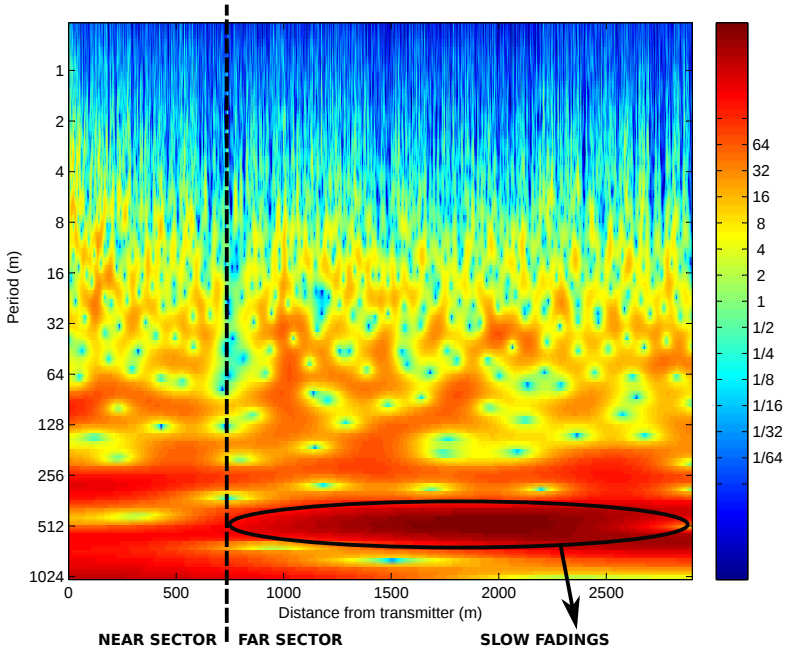

Figure 3.7: Wavelet of the signal versus the distance using the Morlet function.

3.4.1.3 The Wavelet as a Tool for Analyzing Propagation in Tunnels

The wavelet is an appropriate tool for analyzing signals that present singularities. Using wavelets, important information appears through a simultaneous analysis of the signal time and frequency properties [Mallat 99]. Despite being commonly used in the time domain, it also allows frequency information to be analyzed in the spatial domain [Grossmann 84]. A scalogram or spectrogram is the graphical representation of the normalized wavelet power of a signal $f(t)$ in a time-varying frequency domain, within a three-dimensional space: time (x), scale/frequency (y) and power (z).

The spectogram of the wavelet of the signal from Fig. 3.4 is presented in Fig. 3.7. The Morlet mother function was used over the raw signal to avoid frequency information loss. In order to associate phenomena to spatial coordinates, we have reconfigured the working space as: distance from the transmitter (x), spatial period of the fadings (y), and spectral power density (z).

From Fig. 3.7, the wavelet shows that the spectral power is distributed among all spatial frequencies, up to a point where it starts concentrating in specific bands. This point is located at around 750 m, which agrees with the limit between the near and far sector from the analysis

in the previous Sections. After this point, the power concentrates in a band with 512 m of periodicity, highlighting the presence of slow fadings and its uniform behavior in the far sector. The fact that the power is concentrated around the same spatial period for a determined distance demonstrates the uniform periodicity of these phenomena.

Hence, wavelets enable us to determine the limit between the near sector and far sector, the slow fadings period and its behavior, as well as the frequencial behavior of the fast fadings by means of analyzing the spectral power within one graph. To the best of our knowledge, wavelets have never before been used to analyze propagation in tunnel-like fading environments. For an analysis of the remaining frequencies, see [Rizzo 13c].

3.4.1.4 Repeatability of the Fadings in the Temporal and Spatial Domain

Another concern relevant to the present work, but not addressed in the literature, is the repeatability of the fadings in the temporal and spatial domain.

In the temporal domain, the goal is to verify that fadings are repeatable in the same section of the tunnel on different time periods, under the same transmission conditions. To this end, the same experiment, with the same transmitter-receiver configuration, was performed on two different occasions. The transmitter was placed at 1.5 m from the right wall and 2 m high. The receiver was kept at the same cross-section position and was displaced from the transmitter up to 4 km in the longitudinal direction. Measurements of the received power in both experiments are depicted in Fig. 3.8(a), where it can be seen that results from the two trials match each other very well.

In the spatial domain, we aimed to study propagation behavior in two different sections of the tunnel. In each section, the transmitter and receivers were again placed 1.5 m from the right wall and 2 m high. The receiver was than displaced up to 3 km from the transmitter position. The measured received power as a function of the relative position to the transmitter in both sections of the tunnel is shown in Fig. 3.8(b). It can be see that the measurements again match very well, despite the fact that the two sections of the tunnel were not identical. In particular, the lateral galleries in the two sections are not equally spaced and vary in shape and depth.

The notable concordances in terms of received power, signal envelope, mean values and fadings' period and location in all of the experiments leads us to conclude that propagation phenomena are repeatable in both domains. We also verify that the presence of emergency

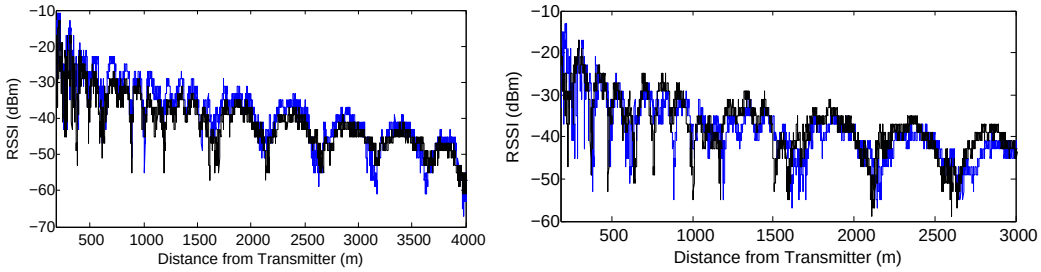

(a) Temporal Domain (b) Spatial Domain

Figure 3.8: Repeatability of the fadings in the Time and Space domain

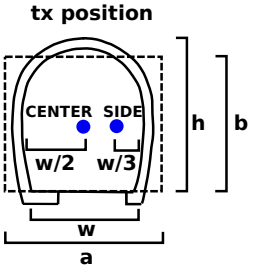

Figure 3.9: Equivalent rectangular waveguide and antenna positions.

vaults and lateral galleries does not have a significance affect on propagation.

3.4.1.5 Equivalent Rectangular Waveguide Determination

As previously mentioned in Section 3.2, in this work, we adopt the Modal Theory Approach, modeling the Somport tunnel as a rectangular dielectric waveguide. This approximation has been widely used in the literature for tunnels with different cross-section shapes, simulating the equivalent rectangular or circular waveguide (depending on the actual tunnel geometry) that best reproduces the experimental measurements. The dimensions of the equivalent waveguide are obtained by minimizing the difference between the theoretical and experimental attenuation rate of the first propagating mode and/or the fadings period [Dudley 07, Molina-Garcia-Pardo 08d].

From the experimental results of Section 3.4.1.2, the slow fadings period for the cited case is about 512 m with a mean attenuation rate close to 4.5 dB/km. From Eq. (3.9) and Eq. (3.7), the equivalent rectangular waveguide that reproduces the measured values is $a = 4.9$ m and $b = 4.3$ m (width and height respectively, see Fig. 3.9), close to the physical dimensions of the actual

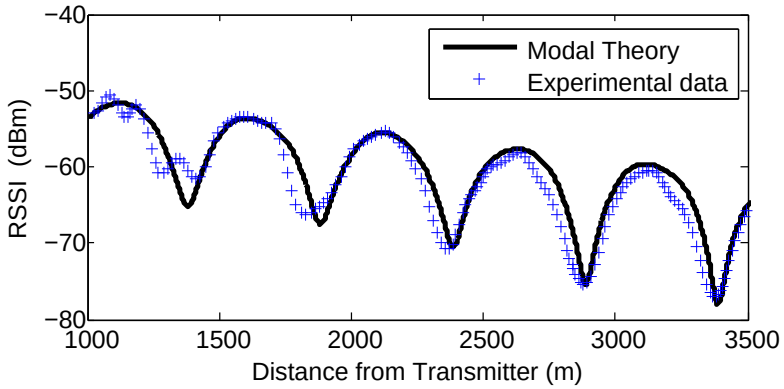

Figure 3.10: Experimental Results vs Modal Theory simulations at 2.4 GHz with Tx and Rx antennas in the *side position*.

tunnel. The wall conductivity and relative permittivity used were 0.01 S/m and 5.5 respectively, both typical values for limestone. The power distribution among the three first modes that best fits to the data is 15% in EH^y_{11}, 84% in EH^y_{21} and 1% in EH^y_{31}, showing dominance of the first two modes in the far sector for this specific transmitter-receiver setup (*side position* in Fig. 3.9). In Fig. 3.10 the experimental data is compared to the Modal Theory simulations, where the two datasets match each other quite well. The signal has been filtered with a 100λ moving average window to mitigate the fast-fadings and highlight the slow fadings [Lienard 98, Masson 09a].

3.4.1.6 Modal Coupling: Influence of Transmitter Position over the Fadings Period

As stated before, the interaction between each pair of modes is responsible for one periodic fading structure. If more than two propagating modes are present, the total electromagnetic field will be the superposition of all of them, producing a structure with irregular fadings period. Fig. 3.11 shows the effects of choosing an arbitrary transmitter position. In this case, several modes with similar attenuation rates and non-negligible power contribution are excited, producing a complex fading structure (fadings with different periods combined).

As our goal is to produce predictable periodic fadings, we aim to promote the excitation and interaction only between two propagating modes. We are interested in the first three propagating modes, as their attenuation constant is low enough to ensure coverage along several kilometers inside the tunnel.

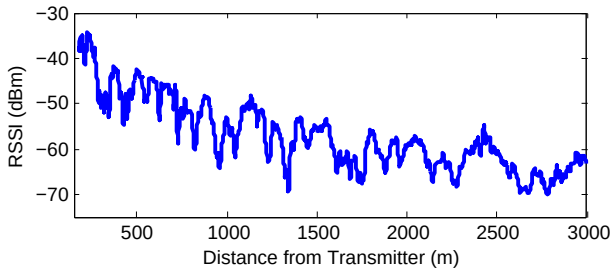

Figure 3.11: Example of inadequate transmitter position: complex fading structure caused by the interaction of more than 2 propagating modes.

Table 3.1: Location of the maxima and minima in the modal interaction

	modes 1 & 2	**modes 1 & 3**
Max	d $\approx$ 0.3*a from wall or $x = x_0 \pm 0.2a$	$d = \frac{a}{2}$ or $x = x_0$
Min	$d = \frac{a}{2}$ or $x = x_0$	$d = \frac{a}{3}$ and $\frac{2a}{3}$ or $x = x_0 \pm \frac{a}{6}$

Tuning the power coupled to a given mode is accomplished by choosing the antenna position in the tunnel cross section. The coupling will be maximized (minimized) close to a point where a given mode has an amplitude maximum (minimum). From Eq. (3.10), Fig. 5.1(b) shows the field distribution of the first three EH^y_{m1} modes (EH^y_{11}, EH^y_{21} and EH^y_{31}, also called *mode 1, mode 2* and *mode 3* throughout this work) along a rectangular waveguide cross section for a fixed (y,z). Moreover, Fig. 3.12(b) represents the absolute value of the field of these modes, highlighting the coordinates where the interaction between these takes maximum and minimum value. These are summarized in Table 3.1, where d is referenced from the tunnel left wall, while x is referenced to the tunnel center, in accordance with Fig. 3.1.

It can be seen that in the *center position* of the tunnel (Fig. 3.1), the interaction between the first and third mode takes maximum value, while minimizing the influence of the second mode. In a similar manner, positions around one third from the tunnel walls (*side position*) maximizes the interaction between the first and second mode, while minimizing the influence of the third mode.

To analyze the received signal fadings, both the transmitter and receiver were placed in the *center* or *side* position in the cross-section dimension. The receiver was then displaced up to 3

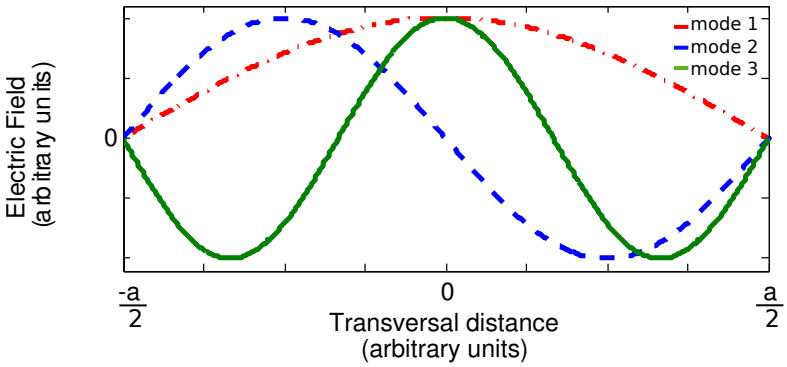

(a) Electric field distribution for the first three propagating modes

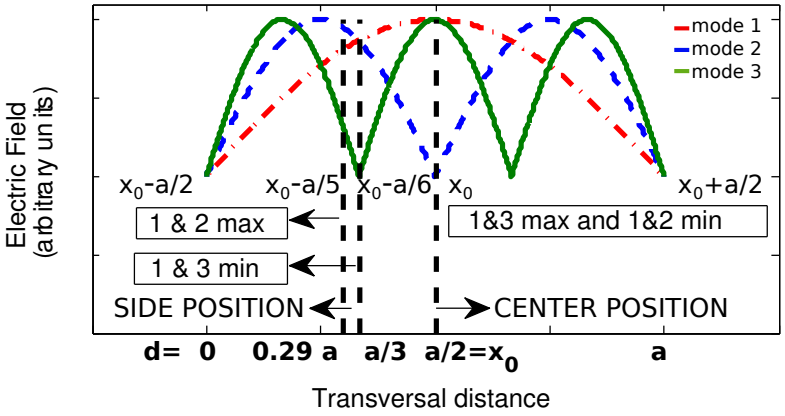

(b) Interaction between the first three modes. The vertical dashed lines represent the places where the sum of the absolute values takes maximum and minimum value

Figure 3.12: Mode 1, mode 2 and mode 3 in a rectangular waveguide

km in the longitudinal direction. The experiments were performed at 433, 868, 1800 and 2400 MHz.

The results are shown in Fig. 3.13, ordered by frequency. The red signals correspond to transmitter and receiver in the *center position*, while the blue signals to transmitter and receiver in the *side position*. Table 3.2 collects the experimental measurements compared to Modal Theory calculations. For all of the studied frequencies, the same rectangular cross section determined in Section 3.4.1.5 was used.

We see that the Modal Theory analysis models the measured received power and period of the longitudinal fadings well. On the other hand, the attenuation rate of the present modes is more difficult to estimate, as it varies for each mode. When the difference between the rates

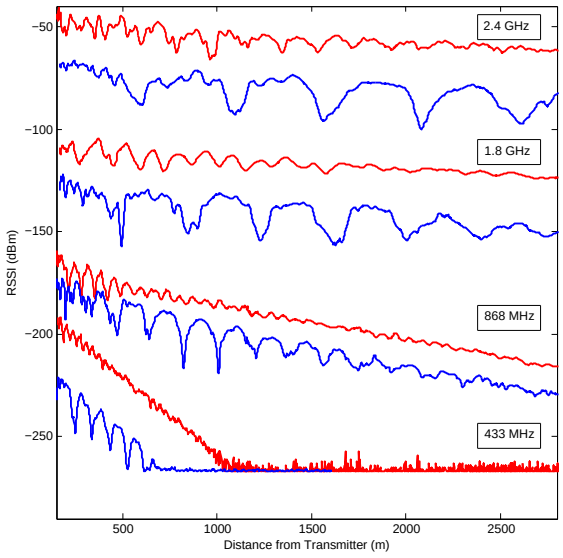

Figure 3.13: Measured received power at: 2400, 1800, 868 and 433 MHz, with both Tx and Rx antennas in *center position* (red), and in *side position* (blue) . The signals have been offset for clarity.

is sufficiently high, as in the case of the first and third modes, the attenuation rate of the first mode can be determined from data taken far enough from the transmitter such that most of the power is concentrated in that mode. However, this is not possible in the case of the first and second modes, as both have similar attenuation rates. At all frequencies, the attenuation rate of the first mode matches with the predictions, except for the case of 2.4 GHz, which is higher in the experimental results than in the predictions. This may be caused by the non-uniformity of the tunnel walls, which becomes significant as its roughness gets comparable to the wavelength of the signal.

From the fadings period, it can be seen that placing the transmitter in the *center position*, excites modes 1 and 3 while minimizing the influence of the second mode. On the other hand, placing the transmitter in the *side position* excites modes 1 and 2 while minimizing the effects of the third mode. It can also be noticed that the lower the operating frequency, the shorter the near sector, the shorter the fadings period, and the higher the attenuation rate. Qualitatively, the obtained fadings are well defined and uniformly periodic. Quantitatively, the modal theory predicted periods and attenuation rate matches quite well with the experimental results.

Table 3.2: Comparison between Theoretical and Experimental Results

Frequency	Tx pos.	Modes	Theoretical / Experimental period (m)	Mode 1 Theoretical / Experimental slope (dB/km)
433 MHz	center	EH_{11}^{y} and EH_{31}^{y}	35 / 34.5	76.2 / 76.2
433 MHz	side	EH_{11}^{y} and EH_{21}^{y}	92 / 91.6	undet.
868 MHz	center	EH_{11}^{y} and EH_{31}^{y}	70 / 71.6	18.9 / 18.6
868 MHz	side	EH_{11}^{y} and EH_{21}^{y}	185 / 184.2	undet.
1.8 GHz	center	EH_{11}^{y} and EH_{31}^{y}	144 / 147.3	4.4 / 4.25
1.8 GHz	side	EH_{11}^{y} and EH_{21}^{y}	384 / 376.2	undet.
2.4 GHz	center	EH_{11}^{y} and EH_{31}^{y}	192 / 187	2.4 /4.5
2.4 GHz	side	EH_{11}^{y} and EH_{21}^{y}	512 / 512	undet.

3.4.2 Transversal Fadings

Once the transmitter positions suitable to appropriately excite the modes of interests were determined, we proceed to perform the transversal fading analysis. That is, we analyze the received signal power along the tunnel cross section with the transmitter fixed in the above studied positions (center and side), separately.

3.4.2.1 Transmitter on Side

With the transmitter placed on the *side position* at an operating frequency of 2.4 GHz, the twelve antenna array was used as the receiver. Instead of moving one antenna along the cross section, the methodology followed was to drive the antenna array in straight lines along a 3 km segment several times (maintaining the same cross-section position each time), until the whole cross section was covered, except for a 0.8 m of safety distance from the walls. The entire set of data is synchronized as explained in Section 3.3.2.

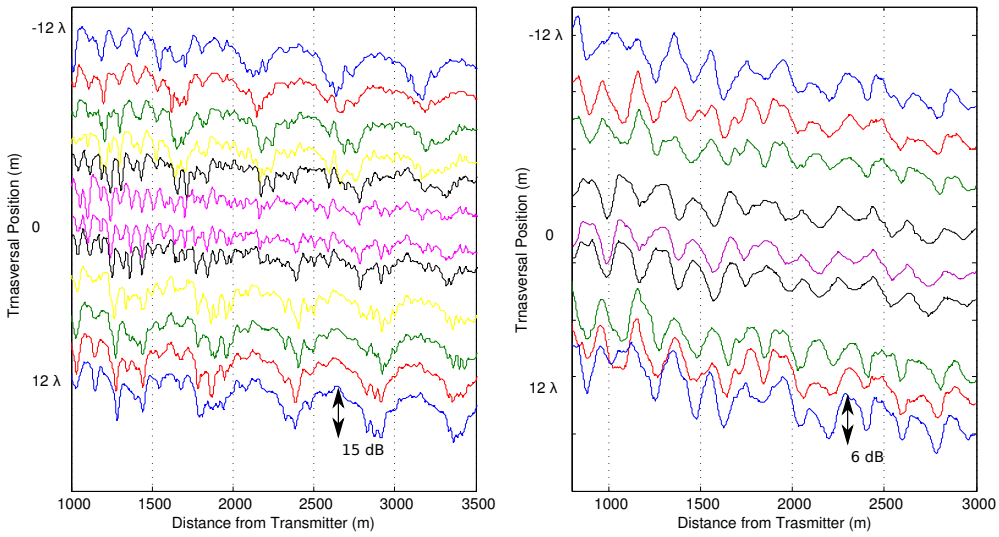

(a) Tx on side - modes 1 and 2

(b) Tx on center - modes 1 and 3

Figure 3.14: Measured Received Power along the tunnel for several antennas in different cross-section positions

Fig. 3.14(a) shows the measured received power as a function of both longitudinal and transversal position, for several antennas located at different cross-section locations. As can be seen, there are longitudinal slow fadings with a spatial period of about 512 m, as studied previously. The fadings are deeper close to the walls, and they seem to mitigate in the center of the tunnel. Also, there appears to be a sudden change in the relative phase between the fadings around the center of the tunnel.

The numerical results for the most relevant antennas are gathered in Table 3.3, where the position is referenced from the tunnel center. The table is divided into two sectors, representing the two halves of the tunnel. Only the data from the 1200 to 3000 m was used, to highlight the contribution of the slow fadings. The phase difference between the fadings is analyzed compared to the leftmost position (antenna closest to the left wall).

It can be seen that the relative phase between the set of signals belonging to the same half of the tunnel is quite similar, but there is a phase difference between signals in different halves of about 180 degrees (i.e. a maximum in one fading matches a minimum in other fading). Also, although the received power in the tunnel center is slightly higher compared to the extremes, the standard deviation is lower. This can be graphically appreciated in Fig. 3.15(a).

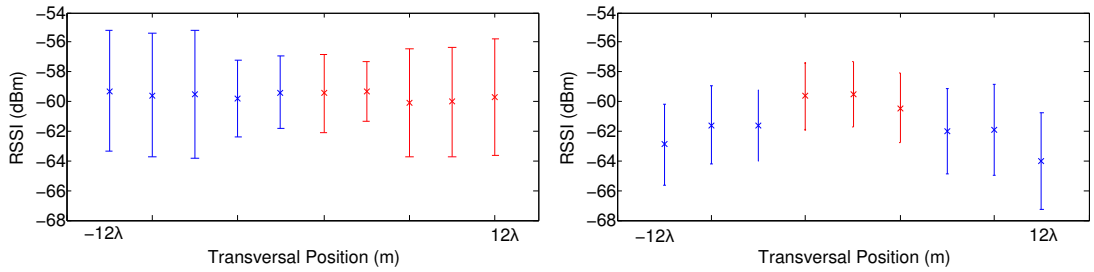

(a) Tx on side - modes 1 and 2

(b) Tx on center - modes 1 and 3

Figure 3.15: Measured Received Power mean value, and standard deviation, along the cross-section of the tunnel. The red values illustrate a phase difference of 180 degrees with respect to the blue values.

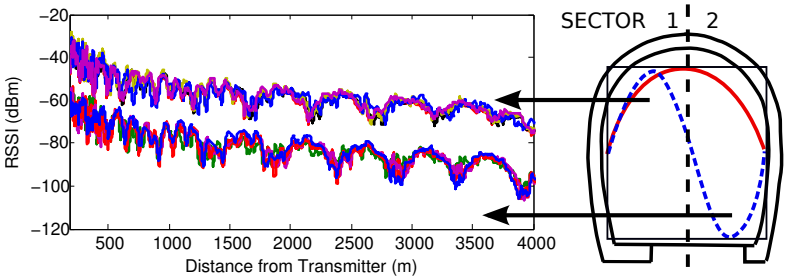

(a) Tx on side - modes 1 and 2

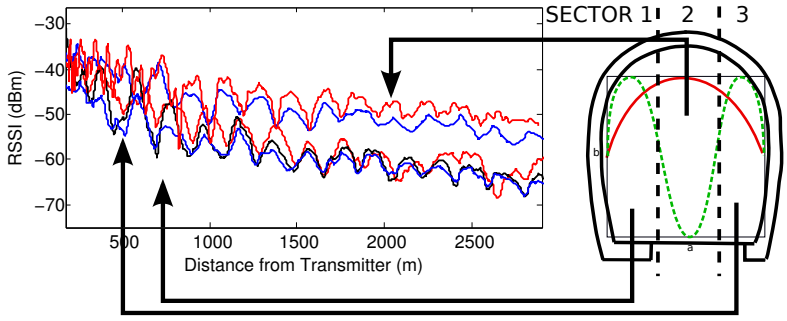

(b) Tx on center - modes 1 and 3

Figure 3.16: Measured Received Power, grouped by sectors according to the interacting modes geometry. The signals have been offset for clarity.

Table 3.3: Quantitative analysis of the received fadings with Transmitter on Side

	Position(m)	**Mean(dB)**	**Std(dB)**	**Phase Difference (deg)**	**Avg. Fading Depth(dB)**
sector 1	-12λ	-59.29	4.09	0	13.4
	-11λ	-59.59	4.18	0	13.1
	-10λ	-59.53	4.30	11.52	12.5
	$-\lambda$	-59.76	2.59	-8.31	7.1
	0	-59.39	2.45	-9.02	6.8
sector 2	λ	-59.45	2.64	172.8	7.2
	2λ	-59.33	2.05	173.52	6.4
	10λ	-60.09	3.64	157.68	13.4
	11λ	-60.02	3.67	164.88	12.9
	12λ	-59.69	3.90	163.44	14.1

Moreover, from Fig. 5.1(b), we can observe that since *mode 1* is even while *mode 2* is odd in the transverse coordinate, whenever constructive interference appears to the left of the tunnel, destructive interference appears to the right, and vice versa. The received signals were grouped by the structure of the second mode, dividing the tunnel in *sector 1* and *sector 2* (Fig. 3.25(a)). It can clearly be seen that the fadings period and relative phase are maintained among all the antennas within each sector.

For clarity, Fig. 3.17 takes the data collected from one antenna from each sector and the antenna placed in the center of the tunnel and compares them with the modal theory predictions (adding a diffuse term as in [Emslie 75]). The 180 degree phase difference between the two halves of the tunnel can again be seen. In the center of the tunnel, the null component in the second mode makes the third mode observable.

An upper view of the tunnel, collecting all the data in both the longitudinal and transversal directions, is presented in a received-power map in Fig. 3.18(a), where the signal power is represented by a color according to its value (from blue to red, with blue being a higher received power). The signal was sampled at 0.125 m in the transverse dimension and 0.1 m in the longitudinal dimension.

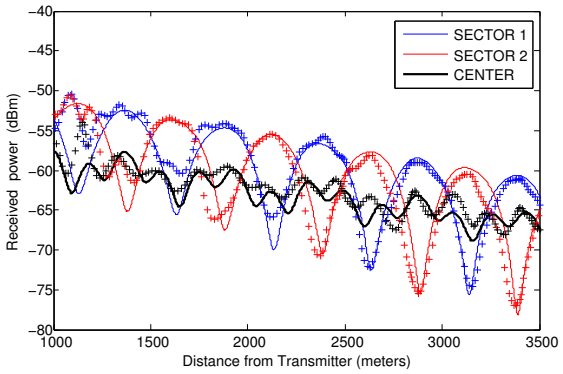

Figure 3.17: Measured received power for three Rx antennas: (*sector 1*, center and *sector 2*), with Tx in *side position*. The solid lines represent the modal theory calculations, and the dotted lines the experimental results.

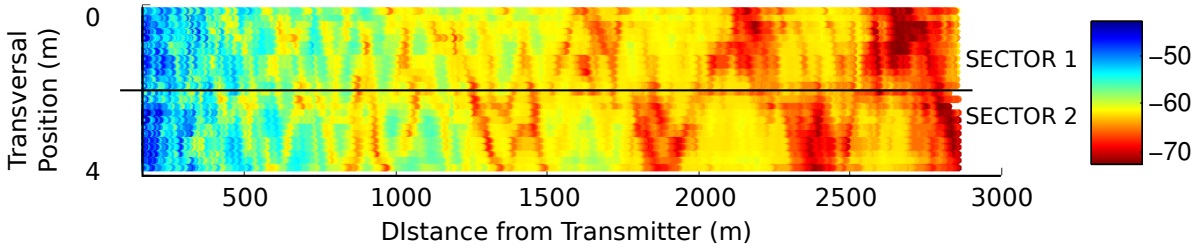

(a) Tx on side - modes 1 and 2

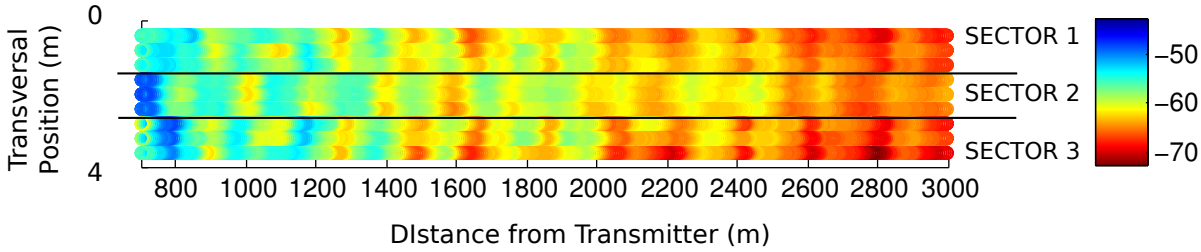

(b) Tx on center - modes 1 and 3

Figure 3.18: Tunnel Upper View. Received-power map.

Table 3.4: Quantitative analysis of the received fadings with Transmitter on Center

	Position(m)	Mean(dB)	Std(dB)	Phase Difference (deg)	Avg. Fading Depth(dB)
sector 1	-12λ	-61.78	2.73	0	5.25
	-11λ	-62.14	2.63	6.1	4.75
	-10λ	-61.95	2.41	3.5	4.62
sector 2	$-\lambda$	-60.09	2.22	172.9	3.87
	0	-60.04	2.19	171	4.12
	λ	-59.99	2.32	181.02	4.19
sector 3	10λ	-62.17	2.85	4.2	5.5
	11λ	-62.12	3.06	9.07	5.3
	12λ	-62.28	3.27	6.05	6.22

3.4.2.2 Transmitter in the Center of the Tunnel

Following the same procedure, the transmitter was located in the *center position* to excite the first and third modes, and the received signal power was recorded over the tunnel cross section. The measured received power for several antennas is shown in Fig. 3.14(b). In this occasion, longitudinal fadings with a period of 190 m take place, matching the results of Section 3.4.1.6. Also, there appears to be two sudden changes in the relative phase between the fadings.

This time, the structure of the third mode suggests dividing the tunnel into three equally sized sectors: each one third of the tunnel width. Fig. 3.25(b) collects antennas from each sector together with the spatial structure of the interacting modes, and in Table 3.4 the numerical results for the most relevant antennas is gathered.

Again, the fadings period is maintained within each sector, matching with the modal theory predictions (Table 3.2). Moreover, agreeing with the structure of the third mode, the extreme sectors (*sector 1 and sector 3*) are in phase and they suffer a relative phase difference of about 180 degrees with respect to the central sector (*sector 2*). Although the received power in the tunnel center is slightly higher compared to the extremes, the standard deviation is lower. This can be graphically seen in Fig. 3.15(b).

The received-power map for this antenna setup is shown in Fig. 3.18(a). A closer view is presented in Fig. 3.19, where can clearly be seen that the extreme sectors are in phase and both

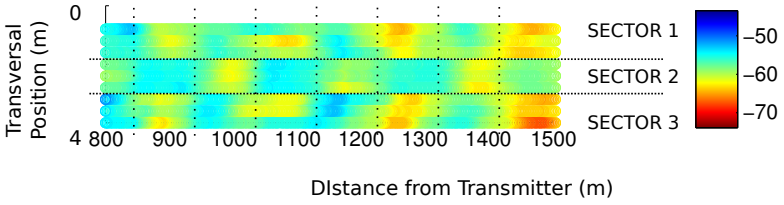

Figure 3.19: Tunnel Upper View. Received-power map with tx on center (closer view of Fig. 3.18(b)).

have a 180 degree phase difference with respect to the center sector. This information will be used in Chapter 4 and Chapter 5 for navigation and localization purposes, respectively.

3.4.3 Vertical Fadings

Consider the case of a flying robot (e.g. a quadrotor) that can modify its height while inspecting a tunnel. It is also fundamental to determine the variations of the received signal power as a function of the vertical position.

According to Eq. (3.10), for modes EH^{y}_{m1} the fadings relative phase remains the same in the vertical dimension regardless the height, but there is a significant variation in the received signal power. To corroborate this, an experiment was performed registering the received power along a straight path, with receivers at the same transversal position but at different heights ($x_{rx} = 1m$, $y_{rx1} = 1.5m$, $y_{rx2} = 2m$, $z_{rx} = 0 - 3000m$). Results are shown in Fig. 3.20, where as expected, the fadings' shape and relative phase are the same, but the received signal power differs in a mean of 3 dB.

Moreover, to analyze the received power variation along the whole vertical dimension, an experiment was performed moving the receiver from the soil to the ceiling in a fixed (x,z) position ($x_{rx} = 1m, y_{rx} = 0 - 4.5m, z_{rx} = 1500m$). The experimental measurements are depicted in Fig. 3.21, together with the first mode structure predicted from the Modal Theory simulations (Fig. 5.1(b)). A good agreement is found overall, with a series of sudden fadings appearing close to the tunnel ceiling, that host a metallic structure for the tunnel lightning.

However, it can be seen that the difference between the measured received power by an antenna located at the center of the tunnel and one located closer to the ceiling or floor can reach up to 25 to 30 dB. This difference can seriously compromise the connectivity with a base station.

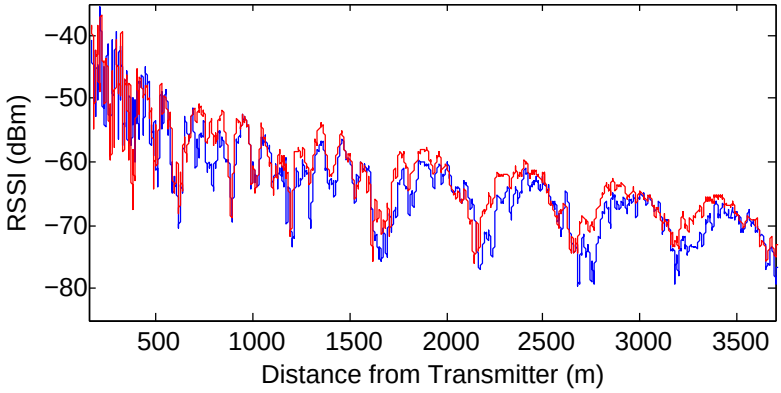

Figure 3.20: Longitudinal fadings at different heights. Measured received power at $x_{rx} = 1m$, $y_{rx1} = 1.5m$ (blue) and $y_{rx2} = 2m$ (red), along $z_{rx} = 0$-$3500m$ with Tx in *side position*

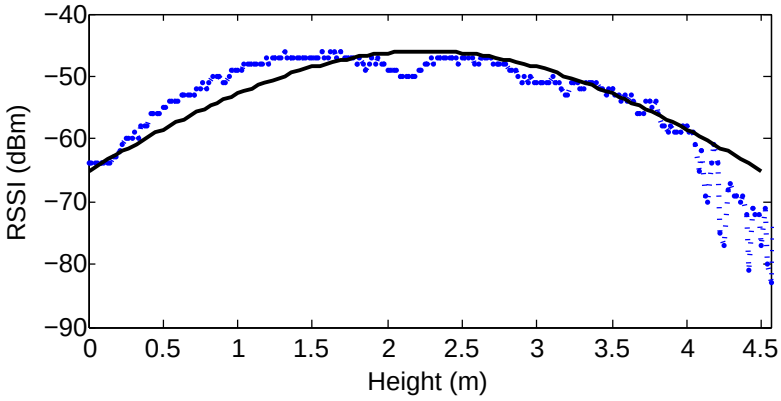

Figure 3.21: Measured received power as a function of the height ($x_{rx} = 1m$, $y_{rx} = 0$-$4.5m$, $z_{rx} = 1500m$), with Tx in *side position*. The dashed line denotes the Modal Theory simulation.

3.5 Rectangular Waveguide Approximation Validation using the Finite Element Method

The drawback of the Rectangular Waveguide Approximation method lies in that a previous measuring campaign is required in order to obtain the equivalent waveguide dimensions, which is time consuming and not always possible.

Since the very beginning of the study of propagation in tunnels and up to the present, numerical methods such as the FEM have been categorized as extremely time consuming and memory demanding in this kind of scenarios [Sadiku 89, Hrovat 14]. Nevertheless, for tun-

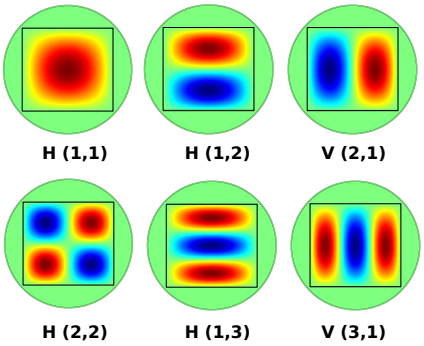

Figure 3.22: Electric field distribution for several modes in a rectangular waveguide, equivalent of the Somport tunnel. The letter corresponds to the Vertical or Horizontal component of the field, and the numbers refer to the respective index in the EH_{mn} modes. Red-yellow shades depict positive values, while the blue shades, negative values. Green represents zero field.

nels with uniform cross section, the FEM calculation of the modal propagation constants and field distribution inside the tunnel is a 2D problem. The effects of surface roughness and wall misalignment are disregarded. In this section, we first validate the rectangular waveguide approximation with a commercial FEM software (COMSOL Multiphysics [COMSOL]) and then compare both solutions for two cases: the previous measuring campaign in the Somport tunnel (with a geometry similar to a rectangle), and literature data for the Roux arched tunnel in France [Molina-Garcia-Pardo 08d] (with a geometry similar to a circle).

To do so, we have split the problem in two physical domains: the air filled tunnel and a homogeneous wall with relative permittivity ε_r and conductivity σ. The model geometry is parametrically defined as a function of frequency. The wall domain extent is fixed as a circle centered at the tunnel with radius 2λ longer than the farther tunnel surface point. A perfectly matched layer (PML) with the wall properties and thickness λ is added as a third domain. A triangular mesh is parametrically built, with element sizes ranging from $\lambda/5$ to $\lambda/10$ in the air and wall domains and from $\lambda/10$ to $\lambda/25$ in the PML. λ is the corresponding wavelength in each domain.

We have solved for the twelve first propagating modes in a rectangular tunnel for the Somport previously estimated (4.9x4.3 m). The field distribution for the first six propagation modes are shown in Fig 3.22. The problem size and execution time -quite reasonable- on a desktop PC (Intel i7-3770K @3.5 GHz processor, 16 GB RAM) for the two extreme frequencies studied are summarized in Table 3.5.

Table 3.5: Computation Characteristics for the FEM

Freq.	Mesh size	Deg. of freedom	Exec. time
300 MHz	17312	121841	17s
2.4 GHz	473716	3319949	610s

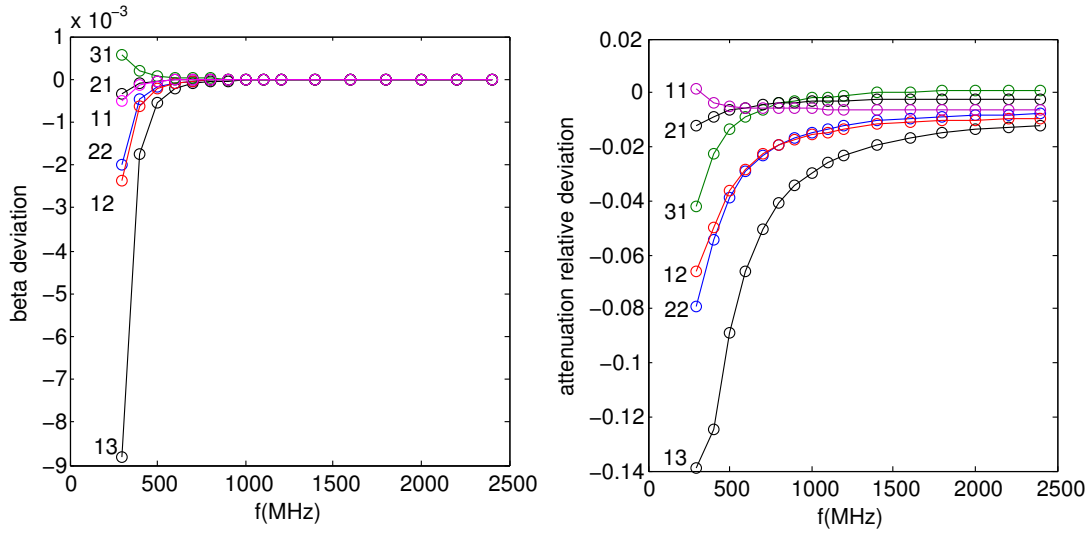

(a) Phase constant

(b) Attenuation constant

Figure 3.23: Difference between the Rectangular Approximation and the FEM solution, for the first propagating modes. The numbers refer to the respective index in the EH_{mn} modes.

For frequencies over 500 MHz, the FEM and Approximate solutions for the phase constant are identical to one part in 10^4. This is shown in Fig. 3.23(a) for the first three horizontal and vertical modes. Both solutions converge as the frequency increases. The attenuation constants are different to a few percent though. The discrepancy in the propagation constant is higher for higher order modes and for lower frequencies (Fig. 3.23(b)). Additionally, the Approximate solution predicts modes purely vertically or horizontally polarized, while the FEM solution evidences cross polarization more pronounced for higher order modes and lower frequencies. Further refinements of the mesh do not cause the FEM solution to approach the approximate one. Solving this FEM problem is easier at low frequencies, while the validity of the approximations in [Laakmann 76] improves for high frequencies. That means that in fact the FEM solution is closer to the real problem solution.

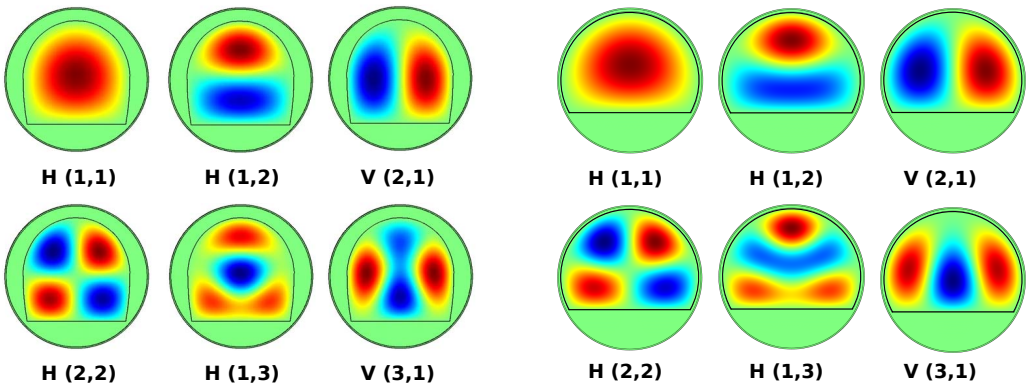

(a) Somport tunnel (b) Roux tunnel

Figure 3.24: Electric field distribution for several modes in the tunnels. The letter corresponds to the Vertical or Horizontal component of the field, and the numbers refer to the respective index in the EH_{mn} modes. Red-yellow shades: positive values. Blue shades: negative values. Green: zero field.

We have applied the same procedure to solve the modal problem in the Somport case, using the real profile of the tunnel cross-section obtained with a 180 degree laser range sensor placed on the floor, and to the Roux tunnel from the published geometry [Molina-Garcia-Pardo 08d]. The field distribution for some of these modes are shown in Fig. 3.24. The comparison of the fadings period produced by the interaction between the first three modes (by pairs), obtained experimentally, by the Rectangular Approximation and by the FEM is shown in Fig. 3.25.

The discrepancy in the propagation constant is higher for higher order modes and for lower frequencies. As for the attenuation, both methods treat the problem as 2D, underestimating the losses caused by non-ideal walls. As a consequence of this, as the studies in the literature estimate the dimensions of the equivalent rectangle using experimental data of the attenuation rate, this causes a more notable error with respect to the propagation constants, and consequently, the fadings period. Additionally, the Approximate solution predicts modes purely vertically or horizontally polarized while the FEM solution shows a cross polarization behavior, more pronounced also for higher order modes and lower frequencies.

The FEM proved to be a powerful tool for predicting propagation in tunnels, solving the problem in 2D with a computer with common processing power nowadays in quite short time. Compared to the experimental data, the FEM produced more accurate results than the Rectangular Approximation, the latter yielding better results as the frequency increases.

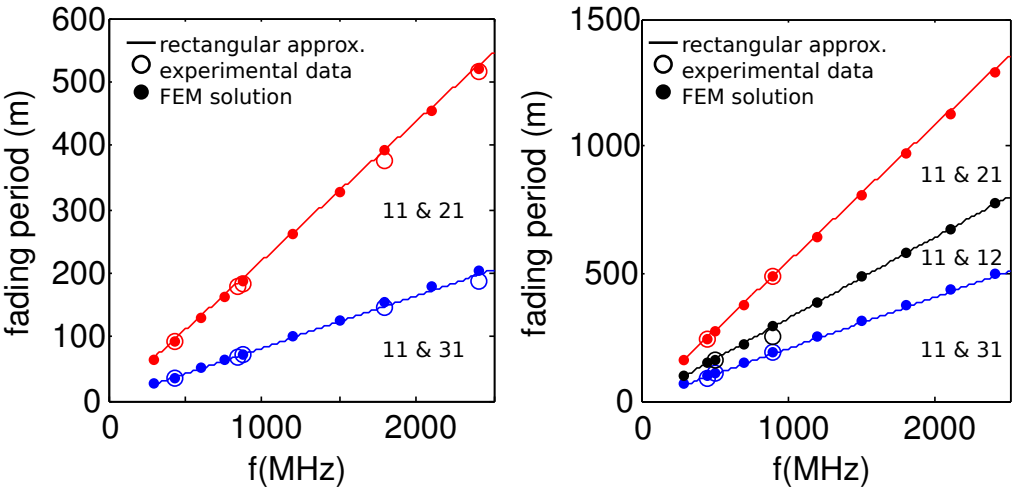

(a) Somport tunnel (b) Roux Tunnel

Figure 3.25: Comparison for the fadings period between: the Rectangular Approximation, the FEM solutions, and the experimental data. The numbers correspond to the respective index in the EH_{mn} modes. The two modes responsible for the periodic fading structure in each case are denoted.

The FEM solution requires only the tunnel cross section (easily obtained, for example, with a laser sensor at the entrance of the tunnel), an thus will be able to predict the fadings period, avoiding the time consuming measuring campaign required by the Rectangular Approximation Method.

3.6 Summary

A deep analysis of RF propagation in the Somport tunnel has been performed based on results from an extensive measuring campaign. The stated qualitative behavior of the tunnel has been determined, comparing it with other cases from the literature and making emphasis on the fadings phenomena. In this context, we have introduced the use of the Wavelet as a powerful tool for analyzing propagation in these environments, enabling us to determine the limit between the near sector and far sector, the slow fadings period and its behavior, as well as the frequential behavior of the fast fadings by means of analyzing the spectral power within one graph.

A study about the repeatability of the fadings has also been performed, an issue not addressed in the literature and relevant for the present work. The notable concordances in terms of received power, signal envelope, mean values and fadings' period and location in all of the experiments leads us to conclude that propagation phenomena are repeatable in both temporal and spatial domain, also dismissing any significant effect of the emergency vaults and lateral galleries in our specific testbed.

In the emitting site, the modal excitation was studied as a function of the modes transversal power distribution, allowing us to determine the transmitter positions to produce noticeable and well defined periodic fadings. In the transversal dimension, the received fadings large-scale structure was directly determined by the present modes power distribution, an issue not addressed in the literature. This could help, as will be discussed throughout this work, to improve spatial diversity schemes, as well as can be exploited to improve the localization and navigation under connectivity constraints.

From the theoretical point of view the Modal Theory Approach was adopted, modeling the Somport tunnel as a rectangular dielectric waveguide. Through experimental measurements it was possible to obtain the equivalent waveguide that best reproduced the actual tunnel behavior. The concordance between the predictions and the experimental results allowed to validate its usefulness in a wide range of frequencies. Nevertheless, the drawback of this method is the requirement of a previous measurement campaign.

Finally, the rectangular waveguide approximation has also been validated with a commercial FEM software. Two cases of study were considered: our own measurement campaign from a horseshoe-shaped tunnel (with a geometry close to a rectangle) and literature data for the

Roux arched tunnel in France [Molina-Garcia-Pardo 08d] (with a geometry close to a circle). Although the FEM has been categorized as extremely time consuming and memory demanding in this kind of scenarios, it proved to be a powerful tool for predicting propagation in tunnels, solving the problem in 2D with a computer with common processing power nowadays in quite short time. Compared to the experimental data, the FEM produced more accurate results than the Rectangular Approximation, the latter yielding better results as the frequency increases. The FEM solution requires only the tunnel cross section (easily obtained, for example, with a laser sensor at the entrance of the tunnel), an thus will be able to predict the fadings period, avoiding the time consuming measuring campaign required by the Rectangular Approximation Method.

3.7 Final Considerations: Comparison of Propagation in Different Tunnel-scenarios

Roughly speaking and disregarding the effects of the transmitter-receiver configuration, propagation in tunnel-like environments depends mainly on the tunnel geometry and materials. We therefore have analyzed the two most common cases in real scenarios: a cylindrical metallic pipe, and a rectangular dielectric tunnel.

In metallic waveguides, there is a well specified cutoff frequency for each propagating mode. To motivate the appearance of periodic fadings, the frequency can be chosen to allow propagation of the desired number of modes (hence, there will be no *near sector*). As each pair of modes is responsible for a periodic fading structure, the fewer the number of modes, the simpler the fading structure. Also, the attenuation per unit length involving these materials is low enough to allow propagation in the order of kilometers in pipes ranging from 3 to 6 m in diameter (common cases of study in the literature and real scenarios: dam pipes, highway and railroad tunnels, nuclear storage facilities).

The case of dielectric tunnels differ. In order to behave as a waveguide and to achieve a wireless communications coverage area in the order of kilometers, the wavelength of the operating frequency has to be much smaller than the tunnel cross-section. This causes multiple modes to propagate, producing a near sector where the signal is characterized with rapid fluctuations. To observe the well defined periodic fadings, the higher order modes must attenuate up to a point where only the lower two or three modes survive. In tunnels with cross-section dimensions ranging from 3 to 6 m, this usually happens during the first kilometer from the transmitter. Also, as the wavelength of the signal has to be much smaller than the tunnel cross section (in the order of hundreds of MHz or some GHz for this scale tunnels), the period of the fadings are much larger compared to metallic waveguides of the same size (as in the latter, the frequency can be chosen to be much lower to cover the same area).

In both cases, the interaction between the first and third modes caused shorter period fadings compared to the interaction between the first and second mode. Therefore, the modes' geometry has been used to appropriately excite and detect the modes of interest, with the final goal of obtaining well defined periodic fadings with the shortest period possible. Also, the evaluation

of the interacting modes geometry allowed us to analyze the spatial diversity structure of the fadings, dividing the cross-section in zones where the fadings present a relative phase difference.

Chapter 4

Navigation

Deploying a multi-robot team in confined environments poses multiple challenges that involve task and motion planning, localization and mapping, safe navigation, coordination of robots and also communications among all of them. In recent years, increasing attention has been paid to these challenges by the robotics community, but many problems remain unresolved. Based on the previous analysis of propagation in tunnels, in this Chapter we address a technique to deploy a team of robots in tunnel-like environments, with the goal of exploring the maximum possible distance while maintaining connectivity of the network formed by the robots and a base station at all moment. To this end, the robots travel in a straight line and use each other as relays to go across the fadings. The system, involving all the above-mentioned robotics tasks, is implemented and evaluated by means of simulations and experiments in a real scenario: the Somport tunnel. Finally, we propose a 2D navigation approach, where a single robot exploits the transversal structure of the fadings to improve the communication quality with the base station.

4.1 Introduction

In recent years, communication issues in multi-robot applications have attracted increasing interest in the robotics community. Dealing with these issues has become a real necessity as real applications are developed. Initially, simple theoretical propagation models considering the distance between the robot and the source were used. However, in the real world such simple models do not work well as a result of the complexity or density of the environments, as well as

for the presence of obstacles.

In the literature, different approaches have been adopted for robot team exploration under connectivity constraints in urban scenarios. For instance, in [Hsieh 08], the authors describe a system to maintain connectivity of a team of robots. A signal map is previously constructed, and subsequently a roadmap connecting areas to be explored is generated, which is used to drive the team to designated targets. The connectivity is maintained through a reactive strategy, which measures the signal strength and compute actions from a potential function that models radio propagation. In [Tardioli 10], the authors develop a system to deploy robots which simultaneously achieve mission tasks and maintain connectivity, also in urban environments. A task allocation technique constrained by the signal strength is also described. In that work, the system reactively constrained the motions of the robots depending on the measured signal to maintain the connectivity at all moment. In [Fink 10], different methods are proposed for modeling and mapping radio signal strength with robots. A maximum likelihood estimation of the source location is provided and a robot-motion control-law is applied to localize the source. The experiments were performed in an indoor laboratory and in an open area. A similar approach is described in [Wadhwa 11a], where the authors improve the characterization of the spatial variations of the Received Signal Strength (RSS) over space using Ray Tracing. They propose an adaptive algorithm which uses RSS averages (short and long term) to estimate both the traveling direction towards the source and how to proceed along the chosen direction. In [Yan 12], the authors develop communication-oriented metrics for optimizing the positioning of robot formations and use them as router to extend the coverage in fading environments. The authors use an objective function based on the Bit Error Rate (BER) in a probabilistic framework under communication power constraints. The method improves the performance of other methods based on disc models, although it does not guarantee the continuous maintenance of communication during the movement of the robots to their optimal positions.

However, as exposed in the previous Chapters, electromagnetic waves do not propagate in tunnels as in regular indoor scenarios nor in free space, even if Line of sight (LoS) is maintained between emitter and receiver. In these scenarios, various applications and projects involving safety in tunnels using robots have been developed. These include robots for fire-fighting, exploration, inspection, sensor deployment or surveillance. However, the connectivity problem is not addressed. For example, in [Walker 09], the authors describe a project involving a robot

for surveillance in underground galleries against smugglers in national borders. The problem of the communications loss is mentioned but no solutions are proposed. In [White 10], the authors present an underwater robot for archaeological teleoperated exploration in cisterns. The work make emphasis on SLAM problems for mapping the cisterns whilst communication issues are not considered. In [Peasgood 06], the authors show a multi-robot path planning algorithm in tunnel-like scenarios. However, only simulation results are shown, and the multi-robot communication problems are not addressed. In [Zhuang 08], the authors develop a robot for inspecting tunnels, capturing images, and registering the concentration of some poisonous gases, also disregarding the connectivity problems.

On the other hand, there are few works addressing the connectivity problem in this kind of environments. In [Parasuraman 14a, Parasuraman 14b], the authors deploy a team of robots to conduct remote inspections and radiation surveys in different areas of the underground facilities at the European Organization for Nuclear Research (CERN). Different radio signal propagation models and stochastic estimation techniques are used to enhance the wireless communication qualities. Furthermore, in [Owen-Hill 13] the authors propose a method to incorporate haptic information into the control commands of a mobile robot to augment the operator's perception of wireless signal strength, also for inspections in the same facilities. However, the experiments in the cited works were performed in segments shorter than 100 m in length. Long tunnels present specific propagation phenomena in the far sector, and special techniques must be adopted in order to ensure reliable communication between the robots.

In this Chapter, we introduce a technique for deploying a multi-robot team in tunnel-like fading environments while continuously maintaining the network connectivity, which takes into account the intrinsic signal-propagation behavior. To the best of our knowledge, multi-robot deployment exploiting the signal transmission characteristics in real and long tunnel-like environments has not been addressed in the literature. Unlike some of the previous works based on reactive motion-control, this work presents a deployment strategy in fading environments that takes advantage of a previously built model, but that is able to react according to actual real-time measurements maintaining continuously the network connectivity.

The Chapter is organized as follows. From the analysis of propagation in tunnels in Chapter 3, the general characteristics of signal behavior are summarized in Section 4.2.1. A deploying strategy for a team of robots is presented in Section 4.3, while Section 4.4 introduces the archi-

tecture of the system used to validate the latter. Finally, in Section 4.5 the method is evaluated by means of both simulations and a real experiment carried out in the Somport tunnel.

4.2 Previous Considerations

In order to propose and evaluate an algorithm to explore a tunnel while maintaining the network connectivity, the following considerations must be taken into account.

4.2.1 Wireless Propagation in the Somport Tunnel: Characteristics and Transmitting Setup

From the previous analysis of propagation in the Somport tunnel, we have summarized the propagation behavior in tunnels relevant for this Chapter as follows:

- There exist spatial slow and fast fadings, caused by the interference of two or more propagating modes.
- The slow fadings are periodic.
- The slow fadings are repeatable in both spatial and temporal domains
- There exist important transversal fadings, whose structure is determined by the transmitter setup.
- The noise introduced by the communications hardware can be considered as a *fast fading*.

The stated qualitative behavior of the tunnel (presence of near and far sectors, presence of slow and fast fadings, periodicity of slow fadings, etc.) can be extrapolated to other tunnels. See for example the results presented in [Dudley 07], [Sun 10] or [Mariage 94] where, although no analyses were performed, the cited behaviors can be clearly observed. However, the value of the parameters depends on the frequency and on the tunnel characteristics.

Fig. 4.1 shows an example of the measured received power along the Somport tunnel, highlighting the previous characteristics. The transmitter was placed at 0.25 m apart from the wall and 2 m above the ground (slightly offset from the *side position* for space-availability reasons).

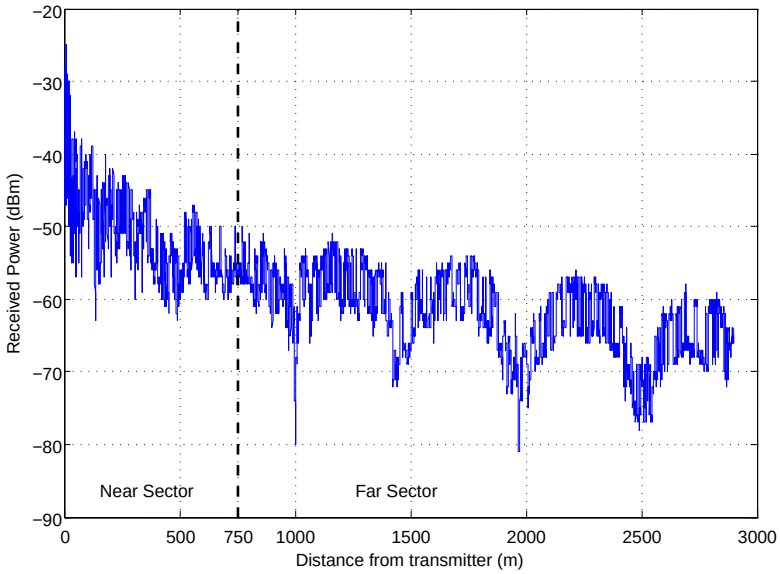

Figure 4.1: Measured Received Power (dBm).

One moving-receiver's antenna was placed at a height of 1.80 m and a distance of 0.60 m from the tunnel axis. It was displaced from the transmitter position up to 2900 m, maintaining the line-of-sight between them.

For availability reasons, this time the experiment testbed was composed of an emitting node based on a PcEngines ALIX3D3 board, which in practice was noisier than the equipment used in the previous Chapters. This was equipped with an Atheros-based chipset wireless card, sealed and designed for operation in hostile environments. It was running a Linux operating system and was programmed to emit broadcast frames periodically. Each receiving node was equipped with an Atheros network card. All antennas used were dipoles, vertically polarized, with a 4.5 dBi gain. The experiments were conducted at 2.142 GHz, and the transmission rate was fixed at 6 Mbps. This setup and the results obtained will be used along this Chapter for the algorithm planing and parameter tuning.

4.2.2 Navigation Path

Given that a temporal repeatability exists, the presence of transversal fadings imposes a restriction in terms of path planning if one robot wants to take advantage of the signal-level information collected by another robot. In fact, a deviation on the order of decimeters in the trajectory could cause strong differences in terms of received power and can provoke a misinterpretation of the

signal characteristics as, for instance, interpreting a decrease in the received power caused by a transversal fading as a longitudinal fading. As a result, all robots must follow the same path when moving. We have chosen the simplest way of accomplishing this requirement in this environment: to force the robots to travel in the same transversal position (maintaining a constant distance to the walls) within one of the Sectors exposed in Section 3.4.2 (Fig. 3.18). That is, to remain within a sector in which the fadings have the same behavior (i.e. same relative phase for the longitudinal fadings). Navigation paths exploiting the transversal structure of the fadings are proposed in Section 4.6.

4.2.3 RSSI Threshold Selection

Link quality measurement and estimation are a critical part of almost every mobile network routing protocol. Primary estimators for capturing the quality of a 802.11 wireless link that have been proposed are Received Signal Strength Indicator (RSSI), Signal-to-noise Ratio (SNR), Packet Delivery Ratio (PDR) and BER (Bit Error Rate). Each of them provides an estimation of the link quality over a period of time with limitations in terms of accuracy. Given that commercial hardware does not provide noise information while receiving packets but only an average estimation, it is quite hard to compute the SNR metric. On the other hand, the use of the PDR involves substantial latency for link quality estimation [Souryal 06]. The BER computation introduces significant overheads and is sensitive to bit sequences [Vlavianos 08]. Finally, the RSSI does not capture the amount of destructive interference in links.

However, RSSI can be a promising metric when its value is above the sensitivity threshold [Srinivasan 06]. Moreover, the use of a token-passing protocol (as in this work, see Section 4.4.3.1) avoids interferences due to simultaneous transmissions. In addition, at low rates [Holland 01] such as 6 Mbps, there is a correlation between the RSSI and the PDR: if the RSSI exceeds a certain threshold, the PDR is almost 100% [Vlavianos 08]. In order to characterize this correlation with the hardware setup considered in this work, a PDR study was performed. The final goal is to establish the RSSI threshold that allows a reliable communication between the nodes, with no packet loss. The resulting threshold will be an important parameter that drastically conditions the robot deployment plan. To this end, measurements were performed at several points in order to obtain the PDR for a large range of RSSI. A scatter plot where it

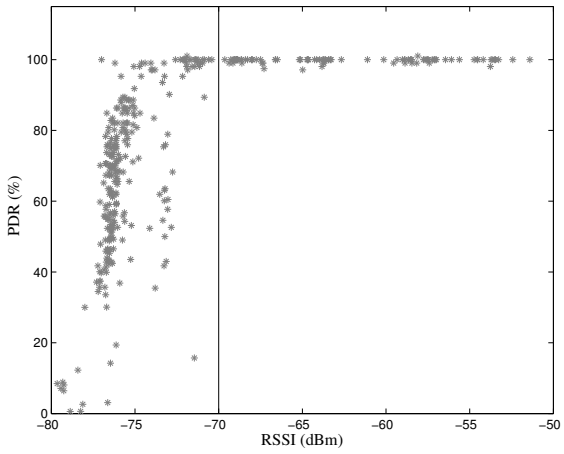

Figure 4.2: PDR vs RSSI. The vertical line denotes the minimum threshold chosen to ensure the acceptable PDR level.

is possible to observe the cited correlation between the RSSI and the PDR in the experiment is shown in Fig. 4.2. It can be seen that in order to obtain a PDR of about 100%, the RSSI should be higher than -70 dBm. This has been selected as the threshold to avoid packet loss between nodes.

4.3 Deployment Planning

In this section, an algorithm to deploy a robot team in a fading environment such as a tunnel is presented. The proposal tries to exploit the wireless propagation characterization presented in Chapter 3 to establish a general strategy for planning the motion of the robots in this scenario. Two main objectives are pursued simultaneously:

- To explore the tunnel while permanently maintaining the connectivity of the network formed by the robots and the Base Station (*BS*).
- To maximize the distance to be explored with the available robots (R_1 ... R_n, R_L).

Using the measured signal presented in Section 4.2.1 and base on the premise that the fadings are repeatable, an off-line deployment plan which would achieve the maximum distance computed from the model without loss of connectivity could be built. But since the real signal

might exhibit changes (although not very relevant ones) it is not possible to ensure that the connectivity will not be lost. Therefore, we suggest that the deployment has to use the real signal measurement for driving the motion in real time.

Even so, the general propagation behavior obtained in the signal analysis allows the definition of a general strategy presented in this Chapter. The analysis allowed us to establish, apart from the *distance path loss*, two main components in the signal, the *slow fadings* and the *fast fadings*. Both pieces of information will be used in the algorithm. The most important aspect to consider in the strategy is how to cross the fadings without losing communication with the base station. To this end, a robot called *leader* will use one or more robots as relays to explore the fadings. The more challenging fadings are the slow ones, that appear in the *far sector* of a tunnel (see Fig. 4.1), because of their width and depth. The information about the fast fadings has been used to make the system capable of tolerating them when they have a RSSI under the chosen safety *threshold* (see Section 4.3.1).

The general strategy is the following. The leader continuously measures the RSSI with respect the *BS*. This information and the above mentioned parameters are used by the system to establish the subgoals for the follower robots, in such a way that there is constant connectivity with the *BS*. When the leader is exploring a fading zone of the *BS* signal and does not find a new zone above the threshold, a new $base \leftarrow R_i$ is set, R_i being the robot closest to the old *base*. From this state, the execution continues taking $base_i$ as the new *base*. Notice that the maximum exploration distance for a fading will be the distance between two consecutive slow fadings. This distance can be computed from the measured signal presented in Section 4.2.1.

4.3.1 Deployment Parameters. Tuning for the Somport Tunnel.

The analysis of propagation in the Somport tunnel described in Chapter 3 (and summarized in Section 4.2.1) allows the parameter tuning of the planning algorithm, in order to execute it in a real scenario (see Table 4.1). The first parameter is the safe RSSI Threshold (TH), defined as the RSSI value that ensures a secure communication between nodes, avoiding packet losses. This is selected as -70 dBm in this case, for the reasons described in Section 4.2.3. The RSSI value between the base station and at least one of the robots must be above the TH in order to keep the network connected. To guarantee that this level is maintained between two adjacent robots, we

introduce the second parameter: the Safe Distance (*SD*). This is the maximum distance that two adjacent robots can move away from each other in order to maintain the RSSI above the TH. As can be seen in Fig. 4.1, in the first 750 meters from a transmission node (the *near sector*), the path loss and fast fadings dominate. The idea is to avoid a fast fading leading a robot into an unsafe zone. Based on our findings, we selected a *SD* of 350 meters, where even with fast fadings fluctuations the RSSI value is maintained above -70 dBm.

The valley-zone (VZ) and peak-zone (PZ) are defined as zones below and above the TH, respectively. Once the robot is located in a valley-zone, the goal is to look for the next peak-zone. The Maximum Fading Distance (MFD) is a parameter that represents the maximum exploration distance within a VZ in which the leader robot can search for a peak-zone before setting a follower as a fixed repeater. Based on our study, a distance of 500 m was chosen, which is the distance between two consecutive *slow fadings*. If a peak-zone is not found within this distance, it does not make sense to continue looking for a peak-zone with the same link. The algorithm sets a follower robot as a new *base*, and the leader starts processing the signal with respect to the new *base*. Finally, in order to switch between zones, the RSSI should be maintained below or above the TH for a distance greater than the Fast- Fading Width (FFW), to avoid a spurious switch in the state machine that controls the system (see Section 4.3.2.2). Hence, the FFW was defined as 20 m, that is the maximum width of 94% of the fast fadings in the Somport tunnel (see Section 3.4.1.2).

4.3.2 Deployment Algorithm

Let R_L be the leader robot and $R_1, ..., R_n$ the follower robots. We assume $n = 2$ throughout this section, however, the algorithm is general for any number of robots. The algorithm is outlined in Fig. 4.3. The deployment begins with all robots at the base station in a chain configuration ($R_1..R_nR_L$) and ready to start. First, a goal at the Maximum theoretical Distance (*MD*) is computed and assigned to the leader robot. Note that this is a function of the number of robots available. The leader begins to move toward this goal while sensing the quality of its link with the *BS* (Fig. 4.3(a)). When it reaches the limit of the safe distance (*SD*) from the closest robot, it creates a virtual rope between itself and the first follower R_n. This provokes the latter to start moving and follow the leader at the *SD* distance (Fig. 4.3(b)). Both robots continue moving

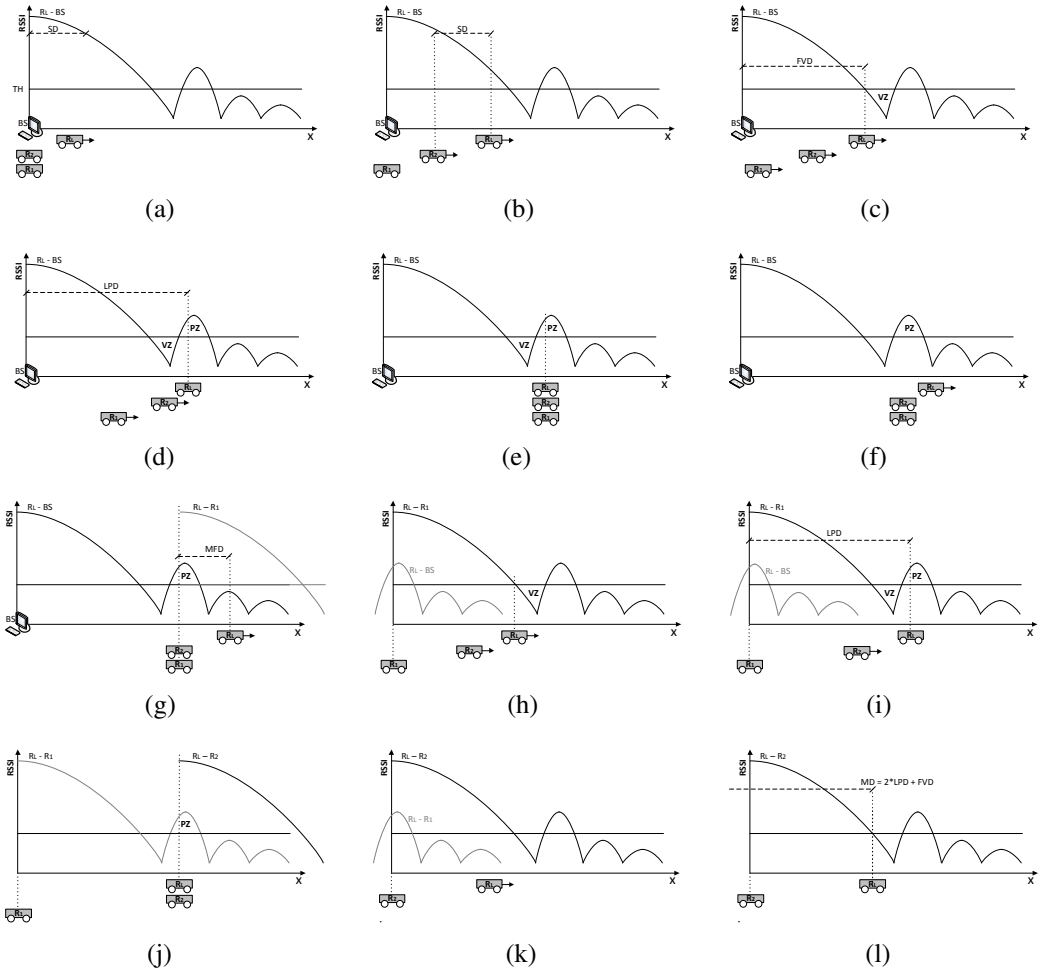

Figure 4.3: Representation of the main steps of the algorithm. In a), Robots R_L, R_1 and R_2 move along the tunnel from the position where base station *BS* is located, keeping a safe distance between them (b). When the leader R_L enters a non-safe zone (VZ), it uses the nodes of the chain as relays to communicate with the base station and continues moving toward its goal (c). R_L looks for a peak-zone (PZ) to reestablish the link with the base station and calls all the following robots in that zone (d). When the grouping is completed (e), the algorithm restarts (f) and the leader moves forward. When the distance between the leader and the followers reaches the MFD distance, a new base station is established for the leader in R_1 (g). R_2 follows R_L (h) when the distance between them reaches the safety distance and the leader continues moving until it finds a valley, but now with respect to the new base R_1, and to find a new peak (i) to regroup with R_2 (j). R_2 now also becomes a stationary relay (k) and the leader R_L reaches the limit of the last safety zone (l), completing the chain that maximizes tunnel coverage with the available robots.

Table 4.1: Parameters and terms used in the deployment strategy. N is the number of follower robots

PARAMETER	DESCRIPTION	VALUE
Safe RSSI Threshold (TH)	RSSI value for PDR=100%	-70 dBm
Safe Distance (SD)	Maximum distance between two adjacent robots to ensure a link above TH	350 meters
Fast-Fading Width (FFW)	Fast-fadings found within this width are not considered	20 meters
Maximum Fading Distance (MFD)	Maximum distance between two consecutive slow fadings	500 meters
Last Peak Distance (LPD)	Distance from a base to last peak above TH	2700 meters
First Valley Distance (FVD)	Distance from a base to the first fading below TH	1000 meters
Maximum Distance (MD)	Maximum exploration distance	n*LPD+FVD meters

until, again, the distance between the first and the second follower exceeds the *SD*. At this moment, the second follower R_{n-1} starts moving to follow R_n. The process is repeated with the other robots in the team until a chain of equidistant robots is created. The situation changes when the leader has traveled a distance equal to the First Valley Distance (FVD) and enters a non-safe zone (valley-zone, VZ) in which its link-quality with the *BS* falls below the TH (see Fig. 4.3(c)). At this moment, the communication between the leader and the *BS* is not yet direct, but R_L uses the nodes of the chain as relays to communicate with it. Even so, the leader continues moving toward its goal, looking now for a new safe zone (peak-zone, PZ) to reestablish the link with the *BS* (see Fig. 4.3(d)). Here, it prepares to stop moving to verify that the peak just found is actually a PZ (and is not due to a fast fading). This filtering is made discarding less-than-twenty-meter-wide peak-zones, the FFW parameter defined in Table 4.1. In the peak-zone, the leader stops and groups all the follower robots. During the grouping, the connectivity is guaranteed by the fact that the leader has a good link quality with the *BS* and the distance among the robots is always below the *SD*. When the grouping is completed (see Fig. 4.3(e)), the algorithm restarts (Fig. 4.3(f)). The leader searches for the next peak. If the leader does not find a new peak-zone within the MFD (Fig. 4.3(g)), it means that it does not exist. When this

situation occurs, the farthest follower (R_1) is fixed as the new base (it will not move anymore) and the leader starts to sense the link quality with respect to this new base (Fig. 4.3(h)). The leader continues moving until it finds a valley, but with respect to the new base R_1. Then it explores in order to find a new PZ where the $n-1$ remaining followers are grouped (Fig. 4.3(i)). After grouping (Fig. 4.3(j)), the process restarts. From this moment until the leader reaches the end goal, all the follower robots are fixed as a new base, following the rules just described. Fig. 4.3(k) represents situations in which R_2 is the new base. The maximum distance is reached when the leader finds a valley-zone and the last follower robot has already been fixed as the new base (Fig. 4.3(l)).

The proposed algorithm uses the communication parameters TH, SD, FFW and MFD (see Table 4.1). These parameters are obtained from the analysis of the measurements described in Section 4.2.1. A poor estimation of these parameters may affect the performance and proper functioning of the algorithm. A qualitative analysis of possible affections follows. The safe RSSI Threshold (TH) does not depend on the propagation characteristics of the tunnel but only on the communication system (hardware, modulation scheme, frequency, etc.). The Safe Distance (SD) is the most critical parameter. Its overestimation can cause loss of communication and, thus, mission failure. An underestimation would mean a decrease in deployment distance. The Maximum Fading Distance (MFD) is used as stop condition. A poor estimation does not represent a threat for the mission, but may increase the deploying time or decrease the maximum distance achieved. Finally, the Fast Fading Width (FFW) is only a filter parameter. An overestimation may decrease the exploration distance because a short peak zone can be interpreted as fast fading, whilst an underestimation can cause an increase in the exploration time since fast fading can be interpreted as peak-zones. The reactivity of the algorithm makes it insensitive to parameter variation in terms of safety. The algorithm can also enable an online signal analysis and then an auto-tuning process could be implemented.

4.3.2.1 Calculation of the Theoretical Maximum Distance

The calculation of the theoretical Maximum Distance (MD) is straightforward. Let LPD be the distance from the Base Station to the last peak-zone in which the signal strength is above the threshold TH, and FVD the distance from the Base Station to the start of the first valley-zone (see Fig. 4.3). This distance is reached when the leader traverses all the valley-zones up to the

last peak with respect to each base, except the last established base, at which the leader stops before traversing the first valley. An upper bound of the exploration distance is:

$$MD = n * LPD + FVD \tag{4.1}$$

where n is the total number of followers. Achieving this bound depends on the relation between the SD, the width of valley-zones and the number of followers. The MD is used to compute the last potential goal to be stated for the leader robot. Nevertheless, the plan for all the robots is computed in real time during the exploration, based on the real signal measurements. In other words, this equation offers an estimation of how far the tunnel can be explored given a certain number of robots, or a rough value about the number of robots needed to cover the whole scenario.

4.3.2.2 Detailed Algorithm

The general Algorithm 1 has been implemented by means of a state-machine. Several states are defined: $BEGIN$ when the algorithm starts, $FIND\_VALLEY$ when the leader is finding the first valley under TH, $FIND\_PEAK$ when the leader is finding a peak zone, $GROUP\_ROBOTS$ when all the robots move for grouping in a location, END when the maximum exploring distance is achieved. The parameters defined in Table 4.1 are used in different states of the algorithm.

4.4 System Description

In order to implement the multi-robot system for the application addressed in this Chapter, we have developed a distributed architecture that integrates different modules in each robot: a COMmunication module (COM), a Navigation Control Module (NCM), a feature-based robot LOcalization Module (LOM) and a SUpervisor Module (SUM). This software architecture was implemented on the onboard computers which run the modular solution presented in Fig. 4.4 and replicated in each robot:

- The NCM module implements the motion planning and reactive navigation techniques and generates velocity commands for the robots, providing a safe navigation towards the goals assigned by the SUM (see below). It uses the information from the robots' sensors

Algorithm 1

$base = 0$, $state = BEGIN$
while *true* **do**
  if $state = BEGIN$ **then**
    $R_L \leftarrow goal(MD)$
    for i in $followers$ **do**
      $set\_rope(R_i, R_{i+1}, SD)$
    $state \leftarrow FIND\_VALLEY$
  else if $state = FIND\_VALLEY$ **then**
    if $found\_valley(R_L, R_{base}, TH, FFW)$ **then**
      if $Card(followers) > 0$ **then**
        $locValley \leftarrow locR_L$
        $state \leftarrow FIND\_PEAK$
      else
        $stop(R_L)$
        $state \leftarrow END$
  else if $state = FIND\_PEAK$ **then**
    if $dist(locR_L, locValley) \geq MFD$ **or**
      $dist(locR_L, locValley) \geq Card(followers) * SD$ **then**
      $set\_new\_base\_station(R_{base+1})$
      $state \leftarrow BEGIN$
    if $found\_peak(R_L, R_{base}, TH, FFW)$ **then**
      $stop(R_L)$
      for i in $followers$ **do**
        $R_i \leftarrow goal(R_L)$
      $state \leftarrow GROUP\_ROBOTS$
  else if $state = GROUP\_ROBOTS$ **then**
    if $robots\_grouped$ **then**
      $state = BEGIN$
  else if $state = END$ **then**
    exit

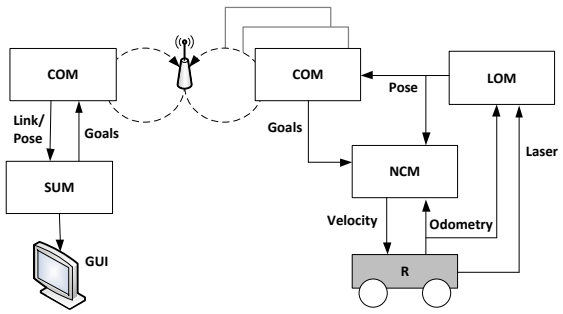

Figure 4.4: Software architecture for the base station and robots.

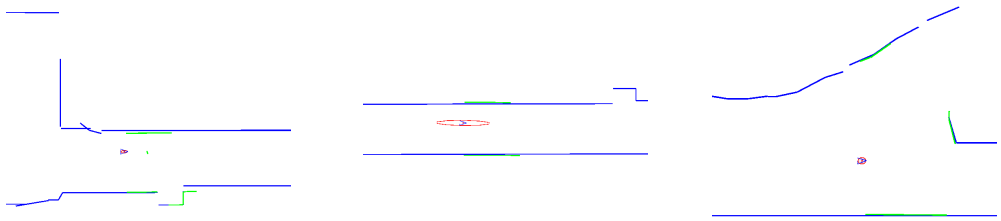

(a) (b) (c)

Figure 4.5: Mapping and robot localization. Three typical zones found in the tunnel. Emergency shelters (also called vaults) (a) and galleries (c) allow accurate localization of the robots, long corridors (b) favor the uncertainty increase (red ellipse). The previous map in blue, the features matched with the map in green.

(odometry and laser rangefinder) combined with the localization provided by the LOM module in order to achieve the navigation.

- The LOM module provides a global localization of the robots, using the information of the rangefinder and odometry sensors and a pre-existing map. This localization information is sent to the COM module that, in turn, sends it through the network to the base station.
- The COM module provides multi-hop, real-time communication among robots and base station, routing the messages over safe paths.
- The SUM module is responsible for collecting the flow of system information (links state, robot localization, etc.) from the network and sending commands to the other modules (goals, emergency stop and resume commands, etc.). The base-station generates such commands, once requested by the operator through its GUI.

The entire system has been implemented on the ROS platform [Quigley 09]. Each node uses its own core, and all communication among different nodes is carried out using the *ros_rt_wmp* node [Tardioli 12] that allows real-time multi-hop communication among the different ROS nodes distributed in different cores.

4.4.1 Localization Module

For a robust autonomous navigation, it is necessary to continuously localize the robots as precisely as possible. The technique used is based on that described in [Lazaro 10]. A segment-

based map is built using a laser rangefinder, which will be used as an a priori map for real time localization while navigating.

The LOcalization Module (LOM) provides the robot pose during the exploration. The Extended Kalman Filter (EKF) localization algorithm segments the laser sensor readings and matches the features obtained with the set of those representing the map. The laser sensor segmentation technique is based on a tracking-like algorithm combined with a validation gate used to group the range readings into regions. These regions are successively split into segments which describe the environment seen by the robot through a polygonal approximation technique. Fig. 4.5 shows some snapshots of the localization algorithm output. It shows the position of the robot during an experiment, the map, and the correctly matched observations. It is worth noting that in this kind of environment (straight tunnels), the uncertainty in the motion direction (x axis) continuously increases because of the planar walls. However, in the particular tunnel used for the experiments, the emergency shelters (vaults) and lateral galleries mentioned in Section 3.3.1 allow this uncertainty to be greatly reduced periodically. This can be observed in Fig. 4.5(a) and 4.5(c) in which the ellipse representing the uncertainty is reduced compared with that drawn in Fig. 4.5(b).

4.4.2 Navigation Module

The goals to be reached by each robot at each moment are set by the planner, as explained in Section 4.3. The navigation control module (NCM) is responsible for providing safe navigation to a given goal.

In order to navigate autonomously in such environments, each of the robots incorporates a navigation system based on the Obstacle-Restriction Method (ORM) [Minguez 05]. This algorithm is an obstacle avoidance method that obtains similar results to the Nearness Diagram family methods [Minguez 04], [Minguez 01] in dense and complex scenarios, but improves trajectory behavior in open spaces (specifically, avoiding oscillations). The algorithm gives a high performance for dense environments, but for this reason the velocities are low in general. The tunnel used for the experiment is not a dense scenario, so higher velocities are possible. We have therefore improved the ORM algorithm with a method based on hinterlands (Fig. 4.6 shows an outline of the technique used). This method combines the ability of the ORM to navigate in

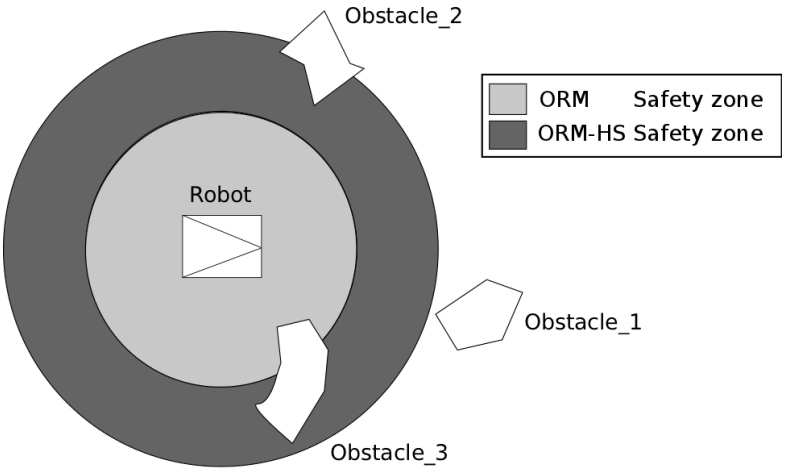

Figure 4.6: Diagram of the safety zones.

dense environments with that of navigating at higher speeds when there are no obstacles nearby.

The method adapts the velocity depending on the safety zone around the robot. Three zones are defined, as can be seen in Fig. 4.6, and a maximum velocity is stated for each zone. In our case these are 1.0 m/s, 0.4 m/s in the external zones, respectively. In the $ORM-HS$ zone, the linear speed is reduced proportionally to the distance to the obstacle. When the obstacles are in the inner zone, the velocity, previously reduced in the $ORM-HS$ zone, is adapted by the ORM method, avoiding the obstacles in an appropriate manner.

4.4.3 Communication Module

The communication among the robots and between the robots and the base station must comply with a set of important conditions and characteristics. Above all, since our solution needs information about the link quality among robots and shares navigation information such as localization and time sensitive data, the COM module must be capable of capturing the link state of each pair of robots and transporting information in a network with real-time guarantees. This last requirement also involves the need for message priority in order to support multiple flows of data. Moreover, the network protocol must support multi-hop communication that is needed by the algorithm presented in Section 4.3.

4.4.3.1 The RT-WMP Protocol

In order to provide information transport with the previously cited characteristics, the COM module bases its communication on the Real Time Wireless Multi-hop Protocol (RT-WMP) [Tardioli 07], designed to connect a relatively small Mobile Ad-Hoc Network ($10-15$ units maximum). In RT-WMP, the end-to-end message delay has a bounded and known duration and it manages global static message priorities. RT-WMP also supports multi-hop communications to increase network coverage. It is based on a token passing scheme and is completely decentralized. The protocol is designed to manage mobility through the exchange of an adjacency matrix containing link quality among nodes.

4.4.3.2 The Link Quality Matrix

When nodes are moving in environments with serious signal fadings, the radio signal, and therefore link quality, among the nodes can change rapidly, and this must be reflected in the global status of the network. Consequently, when a node discovers a change, it has to propagate this information as soon as possible. In RT-WMP, this task is automatically carried out by the protocol token, so the global network link state is updated in each protocol round. The protocol defines the so called Link Quality Matrix (LQM). Each column of the matrix describes the link quality of any node with its neighbors in terms of the RSSI. The information contained in the LQM is shared among all nodes, since it travels with the token and reaches all members of the network in every round. The nodes are responsible for updating the corresponding column of the LQM to inform the other nodes of local signal strength changes. From the point of view of the communication transport layer, the COM module uses LQM to find a reliable path over which to send user or management messages. Fig. 4.7 shows a scheme of the routing algorithm and the corresponding LQM. More details can be found in [Tardioli 10].

4.4.4 Supervisor Module

The Supervisor Module is responsible for executing the deployment algorithm (presented in Section 4.3) and controlling the whole system. It executes the state machine using the information provided by all the nodes involved in the system through the COM module:

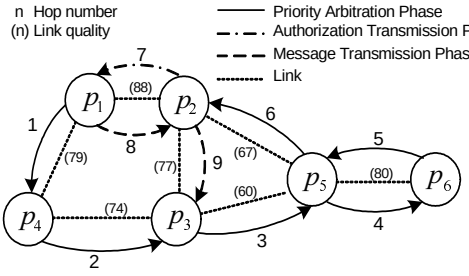

Link Quality Matrix

	p_1	p_2	p_3	p_4	p_5	p_6
p_1	-	88	0	79	0	0
p_2	88	-	77	0	67	0
p_3	0	77	-	74	60	0
p_4	79	0	74	-	0	0
p_5	0	67	60	0	-	80
p_6	0	0	0	0	80	-

Figure 4.7: Message routing using the LQM matrix. The highest link quality is maintained through the nodes.

- *Locations of mobile robots*: the robots periodically send their locations to the SUM module using a real time flow provided by the COM module.

- *Signal Strength among nodes*: the LQM shared among nodes is provided by the COM module to keep the SUM informed about the connection of the network and the link quality among the nodes.

The SUM module also uses the COM to send *goals* or *stop* commands to the mobile nodes in order to ensure the correct execution of the algorithm. Other information, such as laser scans, can travel through the communication network for monitoring purposes. These information flows have a lower priority to avoid the risk of delaying the information needed for control. The SUM also has a graphics user interface (GUI) that permits the visualization of the system state, the link quality among the nodes and the laser readings of each robot.

4.5 Experiments

The evaluation of the system has been carried out by means of both simulations and field experiments. The simulations have been performed using an artificially designed signal to verify the correctness of the algorithm. The field experiments have been performed in the Somport tunnel already described in Section 3.3.1. In all the experiments, the parameters shown in Table 4.1 have been used.

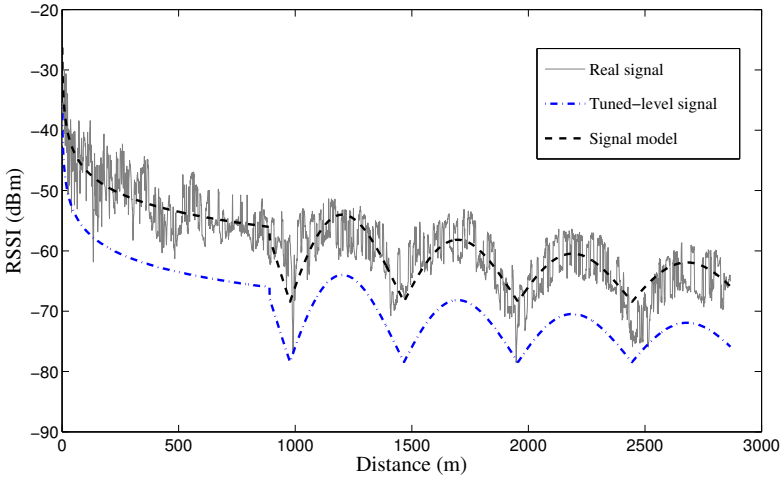

Figure 4.8: Real signal and signal from the model.

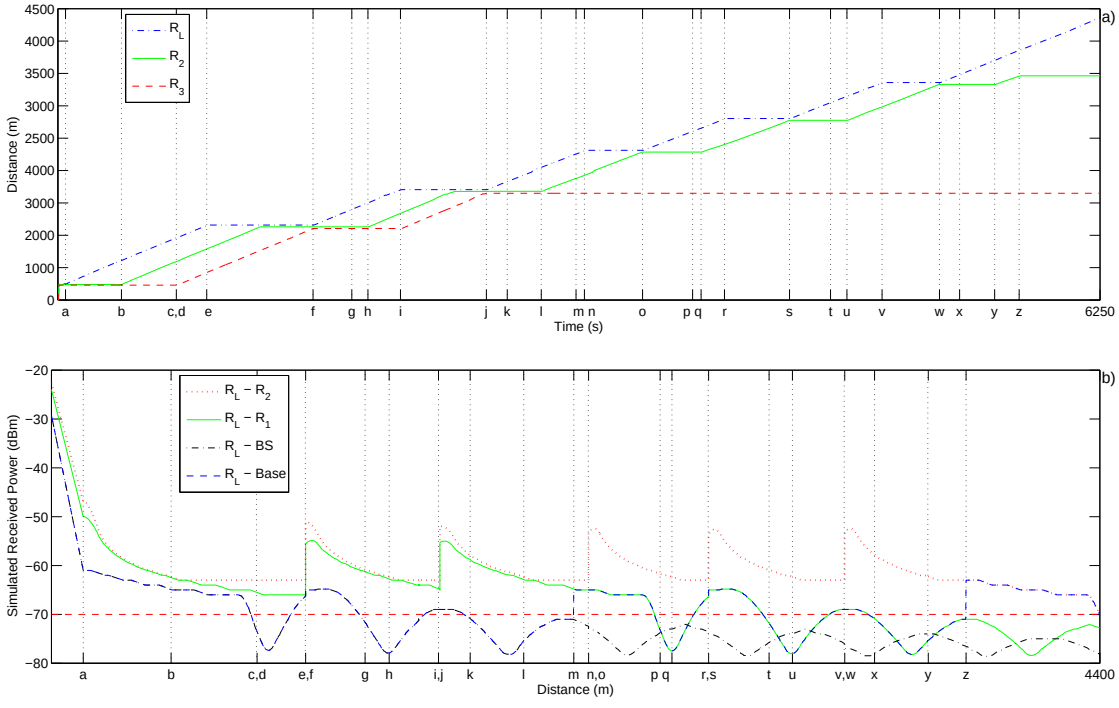

Figure 4.9: a) Robots' position versus time, b) Signal quality versus position. R_L starts (a). R_L finds a peak zone (e, i, n, r and v). R_L finds a valley-zone (c, g, k, p, t and x). Robots meeting points (f, j, o, s and w). Base switching (m and z). Leader pulls followers (b, d, h, l, q, u and y).

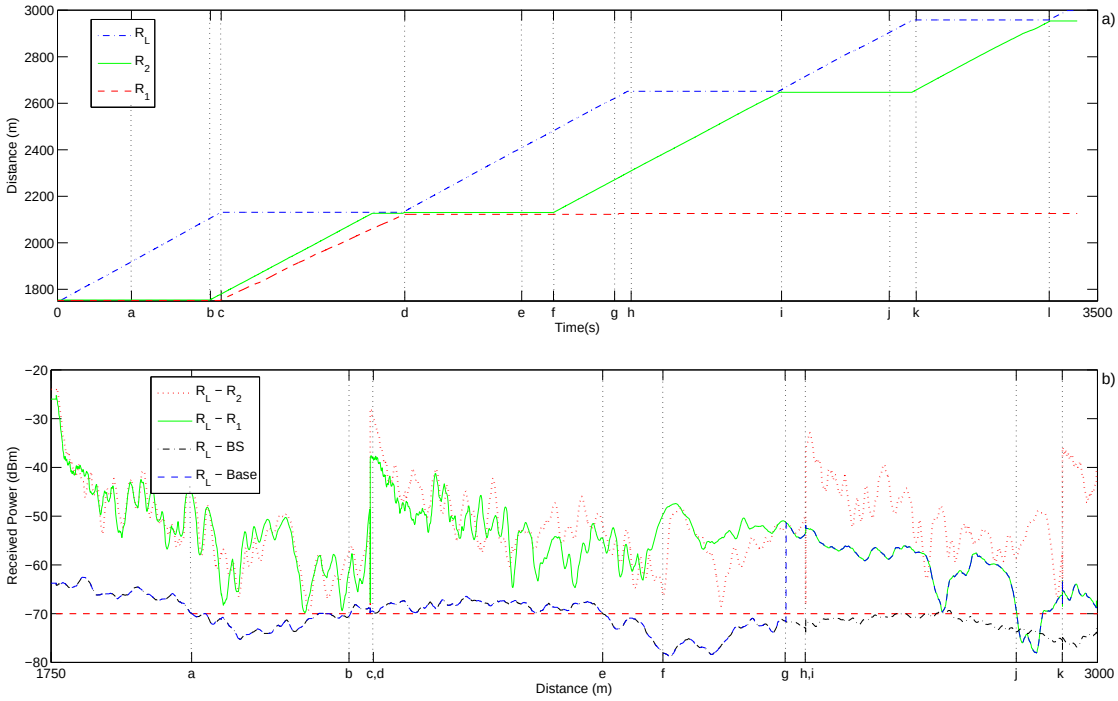

Figure 4.10: a) Robots positions versus time. b) Signal versus position. R_L found a valley-zone (a, e and j). R_L finds a peak zone (c, h and k). Meeting points (d, i and l). Leader pulls followers (b and f). Base switching (g).

4.5.1 Propagation Function Model Design

The propagation of the signal in the tunnel exhibits different behaviors in the near sector and in the far sector (see Section 4.2.1). In the near sector, apart from the fast fadings, the distance path loss dominates following a logarithmic decay in terms of power. In the far sector, the signal power exhibits a characteristic shape (see Fig. 4.1), which for practical reasons can be simulated with a typical *sinc* function. Considering the real data, we tuned such a mathematical function to reflect a similar behavior for $y(x)$ as:

$$y(x) = k \cdot \left| \frac{sin(\frac{\pi}{D} \cdot x)}{x} \right| + C \tag{4.2}$$

where D is the spatial period of the signal, and k and C, the tuning parameters. A least squares optimization technique has been used to find the optimal parameters k, D and C to fit the real data with the artificial curve. In Fig. 4.8 the measured and the designed signals are compared.

The level of the signal used for the simulations has been lowered for bounding its duration and for simplifying the execution of the algorithm while maintaining the same TH level. In this way, only two peak-zones appear during the simulation. A simple analysis of the function allows the automatic computation of the number of slow fadings and of local maxima in which the signal is above the established threshold TH by solving,

$$\nabla_x y(x) = k \cdot \frac{(\beta \cdot cos(\beta) - sin(\beta))}{x^2} = 0 \tag{4.3}$$

where $\beta = \frac{\pi}{D} \cdot x$, which leads to the equation:

$$M = solve(tan(\beta) = \beta) \tag{4.4}$$

where $M = \{m_1, ..., m_{n_f}\}$ is the location of the local maxima found above the threshold corresponding to the n_f slow fadings. From this value, the estimation of the maximum distance LPD defined in Equation 4.1 and the last maximum used to set the initial goal for the leader robot can be computed.

4.5.2 Simulation Results

The complete system has been simulated using the previously calculated signal shown in Fig. 4.8. Three mobile robots were used for simulation within the Stage simulator in the ROS environment, executing the same code as for the real experiment. The three robots started in a chain configuration close to the base station. The results are presented in Fig. 4.9. Fig. 4.9(a) shows the movement of the robots along the tunnel. The distance of the leader robot R_L with respect to all the other nodes begins to increase when it starts moving (a). After 350 meters, at point (b), the distance between R_L and R_2 exceeds the SD and the latter starts to move. After that, the same occurs between R_2 and R_1 and the latter starts to move (c). At the same time the leader finds a VZ with respect to the base station (BS) at (d). The leader continues moving up to the point at which it reaches a PZ (e) and stops. It calls its followers that reach the leader at (f). The algorithm restarts and a similar situation takes place at points (g), (h), (i) and (j) where the leader collects the followers again. After that, the leader restarts and after finding a VZ in (k) continues looking for the next PZ pulling R_2 in (l).

Figure 4.11: Two snapshots from the real experiment.

When it reaches point (m), R_L has explored the valley-zone covering a MFD distance and then R_1 is fixed as the new *base*. From this point on, the leader starts to sense its link with R_1. When it realizes that it is in a peak zone with respect to R_1 (n), it calls R_2 which reaches the leader at (o). After that, the algorithm restarts again with only one follower. The leader traverses the valley-zones (p) and (q) with the help of R_2 reaching the peak zone in (v) where it again calls R_2 which stops at (w). The leader restarts, and finds a new valley-zone in (x). At (y) it tries to pull R_2 again but it has to stop at (z) to avoid leaving the peak zone that permits communication with R_1. The leader fixes this as the new base and continues exploring until the link that connects it with R_2 falls below TH. According to Equation 1, the estimated Maximum Distance (MD) is 4400 meters (LPD=1750, FVD=900), which fits with the final position reached by the leader in the simulation.

Fig. 4.9(b) shows the (simulated) link qualities obtained during the execution of the experiments. It can be seen that the signal level of R_L with the *base* fixed at any moment or with the closest follower is always above TH. At the points (m) and (z) (corresponding to those in Fig. 4.9(a)) it is possible to observe a sudden change in terms of RSSI due to the base switching. In fact, as described, at (m) and (z) R_1 and R_2 become the new base, respectively. It can also be seen that, as expected, the signal is repeated with the same shape after each meeting of the robots ((f), (j), (o), (s), and (w)) and after every switch (m) and (z).

4.5.3 Field Experiment

After completing the simulation experiments, we carried out a field experiment in the Somport tunnel. Fig. 4.11 shows some instances in the experiment. The objective was to verify the results in a real-world scenario using mobile robots and actual wireless communications. We used three Pioneer P3AT mobile robots controlled by three Dell D630 laptops. At the base station we used a Getac B3000 Rugged laptop. All the wireless devices were Ubiquiti Networks SRC 802.11 a/b/g PCMCIA cards based on the Atheros 5004 chipset. For all the nodes we used a dual band 5.2/2.4 GHz Omnidirectional Antenna with a gain of 4.5 dbi in the 2.4 GHz band. The transmission power was fixed at 10 dBm and the frequency at 2.412 Ghz (channel 1 on *802.11 g* band) while the data rate was fixed at 6 Mbps. The results are shown in Fig. 4.10(a) and 4.10(b). Only the stretch between 1750 m and 3000 m has been selected to be shown for being the most interesting and with the end of the making the figure easily understandable. Fig. 4.10 shows the results of the experiment from the moment in which robot R_L starts to move after its stop at 1750 meters. At moment (a) it finds a valley-zone but continues moving up to the point at which the distance with respect to R_2 exceeds the *SD* (b). At this moment, R_2 starts to move to follow the leader but a few meters on, the latter finds a *PZ* in (c) where it stops and calls the followers. It is possible to appreciate a slightly different speed between the two robots due to R_1 having different mechanical parts with respect to the other robots.

When both followers reach the leader at (d), the latter restarts its movement and at (e) finds another *VZ*. It continues moving up to the moment in which the distance between itself and R_2 again exceeds *SD* (f) at which point the latter starts following R_L. After that, in (g) the MFD is reached and R_1 is fixed as the new *base*. From now on, the leader starts sensing the link quality with respect to this new *base*. In the new *PZ*, the leader stops and waits for R_2 which reaches R_L at (h). At this point the latter restarts and, after passing a valley-zone (j), finds another peak in (k). Again it calls its only follower (l) and the process restarts.

Fig. 4.10(b) shows the signals. It is possible to see the beginning of the *VZ* (a), (e) and (j) and the *PZ* (c), (h) and (k) and the switching between the base *BS* and R_1 in (g). It is also possible to observe that the signal between the R_L and the fixed base or between R_L and its closest follower is above the *TH* limit at any moment. Also, it is interesting to appreciate the repeatability of the signal after each grouping of the robots.

Table 4.2: Path of the messages from leader to base station.

Path	Count	Percentage
$BS \rightarrow R_1 \rightarrow R_2 \rightarrow R_L$	12183	35.8%
$BS \rightarrow R_2 \rightarrow R_L$	11649	34.3%
$BS \rightarrow R_1 \rightarrow R_L$	1543	4.5%
$BS \rightarrow R_L$	8659	25.4%

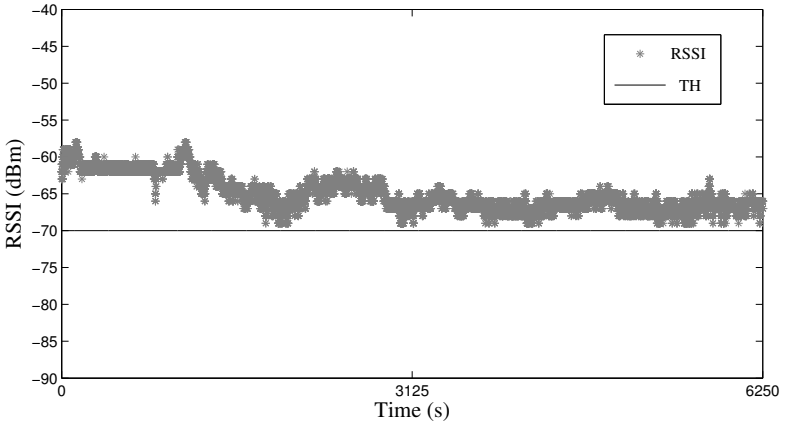

Figure 4.12: Received Signal Strength of the weakest link in the message path.

As expected, during the whole duration of the experiment, the communication was permanently maintained among all the nodes of the network. The varying position of the nodes have provoked different network topologies throughout the experiment and the need for multi-hop communications, as confirmed by Table 4.2 which shows the paths that have been used by the messages sent from the leader node (odometry, position, etc.) to reach the base station and their respective percentages. The specific distribution of these percentages depends in part on the routing algorithm that, in the case of RT-WMP, favors longer safer paths over shorter dangerous ones. Fig. 4.12 shows the RSSI of the weakest link of the chosen path at any moment. Analyzing Fig. 4.10(b) and 4.12 together, it can easily be inferred that the communication would not be possible without multi-hop support. In fact, the first figure shows that in many cases the RSSI of a single link falls below the minimum admissible threshold TH but the second confirms that all the paths used during the operation of the system accomplish the goal of having all the links above such a safety level. This fact has permitted the PDR to be above 99.5% during the whole duration of the experiment, as expected given the results described in Section 4.2.3.

4.6 2D Navigation Extension

In the previous Sections, a technique for deploying a team of robots in a tunnel while maintaining the network fully connected has been presented. The robots traveled in a straight line along the tunnel (which is the most intuitive navigation path for tunnel exploration), and use each other as relays to go across the fadings. Also, by means of detecting and traversing the longitudinal fadings, the information gathered can be used for localization purposes, as will be presented in Chapter 5.

Nevertheless, if only a single robot is available for the tunnel exploration, it is evident that traveling in a straight line and traversing the fadings will cause the robot to fall in hazardous areas in terms of communications (fadings minima or valley zones), where a RSSI below the selected threshold causes data loss and may even result in a completely loss of connectivity between the robot and the base station. In this situation, the transversal structure of the fadings can be exploited to improve the communication with the base station compared to the case of traveling in a straight line.

As seen in Chapter 3.4.2, the spatial structure of the fadings is directly determined by the interacting modes' electric field distribution, which in turn is a consequence of the transmitting antenna setup. The two setups explored to obtain well-defined fading structures consisted to place the transmitting antennas in the center of the tunnel, and at one third of the tunnel width from the tunnel walls. The latter divides the tunnel in two sectors, and the received signal fadings present the same relative phase within each sector, and a phase difference of about 180 degrees between sectors. The transmitter in the center generates a received fading structure that divides the tunnel in three sectors, where the extreme sectors are in phase and present a relative phase difference of 180 degrees compared to the center sector.

If the transmitter is placed in the *side position*, it is seen that the robot should follow an *s-like* or *zig-zag* trajectory (depicted as a black dashed line in Fig. 4.13) , traveling from the fadings maxima in one half of the tunnel (*sector 1*) to maxima in the other half (*sector 2*), avoiding the valley zones, in order to ensure a better link quality in comparison to the case of traveling in a straight line.

On the other hand, if the transmitter is placed in the center of the tunnel, the robot can locate the fadings' maxima traveling from one extreme of the tunnel to the opposite one (*sector*

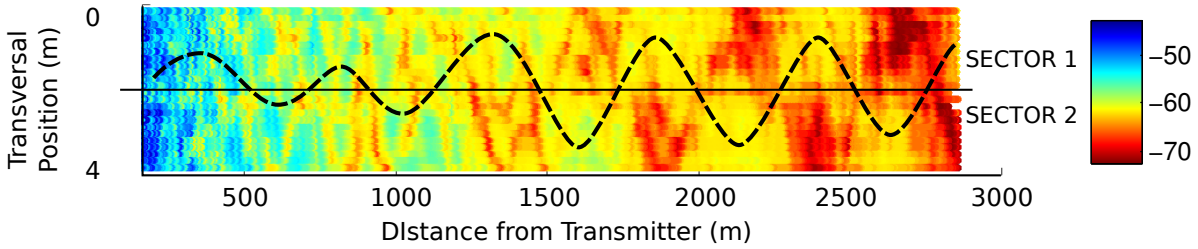

Figure 4.13: Tunnel Upper View. Received-power grid at 2.4 GHz with tx on side. The black dashed line illustrates the robot's navigation path.

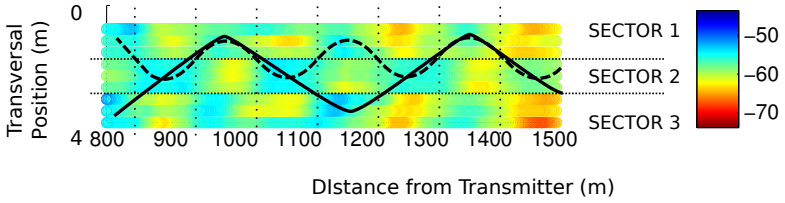

Figure 4.14: Tunnel Upper View. Received-power grid at 2.4 GHz with tx on center. The black dashed and solid lines illustrate the robot's navigation paths.

1-sector 3-sector 1..., depicted as a solid line in Fig.4.14), or within the same half of the tunnel (*sector 1-sector 2-sector 1*, or *sector 3-sector 2-sector 3*, represented with a dashed line).

In order to locate the fadings maxima, the proposed navigation can benefit from RF-source localization approaches such as those presented in [Sun 08, Han 09, Wadhwa 11b, Yu 11], taking into account some considerations. Particularly in [Twigg 12], the authors sample the RSS and estimate the 2D gradient through gently oscillatory navigation paths to guide a ground robot to a RF source.

The case of 2D navigation inside a tunnel is slightly different, though. In the near sector, the robot must actually move against the base station, in the direction in which the RSSI decreases. Once in the far sector, the fadings maxima can be considered as the RF sources in the previous approaches.

In order to avoid local maxima, a global navigation goal must be set. Also, as the transmitter position is a known variable (and consequently the transversal fading structure produced), the navigation planning can benefit from this knowledge to optimize the paths. As an example, once located a fading peak, it is known that the adjacent maximum is located within the other half of the tunnel (in the case of placing the transmitter in the *side position*). Also, the period of the

fadings can be used to smooth the trajectories.

Finally, if more than one receiver is available per robot, Section 5.4 addresses the simultaneous localization and navigation taking into account the connectivity constraint to propose spatial diversity schemes.

4.7 Summary

A technique for deploying a team of robots in confined and fading environments has been developed. This has been integrated in a complete system through a distributed architecture, in order to work in real environments. There were two main objectives: i) to maintain constant network connectivity; ii) to reach the maximum possible distance in the exploration with the available robots. To simultaneously achieve both objectives, the communication quality among all the elements of the network, robots and base station, must be sufficient to ensure that the signal strength remains above a threshold which allows transmission and reception at maximum PDR.

A general deployment planning technique for this kind of environment has been described. It uses the signal parameters characterized in the previous Chapters to particularize the strategy to the specific scenario. It will thus be necessary to estimate these parameters for other fading-like scenarios, but the strategy is general. The leader robot uses the real signal that it measures to plan its motion in real time and the deployment of the follower robots which act as repeaters.

The signal in this kind of environment has a typical shape in which slow fadings and fast fadings appear. This shape allows the multi-robot deployment to be enlarged in such a way that the distance to be reached with the available robots can be maximized without loss of connectivity in the network. The slow fadings are most important in the strategy since the algorithm takes advantage of them for placing the robots so as to maintain the maximum PDR. The simulated and real experiments conducted over three kilometers of the tunnel demonstrate the good performance of the technique based on the signal strength parameters.

In both the simulated and the real scenarios, the system worked as predicted even though the simulated and real signals did not share exactly the same behavior. The network connectivity was maintained during the real experiment, guaranteeing the existence of a safe path among all the robots at all time.

Finally, if only one robot is available for the tunnel exploration, traveling in a straight line and traversing the fadings will cause the robot to fall in hazardous zones in terms of communications. To solve this, a 2D navigation algorithm has been proposed to improve the communications with the base station. Taking into account the transmitter setup, the robot should follow a *zig-zag* navigation path, traveling from maxima in one of the mentioned sectors (according

to the transversal structure of the fadings), to maxima in the other sector, avoiding the valley zones. Also, as the transmitter position is a known variable and hence the expected fadings period and transversal structure, the navigation planning can benefit from this to set the subgoals and smooth the navigation paths.

Chapter 5

Localization

Accurate localization is a challenge in confined environments such as tunnels or pipes because of the hostile conditions, dimensions, and the general lack of distinctive visual and/or structural features. Standard indoor localization techniques (e.g. visual SLAM) do not perform well in pipelines given the lack of exploitable visual features, while outdoor techniques (Global Positioning System (GPS) in particular) do not work inside metal pipes or tunnels. In this Chapter, we present an RF odometry-like method to localize a robot along a pipe (1D localization), using an RF signal transmitter and a receiver, and the setups explored in the previous Chapters to obtain periodic fadings. The robot counts the number of RF received-power maxima and minima encountered to estimate its position from the transmitter along the pipe, given the (theoretically determined) period of the fadings. The method is tested experimentally with ground robots in a small-scale pipe and in a real large-scale drainpipe. We also present the results of propagation in bent pipes and in pipes with one closed end, to extend the methodology for pipes such as those encountered in hydro electric power stations. Subsequently, we suggest methods to address propagation-related issues characteristic of tunnels, such as localization in the messy near sector, and show preliminary results of a hexrotor flying inside the Somport tunnel.
There are two main advantages of the proposed system. First, the sensors are easy to install and can be used with any (ground, aerial) robot. Second, as the fadings obtained are periodic, the method avoids cumulative errors in localization.

5.1 Introduction

Regular inspections of pipe environments, such as sewers, Liquefied Natural Gas (LNG) pipelines, gasoducts, and dam drainpipes, are required in order to identify rusty areas and to prevent fissures, or to locate and repair cracks and leakages that could compromise the whole infrastructure and cause economic damage and even loss of life.

Due to the nature of such environments, which are commonly dark, humid, and dusty, and other limitations such as the physical dimensions, robots are the most suitable and sometimes the only possible devices capable of performing inspection tasks. In this context, determining the position of the robot inside the pipe is necessary to help localizing the affected area to subsequently repair the damage. Unfortunately, due to the previously discussed nature of the environment and other aspects such as the Faraday cage effect, the number of sensors that can be used to provide useful information for localization is severely reduced. Although it is not difficult to localize a robot in the cross-section dimensions with a laser sensor, for instance, localization along the longitudinal axis (length) remains a problem as pipes are much longer than they are wide.

In [Hansen 11], the longitudinal position inside a pipe is estimated using monocular cameras and implementing visual odometry algorithms (dense and sparse). Similarly, [Lee 09] and [Lee 11] recognize landmarks to localize a robot inside a small pipe. However, such algorithms can only work if there are identifiable surface features or irregularities such as rust. A similar problem arises with SLAM, which need to find and match features in order to reduce the localization uncertainty. Nevertheless, if the pipe is smooth and lacks either visual or texture features for cameras or lasers (as is the case in penstocks in hydro electric power stations), the localization uncertainty will continuously increase and cannot be easily reduced without loop closure.

Other methods rely on wheel odometry systems for localization, but pipes tend to be slippery due to their circular geometry, humidity, and the presence of fluids and mold. Hence, the robot wheels tend to slide, accumulating errors and thus making this system unreliable for position estimation. Besides, wheel odometers are not suitable for every kind of robots (such as aerial vehicles).

In this Chapter, the waveguide effect explored in the previous Chapters is used to design

and implement a localization methodology suitable for tunnel-like environments, based on the promotion of periodic fadings, using only an RF transmitter and a receiver. As the proposed system is completely independent of odometers, it can be implemented in wheeled or flying robots, as a potential solution for localization in inspection tasks with aerial robots such as in [Ozaslan 13]. Moreover, as a result of the periodic nature of the fadings, the RF signals data can be used alone or together with information from other sensors to correct or reset the position estimation errors accumulated by other systems.

5.2 Localization in Pipes

5.2.1 Algorithm Formulation

In the previous Chapters, the most suitable setups to obtain periodic fadings inside a pipe and a tunnel were explored. In particular, the effects of the operating frequency, as well as the transmitting and receiving antennas cross-section's positions and orientations were studied.

In the case of metallic pipes, recall Section 2.4, where two cases of study were highlighted: to propagate two or three modes (bimodal and trimodal propagation). In all cases, the fadings period is a function of the pipe diameter and the operating frequency, which has to be set higher than the n^{th} mode's cutoff frequency but lower than the $n^{th}+1$ mode's cutoff frequency in order to propagate n number of modes. Tuning the antenna position and orientation allows for enhancement of the excitation and detection of the modes of interest (in the case of trimodal propagation, to perceive the first and third modes while disregarding the second one).

While displacing the RF receiver from the transmitter, the basics of the algorithm is to discretely determine the distance traveled (one-dimensional localization in the longitudinal axis), by counting the fadings maxima and minima encountered (e.g. detecting the changes in the slope), creating some sort of RF-odometry. As two changes in the slope take place within one fading (minimum and maximum), the localization resolution is equal to one half of the (easily calculated) period of the fading. In this case, the shorter the period, the better the localization resolution. Finally, the direction of movement is used to increase or decrease the distance traveled after detecting the changes in the slope. Fig. 5.1 illustrates the algorithm by means of simulating bimodal propagation in a generic metallic pipe (although it can be extrapolated to

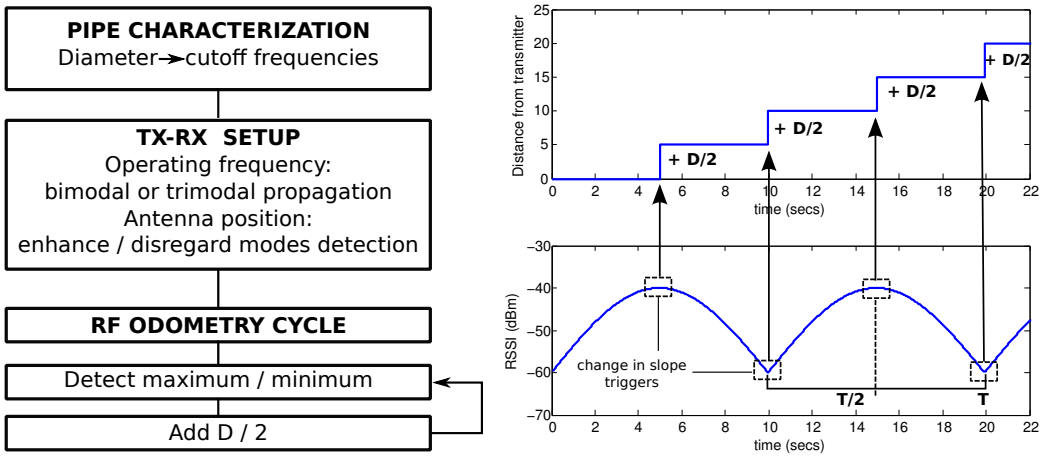

(a) Diagram (b) RF odometry

Figure 5.1: Discrete Localization: (a) Algorithm and (b) Example using a generic periodic signal. T denotes the time period of the fadings, and the dashed squares the changes in the slope used as triggers, adding $D/2$ to the current position each time detected (being D the spatial period of a fading).

Table 5.1: Experiments with Different Pipes

	Small pipes	**Gasoduct**	**Santa Ana dam drainpipe**	**Allatoona dam penstock pipe**
Diameter (m)	0.15	0.40	4	6
2nd mode f_c	1.5 GHz	574 MHz	57 MHz	38 MHz
3rd mode f_c	1.9 GHz	729 MHz	73 MHz	48 MHz
4th and 5th mode f_c	2.4 GHz	914 MHz	91 MHz	60 MHz
Bi-modal fadings period (m)	0.5	1.3	13	20
Three modes fadings period (m)	0.28	0.75	7.5	11

any periodic signal).

For practical purposes, Table 5.1 summarizes the most relevant characteristics of pipes in which we have performed measuring campaigns, such as the penstock pipe of the Allatoona dam (Georgia, USA), and common cases of study in the literature.

It can be seen that ranging from 6 to 0.15 m in diameter, the appropriate working frequencies vary from 50 MHz to 2.5 GHz, in order to obtain fadings with periods from 10 m to 0.3 m.

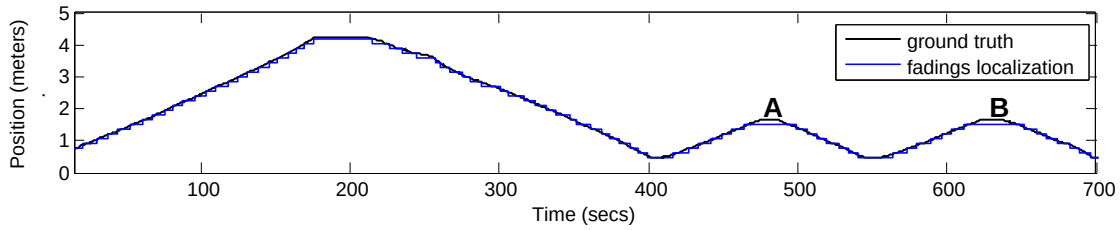

(a) Estimated position and ground truth

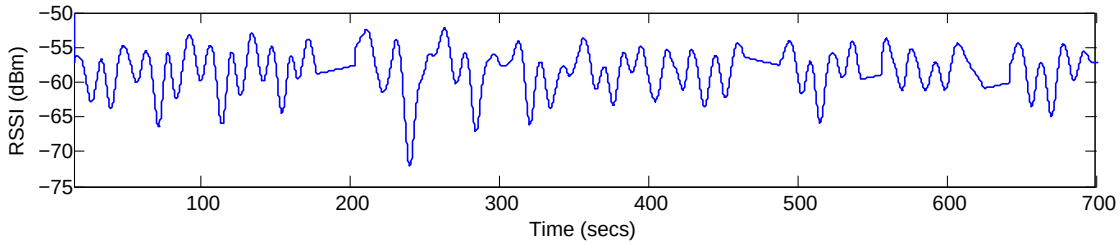

(b) Measured received power

Figure 5.2: Discrete Localization algorithm test in the small-scale pipe

Commercial devices operating at the mentioned frequencies are available for relative low cost (less than 500 euro for both the transmitter and receiver in the study performed at the Santa Ana dam, as an example), making them suitable for practical applications.

5.2.2 Experimental Evaluation in Pipes

5.2.2.1 Small-scale Pipe Experiment

The algorithm was first tested in the laboratory small-scale pipe, using a Continuous Wave Signal Generator as the transmitter (Agilent model E4432B), and a portable spectrum analyzer (RF Explorer model 3G) placed on the small motorized robot as the receiver (see Section 3.3.2). Based on the previous results, the configuration was chosen to propagate three modes (f=2.6GHz) under the C-H configuration for the transmitter (cross-section center with horizontal orientation) and the C-V configuration for the receiver (cross-section center with vertical orientation), yielding theoretical fadings period of 0.29 m and a discrete localization resolution of 0.145 m. Recall that despite the fact that all three modes are propagating inside the pipe, the tx-rx setup enhances the excitation and detection of the first and third modes, and hence the detected fadings are caused by their interaction.

In the experiment, the robot was programmed to run forward and backward several times, ending up in the same starting point. Fig. 5.2(b) shows the measured received power as a function of the time, and Fig. 5.2(a) compares the estimated position with the ground truth, obtained with the laser sensor pointing at the robot. For the position estimation, the theoretical fadings period was used (calculated with Eq. (2.16)).

Besides the discretization, Fig. 5.2(a) shows that the maximum errors occur at points A and B, with values of 0.143 and 0.144 m respectively. This situation occurs when the robot approaches a fading maximum or minimum, but changes direction before reaching the change in the slope (trigger). Fig. 5.2(a) also shows that the ending point corresponds to the starting point after several forward and backward travels, demonstrating that this method avoids cumulative errors since the fadings are stationary and periodic.

In this particular experiment the position estimation was done online. The receiver sampling frequency was 16 Hz and a moving average of 10 samples was applied to the received signal power, causing a delay of 0.625 s. Nevertheless, as the robot maximum speed is 0.025 m/s, this represents a maximum error at the longitudinal position of about 0.015 m caused by the filtering delay.

Although not the case with this experiment, it is true that mis-counting the number of maxima and minima that have been traversed (cycle slipping) would cause a more significant error in the position estimate. To deal with this situation, more complex approaches including a process model can be developed. For example, one might consider using a particle filter or a Kalman filter with the signal model and an Inertial Measurement Unit (IMU) to estimate the direction of movement, and potentially the acceleration, which can lead to better position estimates.

5.2.2.2 Large-scale Pipe Experiment

In order to check the validity of the proposed algorithm in a real situation, a Pioneer P3AT wheeled robot was used inside the large-scale drainpipe at the Santa Ana dam, simulating a service routine. The platform was equipped with two RF receivers (in order to exploit the spatial diversity, as will be explained later), as well as two odometers and a 180 degree SICK laser, which provide sensor data used in SLAM algorithms (Fig. 5.3(a)). As the pipe has no structural features, a series of landmarks were added at the the laser field-of-view level (separated 10 m one from each other) in order to implement standard localization algorithms for comparison

(a) Instrumented Pioneer P3AT robot inside the large-scale pipe

(b) Structural landmarks for laser localization

Figure 5.3: Large-scale pipe experimental setup

Figure 5.4: Map of the pipe obtained with the GMapping algorithm

purposes (Fig. 5.3(b)).

First, a map of the pipe was built to subsequently localize the robot. To this end, the GMapping algorithm was used [Grisetti 05, Grisetti 07, GMapping]. This algorithm is one of the most commonly used in the literature for map building and localization. Despite the presence of landmarks, Fig. 5.4 evidences that the obtained map is curved, even though the pipe is straight and the robot traveled in a straight line. The map was then corrected and refined with knowledge of the pipe geometry and landmarks spacing.

For the RF odometry, the trimodal propagation was chosen over the bimodal case to obtain shorter period fadings. The selected frequency was f=71MHz, producing fadings with a theoretical period of 8.2 m and a discrete localization resolution of 4.1 m. The transmitter antenna was placed horizontally at 1 m from the soil, and the two receivers at 1.5 m and 2.5 m in height (0.5 m upper and below the pipe center). Under this configuration, it is expected a relative phase difference of about 180 degrees between the receivers (as seen in Section 2.5), a property that will be exploited to improve the localization resolution.

In the experiment, the instrumented robot was displaced inside the pipe up to 70 m from the transmitter, streaming the data from the sensors to a computer running ROS over Ubuntu

12.04. Fig. 5.5(a) shows the results for the position estimation using four methods. The black line shows results from the localization method used in [Lazaro 10], which mixes information from the odometers and the laser sensor over the previously built and corrected map of the pipe. We consider this as ground-truth. The blue line shows the discrete position estimation from the fadings localization algorithm (with a resolution of half of the period of the fadings), using just one of the RF receivers. The fadings maxima and minima of the signal shown in Fig. 5.5(b) were used as triggers. The green line shows a purely odometric position estimation (which is the result of removing the landmarks for the laser). It is clear that the error of the pure odometric estimation accumulates with the distance, while the fadings estimation error is discrete and bounded (disregarding mis-counting the fadings maxima or minima).

Moreover, Fig. 5.5(c) shows the measured received power with each of the two receivers. It corroborates the expected relative phase difference of 180 degrees (a maximum in one signal that matches a minimum in the other). In this case, two more triggers can be perceived within a fading: where the two signals cross each other. These two extra triggers allow us to improve the localization resolution from one half the period of the fading to one quarter, shown in red in Fig. 5.5(a).

5.2.3 Considerations for Dam Penstock Pipes: Elbows and Closed-ends

Consider the case of a quadrotor used for penstock pipes inspection, such as in [Ozaslan 13]. These pipes usually have one or two straight parts and an inclined one. The segments are joined by elbows. Also, one of the extremes is closed with a penstock to prevent flooding from the lake when performing inspection or repairing labors. Fig. 5.6 shows the schematics of the Glen Canyon Dam, in Arizona, highlighting the elbows and penstock.

To evaluate the applicability of the method in such environments, as well as in others with similar characteristics, a series of experiments was performed.

5.2.3.1 Propagation in Bent and Irregular Pipes

To evaluate if the guided wave propagation would be preserved in bent pipes, a series of experiments were performed in both rigid and corrugated metallic pipes of about 0.125 m in diameter

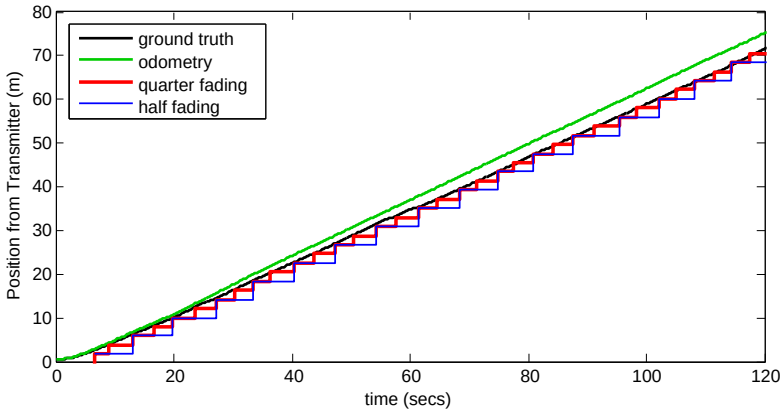

(a) Position estimation

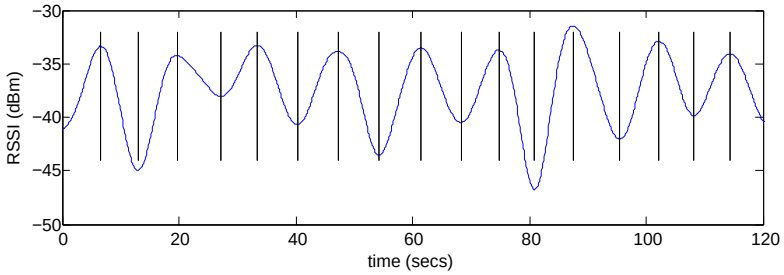

(b) Signal fadings using one receiver. The vertical lines denotes the triggers

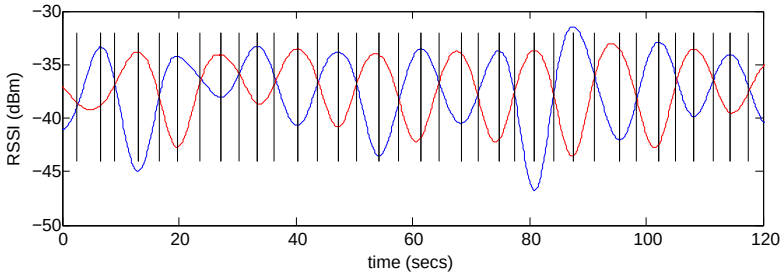

(c) Signal fadings using one receiver in the upper half and one receiver in the lower half of the pipe.

Figure 5.5: Comparison of localization methods in the large-scale pipe

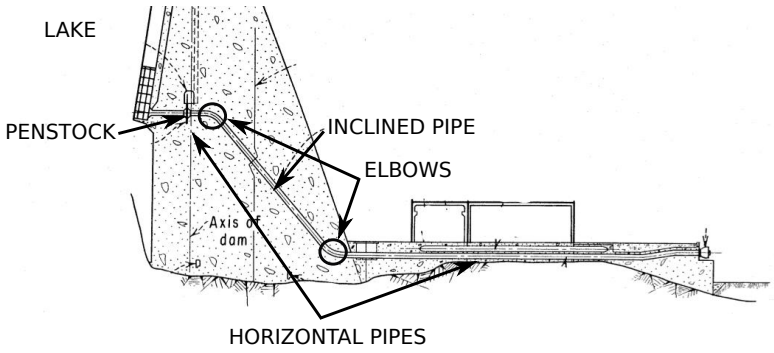

Figure 5.6: Schematics of the penstock pipe at the Glen Canyon Dam, Arizona, USA [GlenDam]

(used for commercial heating and air conditioning installations). In particular, the effects of the elbows on the fadings period was analyzed. Four cases of study were contemplated: a 90°elbow in a rigid pipe (Fig. 5.7(a)), a 90°elbow in a corrugated pipe (Fig. 5.7(b)), a 90°+ 90°elbows (Fig. 5.7(c)), and finally a 90°+ 180°+ 90°elbows (Fig. 5.7(d)).

The transmitter was placed in horizontally in the pipe center (C-H) and the receiver vertically in the pipe center (C-V). The frequency was set to 2.65 GHz to induce trimodal propagation. In all cases, the transmitter was placed in the straight segments before the first elbow, and the received signal power measured in the whole straight segment after the last elbow. Measurements in the elbow itself were not possible due to dimensional limitations of the receiver within the pipe.

It can be seen that in all cases, the fadings period is maintained and its mean value is about 0.3 m, matching quite well with the simulations of the same signal propagating in the equivalent ideal metallic pipe.

The signal is noisier compared to the previous experiments in rigid pipes, though. This may be caused by the non-uniformities and reflections in the elbows. Hence, as the slope detector may become inaccurate as a trigger, filtering approaches including the signal propagation model should be explored to detect the fadings maxima and minima.

5.2.3.2 Standing Wave for Closed-end Pipe

As in penstock pipes, consider the case of a pipe with one or both extremes closed. In this situation, the propagating wave will reflect off the closed end and travel in the opposite direction

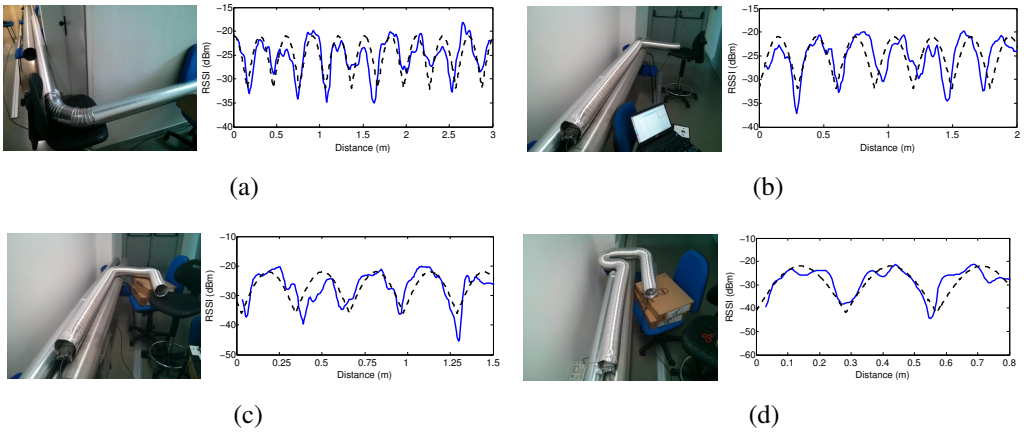

Figure 5.7: Received-signal fadings in bent pipes: (a) rigid pipe and 90°elbow (b) corrugated pipe and 90°elbow (c) corrugated pipe and 90°+ 90°elbows (d) corrugated pipe and 90°+ 180°+ 90°elbows. The black dashed line represents the simulation in a smooth metallic pipe.

of the incident wave, producing interference and hence a standing or stationary wave pattern.

To avoid interference with other modes, the most adequate setup to obtain a strictly periodic and well defined fadings structure is to propagate the dominant mode (monomodal propagation). Unlike the case of monomodal propagation in a pipe with both extremes open (where a signal with low attenuation and no fadings was obtained, see Fig. 2.7 in Section 2.4.1), this case will produce a periodic structure caused by the standing wave. The period of the fadings is one half of the wavelength of the signal in the pipe (λ_g)

$$D = \frac{\lambda_g}{2} = \frac{c}{2f\sqrt{1-\left(\frac{f_c}{f}\right)^2}} \tag{5.1}$$

where f_c is the cutoff frequency of the first mode in the case of monomodal propagation (recall Section 2.2 for more details). In this situation, the period of the standing wave is actually shorter compared to the fadings period of bimodal and trimodal propagation. This allows to improve the discrete localization resolution of the RF odometry even more.

Fig. 5.8 shows a comparison between the fadings due to a standing wave, created when one of the extremes of the pipe was blocked with a metallic plate, and those due to bimodal and trimodal propagation. It can be seen that the fadings period is shorter compared to the other cases.

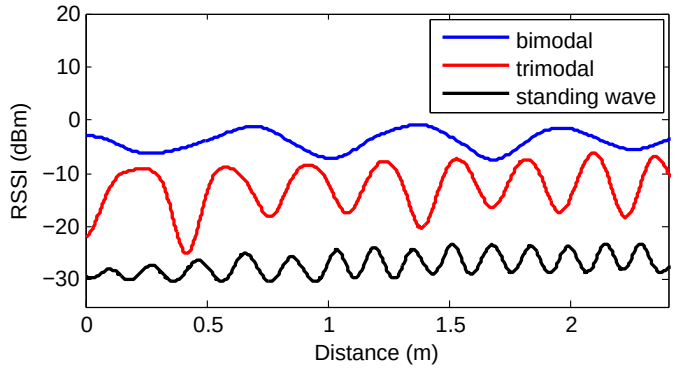

Figure 5.8: Fadings inside a pipe caused by: bimodal and trimodal propagation, and a standing wave. The signals are offset for clarity.

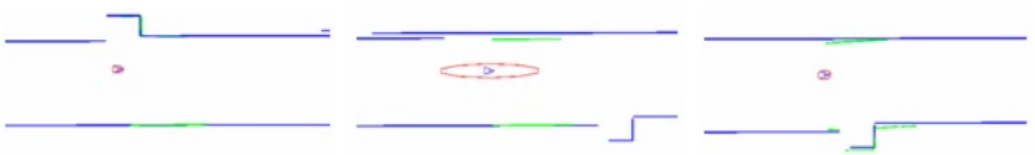

(a) (b) (c)

Figure 5.9: Localization inside tunnels using laser data (green) over a previous built map (blue). The uncertainty (red ellipse) continuously grows from (a) to (b) in the absence of lateral shelters, until the laser matches a new one (c).

5.3 Localization in Tunnels

Similar to the case of pipes, the hostile conditions, GPS-denied nature, and lack of visual and structural features make standard localization techniques perform erratically in tunnels. If not for the periodic emergency shelters in the Somport tunnel (a special characteristic of our test bed), the localization uncertainty caused by the absence of features would continuously grow. Fig. 5.9 illustrates the situation, where the localization algorithm described in [Lazaro 10] was used to localize a Pioneer P3AT robot over the tunnel's map (in blue) using laser data (in green). It can be seen that at just 25 m (the distance between adjacent emergency shelters), the uncertainty ellipse (in red) continuously grows in the longitudinal axis of the tunnel up to one meter in the major axis (Fig. 5.9(b)), up until the moment where the laser matches the subsequent shelter (Fig. 5.9(c)).

In this situation, the information from the RF sensors can be used to estimate the position

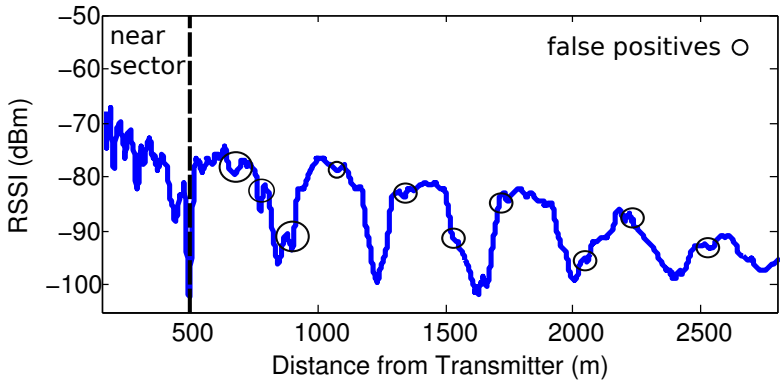

Figure 5.10: Near sector and false positives (change in the slope that may be detected as a maximum or minimum), using a real 1800 MHz signal in the Somport tunnel.

(as previously) or to correct the accumulated error from other sensors, such as odometers. The fadings maxima and minima would play the same role as the emergency shelters in the Somport tunnel, allowing for correction or reset the odometric errors periodically.

Nevertheless, recall from Chapter 3 that in order for these scenarios to behave as a waveguide, the wavelength of the signal has to be much smaller than the tunnel cross section, which allows the propagation of a large number of modes that create the near sector (where the signal is characterized for rapid fluctuations). After the higher order modes have attenuated, the lower order modes survive, producing the periodic fadings useful for localization. However, the signal is susceptible to fast-fadings due to interfering modes, and consequently, the received fadings seem to be irregular. For these reasons, the fadings maxima and minima are not accurate recognized by detecting the change in slope, as previously done. Fig. 5.10 shows an example using a real 1800 MHz signal in the Somport tunnel.

In this section, the solutions to the problems associate to tunnels are theoretically addressed, showing some preliminary results in the Somport tunnel.

5.3.1 Transmitter-receiver Setup

In Section 3.4.1.6, the setups to create periodic fadings in tunnels were explored. In particular, the effects of the operating frequency and the antenna cross-section position were studied. The optimal position was determined by means of analyzing the modes' geometry, where the goal was to enhance the excitation and detection of the modes of interest while reducing the influence

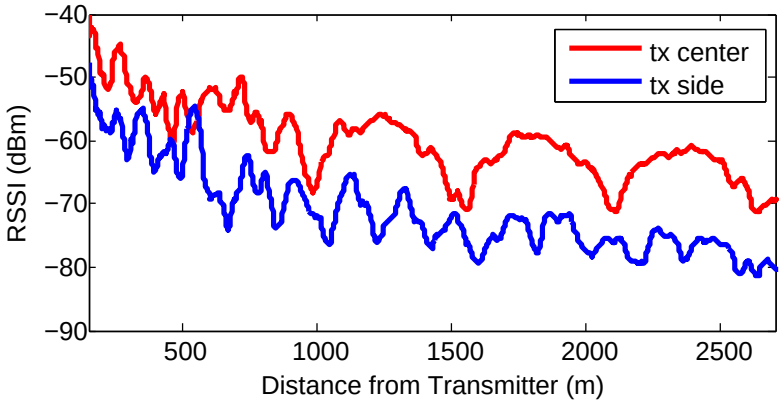

Figure 5.11: Effects of transmitter position. Measured received power at 2.4 Ghz with Tx on center and side. Signals are offset in the vertical axis for clarity.

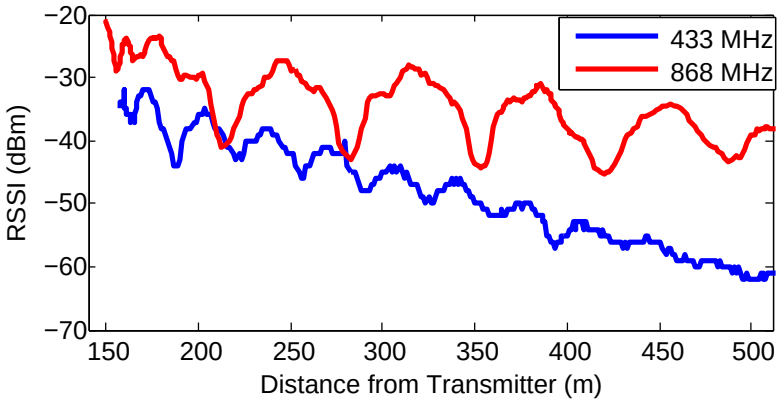

Figure 5.12: Effects of transmitter frequency. Measured received power with Tx on center at 433 and 868 MHz.

of the others.

Fig. 5.11 shows, as an example, the effects over the fadings period of different antenna positions (tunnel center and side) for a fixed frequency (2.4 GHz), while Fig. 5.12 shows two different frequencies (868 and 433 MHz) for the same transmitter antenna position (tunnel center). Summarizing, the shortest period fadings were obtained by placing the transmitter in the center of the tunnel (in both x and y). Also, the lower the frequency, the shorter the fadings period and *near sector* length, but the higher the attenuation rate.

5.3.2 Determination of the Fadings Period

After determining the transmitter setup to propagate the modes of interest, the fadings period is a function of the equivalent waveguide dimensions, which is not directly obtained from the actual tunnel dimensions. In the literature, these dimensions are obtained by finding the equivalent rectangle (or circle) that best reproduces the experimental measurements (e.g. the attenuation rate of the dominant mode). However, if a previous measuring campaign has not been performed (as is the most probable case in an emergency situation), the equivalent dimensions would not be able to be determined, and consequently, neither could the fadings period.

To solve this issue, an analysis of propagation using the FEM was performed in Chapter 3.5. Results show that the FEM treats the problem as 2D to obtain the propagation constants and consequently the fadings period (even more accurately than with the rectangular approximation) quickly using computers with common processing power nowadays. In order to do this, only the real profile of the tunnel is required, which can be obtained, as in our case, with a laser scanner range sensor.

5.3.3 Navigation Path Constraints Caused by the Transversal Fadings

In Section 3.4.2, the transversal structure of the fadings was determined by interpreting the interacting modes' geometry, dividing the tunnel in two sectors if the transmitter is placed in the *side position* (exciting modes 1 and 2), or in three sectors if it located in the center (exciting modes 1 and 3). Within each sector, the longitudinal fadings have the same relative phase. Hence, in order to benefit from the periodicity of the fadings to localize, it is important to travel in a straight line and within one of the above mentioned sectors. Spatial diversity schemes to improve the communications while benefiting from the periodic fadings to localize will be addressed in Section 5.4.

5.3.4 Preliminary Experiments

To test the concepts in a practical experiment, a DJI F550 hexrotor was used as a moving receiver. It was instrumented with the portable spectrum analyzer previously used and connected

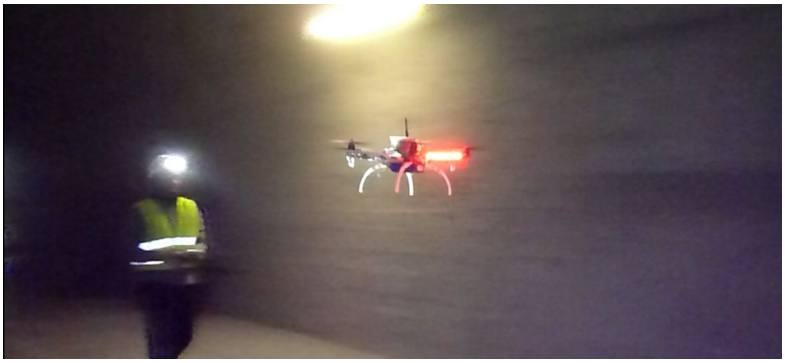

Figure 5.13: Preliminary experiments of localization in the Somport tunnel with a hexrotor.

to an onboard computer (RaspberryPi model B) running a version of ROS for RASPBIAN operating system. The transmitter antenna was placed in the center of the tunnel, and the operating frequency was set to 868 MHz. It was corroborated that the electronic motors and speed controllers did not interfere with the receiver at this working frequency. This setup produces periodic fadings with a theoretical period of about 68 m.

The hexrotor's cross-section position was kept in the tunnel center, and it was flown in a straight line along a 550 m segment, approximately at a constant speed. A snapshot of the experiment is shown in Fig. 5.13.

Two trials were performed to evaluate the repeatability of the results, shown in Fig. 5.14, along with the results of a simulation of the same signal propagating in the equivalent hollow dielectric waveguide. The power coupling and received power was calculated as explained in Section 3.2.

Although a high resolution point-by-point numerical comparison is not yet possible as the complete system is in the development stage, according to modal theory, a number of eight fadings should appear in the 550 m traveled (Fig. 5.14). In the experiments, the measured power was plotted over the same covered distance assuming a constant speed, and it can be seen that the 8^{th} is almost but not completely appreciated (i.e. the 8^{th} fading trigger has not been detected yet). In a discrete algorithm such as the one previously explained, this would translate into a 6.2% localization error over the whole covered distance.

Based on the agreement between the received signal and the simulation, we believe that filtering approaches, such as using a Particle Filter or Kalman Filter with the signal propaga-

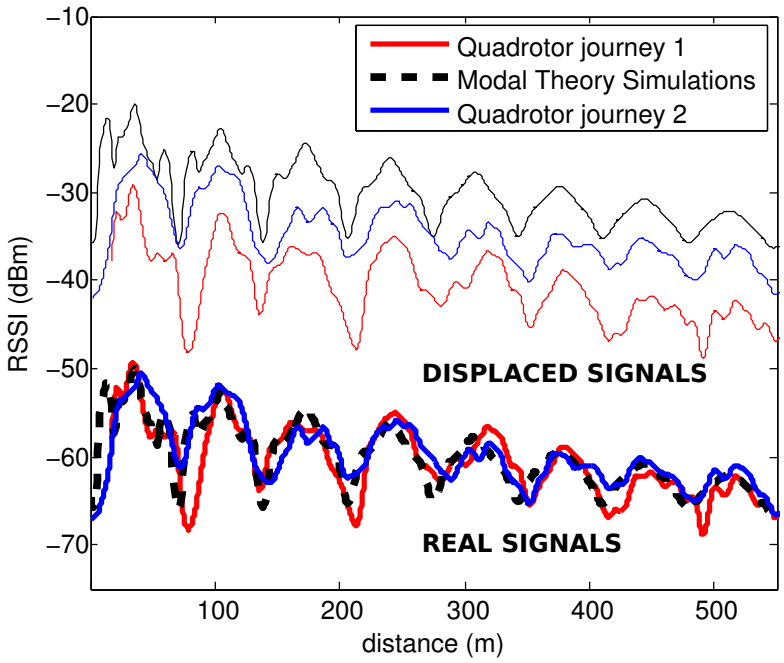

Figure 5.14: Measured signal power with the hexrotor and Modal Theory previous simulations (displaced and overlaid with the experimental results to notice the agreement).

tion modes and an IMU to estimate position, can lead to precise localization in this kind of environments.

5.3.5 Exploiting the Transversal Structure of the Fadings to Improve the Localization Resolution

As in the case of pipes, by exploiting the transversal structure of the fadings, the localization resolution of the method can be improved. Fig. 5.15 shows, as an example, the measured received power at 2.4 GHz if two receivers are placed in different halves (keeping the transmitter in the *side position*).

If only one receiver is used, for instance, the one located on the left side (blue signal in Fig. 5.15), only two triggers can be perceived within one fading distance. These triggers are denoted as $T1$, corresponding to the maximum and minimum value within one fading. Furthermore, by detecting two signals with a relative phase shift of 180 degrees, two more triggers can be perceived: where the two signals cross each other (denoted as $T2$ in Fig. 5.15). These two extra

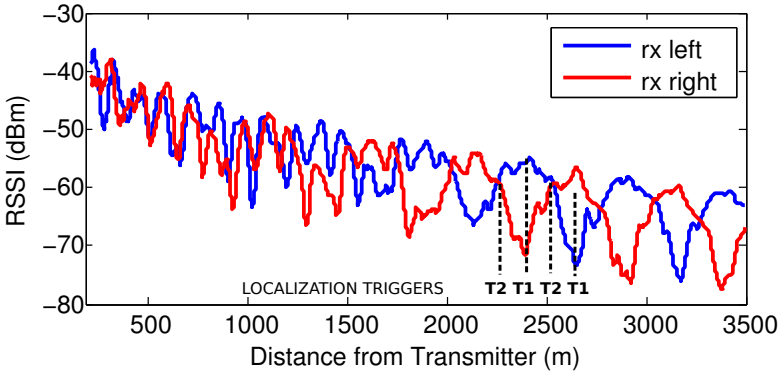

Figure 5.15: Measured Received Power at 2.4 GHz with two receivers in the right and left half of the tunnel (with tx on *side position*). T1 denotes the triggers due to the fading maximum and minimum, while T2 denotes the two extra triggers, where the signals cross each other.

triggers allow to improve the localization resolution from one half the period of the fading, to one quarter of the period of the fading.

5.3.6 Overcoming the Near Sector Issues

In order to cover longer distances, lower attenuation rates should be met by means of working at higher frequencies. This produces an elongation of the *near sector*, where multiple fast-fadings appear and accurate localization may be difficult to determine.

To overcome this issue, two signals - one at *low* frequency and one at *high* frequency - can be used simultaneously. As in the low frequency signal the *near sector* is shorter, it can be used to perceive the fadings and estimate the position during the *near sector* of the higher's frequency signal. Once exceeding this distance, the localization method can switch to localize with the high frequency signal.

Fig. 5.16 shows an example of such situation, where an 868 MHz signal was used to deal with a *near sector* of around 1 Km of a 2.4 GHz signal.

5.3.7 Multiple Fading Structures for Robust Localization

For more robust localization, the transmitting position or frequency can be multiplexed in order to obtain multiple fadings structures (n^{th} order),'at the same time', using n number of transmitters positions (appropriately chosen) or frequencies.

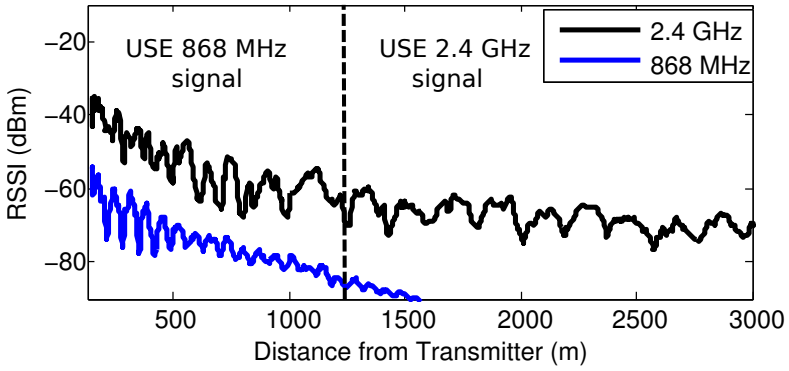

Figure 5.16: Low frequency and high frequency signals combined to overcome the near sector issues. The signals are offset in the vertical axis for clarity.

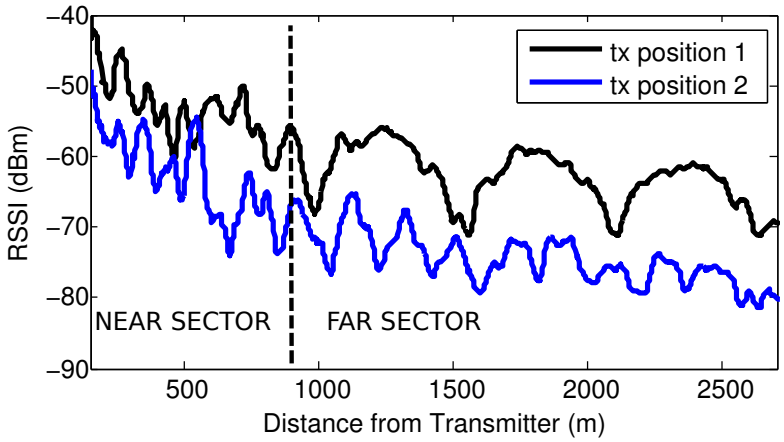

Figure 5.17: Received signals after multiplexing the transmission at 2.4 GHz. Each signal corresponds to a different transmitter position. The signals are offset in the vertical axis for clarity.

As an example of position multiplexing, one transmitter can be located in the center of the tunnel and another transmitter near to the tunnel walls (both positions studied in Section 3.4.1.6). This would yield a fading structure caused by modes EH_{11}^{y} and EH_{31}^{y}, and another structure with a different period caused by modes EH_{11}^{y} and EH_{21}^{y}. By means of multiplexing the transmission in the time domain, both fading structures can be detected using the same receiver.

The result of such system is shown in Fig. 5.17. In this experiment, two commercial WiFi devices (Ralink chipset network cards) were used as transmitters, placed in the above-mentioned positions. One laptop running Ubuntu 12.04 broadcasted frames every 5 milliseconds, multiplexing the transmission between the network cards. A *source* field was added to the transmitted

data packet to discern between emitters. The receiver (also a network card with Ralink Chipset placed on the all-terrain vehicle) was displaced 2700 m from the transmitter, maintaining the same cross section position (2 m in height, at 1/6 of the tunnel width from the left wall), and an average speed of 20 Km/h. Under this configuration, approximately one frame was received each 0.03 m, and hence one frame each 0.06 m coming from the same transmitter or position (which is one half of the wavelength of the signal at 2.4 GHz).

It is important to notice that the receiver should not be located in a position associated with a null component of the electric field of the interacting modes in order to perceive all the fading structures. In this example, the receiver was located at 1/6 of the tunnel width from the wall, where none of the interacting modes (EH^y_{11}, EH^y_{21} and EH^y_{31}) have null components (see Fig. 3.12 in Section 3.4.1.6).

5.4 Spatial Diversity Schemes

A localization technique based on traversing periodic fadings inside tunnel-like environments has been presented. However, if the received power is lower than certain threshold (usually determined by the correlation between the RSSI and other metrics, see Section 4.2.3), the connectivity with the base station may be compromised, causing a decrease in the PDR, data loss, or even complete loss of connectivity between the base station and the robot.

To deal with this situation in a multi-robot context, a fading-crossing navigation technique was presented in Chapter 4.3, where multiple robots are used as relays to cross the fadings while ensuring the connectivity with the base station at all times. If only one robot (with a single receiver) is available, other techniques must be explored, as those proposed in Section 4.6.

In this section, we consider the case of having more than one receiver per robot in order to propose spatial diversity schemes, exploiting the spatial structure of the fadings, with the final goal of perceiving the fadings for localization, while improving the communication with the base station.

Lienard et al. propose to replace the concept of spatial diversity with modal diversity on the basis that an increase in the channel capacity is related to the presence of several propagating modes [Lienard 06]. As the number of modes rapidly decreases with the distance, the authors claim that a full benefit from the spatial diversity can not be obtained at distances far from the

transmitter [Molina-Garcia-Pardo 08c]. However, our approach differs in that we aim to study the transversal fadings structure to establish a secure zone for communications. That is, instead of increasing the channel capacity, we ensure a link quality above a certain threshold to maintain the communication with a base station, while benefiting from the periodic fadings to localize.

The results in Section 3.4.2 show that the modes geometry directly determines the transversal fadings structure. In a multi-antenna context, in order to take full advantage of the *spatial diversity* in the *far sector* (i.e. to ensure a communication link above certain threshold), the involved modes' geometry should be taken into account when determining the separation between antennas. Moreover, what is actually relevant is not the separation between antennas, but their cross-section position in the tunnel.

Consider the case of placing the transmitter or base station in the *side position* (Fig. 3.1), and a single robot with two antennas as the receiver. By placing one of the receiving antennas in each half of the tunnel, a better quality link with the base station in comparison to the case of placing both antennas in the same half of the tunnel can be provided. As in [Lienard 03, Cocheril 09], the array elements is placed in the transverse plane instead of the longitudinal one, the latter yielding highly correlated fields.

Fig. 5.18(a) shows the received power by each of the antennas in such situation, where the difference between them can reach up to 25 dB. The horizontal dashed line denotes a RSSI threshold of about -70 dBm to ensure a PDR of 100%, as studied in Section 4.2.3. Notice that if only one of the antennas is chosen, there are several zones where the received power drops below the RSSI threshold, risking the connectivity.

Furthermore, Fig. 5.18(b) shows, in blue, the received signal power when the higher RSSI value between both antennas is chosen, and in red, the contrary case. This time, the blue signal is always above the RSSI threshold. By simultaneously using both antennas, it is possible to communicate securely (i.e. to establish a link above the RSSI threshold), as well as perceiving the fadings maxima and minima to localize. Moreover, as exposed in Section 5.2.2.2, it allows to improve the localization resolution of the discrete method by adding two extra triggers where two 180 degree delayed-signals cross each other.

Analogously, if the transmitter is placed in the center of the tunnel, one antenna should be kept in the central zone (*sector 2*) while the other can be located in any of the extremes (*sector 1* or 3) in order to benefit from the relative 180 degrees phase difference for both communication

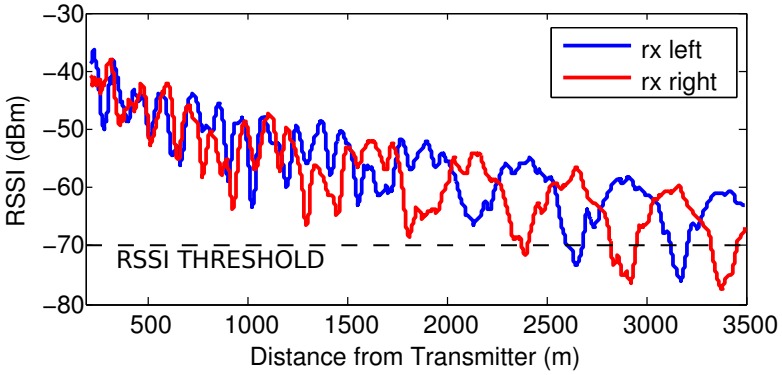

(a) Antenna from *sector 1* (blue) and *sector 2* (red).

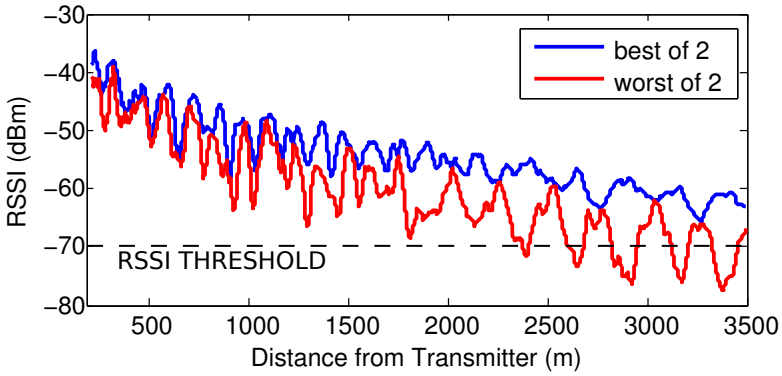

(b) Best and Worst of both antennas

Figure 5.18: Effects of spatial diversity over the measured received power.

and localization.

5.5 Practical Considerations

In order to implement the system and obtain an idea about its practicability, we have summarized the important aspects as follows:

- The sensors are easy to install and the system is suitable for any (ground, aerial) robot.
- In our cases of study, most of the chosen frequencies are part of the ISM band. Transceivers for these bands are commercially available for a relatively low cost.
- The transversal structure of the fadings can be exploited to improve the localization resolution (from one half of the period of the fading, to one quarter of it), allowing to add two

more triggers within one fading: where two 180 degree of phase-difference signals cross each other.

In the particular case of metallic pipes:

- The fadings period is given by the pipe diameter and frequency, which in turn determines the number of propagating modes. In order to propagate n modes, the operating frequency must be greater than the n^{th} mode cutoff frequency but below the $n^{th}+1$ mode cutoff frequency.
- Inside metallic pipes, the Faraday cage effect avoids interference from external RF sources, so that the received signal is low in noise.
- The maximum possible length to cover is given by the pipe diameter, material, and equipment sensibility. Metallic pipes have low attenuation rate. In our case of study, the Large-scale pipe was carbon steel with an attenuation rate of less than 9 dB/Km, and our low cost receiver has a sensibility of -105 dBm. This provides a maximum possible coverage length of several kilometers.
- In bent pipes, the fadings period is maintained in the straight parts despite the elbows, even in the case of using four 90 degree elbows.
- In pipes with one closed end, monomodal propagation produced a fading structure. In this situation, the wave reflects on the closed end and travels in the opposite direction, causing interference with the incident wave, hence producing a standing wave. The period of the fadings is shorter compared to the case of bimodal and trimodal propagation.

In the case of the tunnels:

- Modes EH^y_{11} and EH^y_{31} create shorter period fadings than modes EH^y_{11} and EH^y_{21}. The transmitter located in the center of the tunnel excites the former, while closer to the walls the latter. In the vertical dimension, the center of the tunnel is preferred over positions close to the soil/ceiling.
- The lower the operating frequency the shorter the fadings period and *near sector* length, but the higher the attenuation rate.

- Besides the operating frequency, for vertical polarization the fadings period is determined by the equivalent tunnel width, while the height influences much more in the attenuation constant. Using the FEM, the period can be previously determined with the actual tunnel profile, avoiding the time consuming (and not always possible) measuring campaign required by the Rectangular Approximation Method.

- Combinations of two or more signals (different frequencies and/or different transmitter positions) can be used to overcome the *near sector* issues and/or to achieve a more precise and robust localization.

- The agreement between the modal theory simulations and the experimental results suggest that a more precise localization can be achieved by means of including the model in a Kalman Filter or Particle Filter approach, as an example.

5.6 Summary

A RF odometry-like localization method designed for tunnel-like environments has been developed, based on the promotion of periodic RF signal fadings (repeatable and predictable). The robot counts the fadings maxima and minima traversed, and estimates its position from the transmitter given the known period of the fadings. The technique is non intrusive and does not require environment modifications (conversely to the case of a laser-based localization system inside a pipe). It requires an RF transmitter and a receiver for the simplest setup.

The method has been validated by means of experiments in two scenarios: a small-scale and a large-scale pipe. The method proved not to accumulate errors, contrary to the case of wheel odometry systems. In the large-scale pipe, the spatial diversity could be exploited to improve the localization resolution (from one half of the period of the fading to one quarter) allowing to add two more triggers within one fading: where two 180 degree delayed signals cross each other. Also, an extension for penstock pipes has been proposed by means of analyzing propagation in pipes with one closed end (where monomodal propagation yield a periodic stationary wave pattern, being the period shorter compared to the bimodal or trimodal case) and in bent pipes (where the period of the fadings weren't affected).

Discrete and non-discrete approaches can be implemented depending on the required accuracy. While this study only addressed the exploitation of the waveguide effect for discrete localization, clearly any real implementation would greatly benefit from filtering approaches including process models. For example, one might consider using a particle filter or a Kalman filter with the signal model and an IMU to estimate the direction of movement, and potentially the acceleration that can lead to better position estimates. The position estimation algorithm can use the maxima and minima in signal fadings as triggers to correct the position, as in the case of GPS + IMU systems, or to reset the accumulated errors with visual/wheel odometry systems. In order to adapt the methodology for tunnels, combinations of two or more signals (different frequencies and/or different transmitter positions) can be used to overcome the near sector issues and/or to achieve a more precise and robust localization. A preliminary experiment was performed with an hexrotor as the moving receiver. The agreement between the modal theory simulations and the experimental results let us believe that a more precise localization can be achieved by means of including the model in a Kalman Filter or Particle Filter approach, as an

example.

Finally, large-scale spatial diversity schemes were proposed to facilitate the navigation while improving the localization and communications. Contrary to the usual small-scale spatial diversity schemes found in the literature, in tunnel scenarios the transversal structure of the large-scale fadings deserves special attention that cannot be ignored when designing such techniques. Moreover, we have highlighted the importance not only of the separation between antennas, but its cross-section position.

Chapter 6

Conclusions

6.1 Conclusions

In this thesis, we have solved relevant robotic-related issues in order to provide some tools necessary for robotics exploration in tunnel-like environments under connectivity constraints. Although fadings in these confined environments are unavoidable and are considered a serious problem for communication purposes, we have shown an interesting way to address this issue by appropriately generating and detecting known-geometry periodic fading structures, demonstrating how to navigate to deal with these fadings to maintain the connectivity of the wireless network formed by robots and a base station, and how to benefit from the fadings' periodicity to localize in these challenging featureless environments. The thesis has a solid experimental background, validating the proposed algorithms in real environments.

First of all, we have performed an in-depth theoretical and experimental analysis of propagation in two of the most common tunnel-like environments: tunnels and pipes. In **Chapter 2**, we have analyzed wireless propagation in cylindrical metallic pipes with emphasis on the fadings phenomena. By adopting the Modal Theory approach, it was determined that fadings are caused by the interaction between the propagation modes, which propagate along the pipe with different wavelengths. Each pair of modes interact and produce a strictly periodic fading structure. Hence, the higher the number of propagating modes, the more complex the resulting fading structure. Therefore, the best manner to produce periodic fadings is to motivate the interaction between two propagating modes. By means of analyzing the interacting modes' ge-

ometry, as well as the electric field distribution, we were able to find optimal antenna positions and orientations that enhance the power coupled to a given mode, improving the modal excitation and detection. Experimentally the concepts were tested in a small-scale laboratory pipe, and in two large-scale real scenarios: the penstock pipe of the Allatoona dam (Georgia, USA) and a drainpipe in the Santa Ana dam (Castillonroy, Spain). In both cases, periodic fadings were obtained by propagating two or three modes (bimodal and trimodal propagation, respectively). The bimodal propagation yielded higher period fadings compared to trimodal propagation. In the latter, the fadings were produced by the interaction between the first and third mode, and the antenna setup allowed us to minimize the power coupled to the second mode, obtaining a well-defined periodic fading structure. Also, the transversal structure of the fadings was determined. The pipe was virtually divided in two halves (vertically or horizontally), and depending on the chosen setup, the received fadings corresponding to each sector were in phase or presented a relative phase difference of about 180 degrees (i.e. where a maximum in one fading matches a minimum in the other). Propagating more than three modes yielded more complex structures due to the mutual interaction among all the modes involved.

In **Chapter 3**, we performed an extensive analysis of wireless propagation in a horseshoe-shape dielectric tunnel, again, emphasizing the fading phenomena. Firstly, we performed a classical study of propagation in tunnels, as in the literature, highlighting the presence of the near and far sectors, and fast and slow fadings. To do so, we introduced the use of the wavelet as a powerful tool to analyze propagation in tunnels, which allowed us to observe all the above mentioned characteristic in one graph. Analogous to the case of pipes, we studied the modal excitation as a function of the modes' electric field distribution, allowing us to determine the transmitter positions to motivate the appearance of noticeable and well defined periodic fadings. In the transversal dimension, the received-fadings' structure was directly determined by the present modes' electric field distribution, allowing us to divide the tunnel in sectors in which the fadings are in phase, or present a phase difference of 180 degrees. We also demonstrated that these fadings are repeatable in the temporal and spatial domain, a result relevant for localization and navigation.

To perform the modal analysis, the tunnel was modeled as a rectangular waveguide, where we used the rectangle dimensions that best reproduce the experimental measurements, as in the literature. The concordance between the predictions and the experimental results allowed us to

validate the usefulness of this method in a wide range of frequencies. Nevertheless, the drawback is the requirement of a previous measurement campaign. We have provided a validation of the method using the FEM. Although this method is traditionally viewed as extremely memory demanding and time consuming, we proved that in uniform tunnels, the variables of interest (phase and propagation constants) can be obtained through a 2D analysis instead of in three dimensions. This reduces the computation time to a few minutes with computers with common processor power. Comparing both methods to experimental results from our measuring campaigns and examples from the literature, the FEM produced more accurate results. Besides, the FEM solution requires only the tunnel cross section (easily obtained, for example, with a laser sensor at the entrance of the tunnel), and thus will be able to predict the fadings period, avoiding the time consuming measuring campaign required by the Rectangular Approximation Method.

Comparing both tunnel scenarios, in metallic waveguides there is a well specified cutoff frequency for each propagating mode, and it is possible to choose a frequency to propagate the desired number of modes. In the case of dielectric tunnels, there is no a well-defined cutoff frequency for each mode. In order for dielectric tunnels to behave as waveguides and to achieve a wireless communications coverage area in the order of kilometers, the wavelength of the operating frequency has to be much smaller than the tunnel cross-section. This causes multiple modes to propagate, producing a near sector where the signal is characterized by rapid fluctuations. To observe the well-defined periodic fadings, the higher order modes must attenuate up to a point where only the lower modes survive.

Once the setups to obtain predictable periodic fadings were explored, and after determining its structure in the cross-section, in **Chapter 4** we have presented a technique for deploying a team of robots for tunnel exploration. In particular, our technique maintains connectivity of the network formed by the robots and a base station at the entrance of the tunnel. In order to ensure a PDR as close as possible to 100%, the received power level must be maintained above a certain threshold. The robots traveled in a straight line (1D navigation) and used each others as relays to go across the slow fadings. The system was evaluated by simulations and real experiments, conducted over a length of three kilometers of the tunnel. The network connectivity was maintained during the real experiment, guaranteeing the existence of a safe path among all the robots at all times. Although the deployment used the signal parameters characterized in the previous Chapters to particularize the strategy to the specific scenario, the algorithm is general

and can be adapted to any tunnel-like fading environment. Moreover, the received-power was measured by the robots to plan, in real time, the deployment of the leader and follower robots (acting as repeaters). On the other hand, if only one robot is available for the tunnel exploration, a 2D navigation algorithm was proposed to improve the communications with the base station, compared to the case of a single robot traveling in a straight line. Taking into account the transmitter setup, the robot should follow a zig-zag navigation path, traveling from maxima in one of the mentioned sectors (according to the transversal structure of the fadings) to maxima in the other sectors, avoiding the valley zones (fadings minima).

The localization of the robots during the navigation experiments described in **Chapter 4** was possible as a result of the identification, using laser sensors, of periodic emergency shelters characteristic of the Somport tunnel. However, in the absence of these shelters (as is the case of most tunnels), the laser would only detect two featureless straight lines. Hence, the odometric error accumulated along the tunnel would not be able to be corrected. Moreover, if an aerial robot is used instead, no reliable localization system can be used inside the tunnel: the lack of structural features, the darkness, the GPS-denied nature, and the impossibility of carrying wheel odometers disable the possibility of using standard localization algorithms based on lasers, cameras, GPS, or odometers. To solve this situation, in **Chapter 5**, we presented an RF odometry-like localization method designed for tunnel-like environments that benefits from the (proved repeatable) periodic fadings obtained in the previous setups. The robot counts the fadings maxima and minima traversed and estimates its position from the transmitter with previous theoretical knowledge of the period of the fadings. The discrete resolution of the method is half of the spatial period of the fadings, which is the distance between two consecutive triggers (maximum and minimum). Several experiments were conducted to validate the algorithm in two scenarios: a small-scale laboratory pipe and a large-scale drainpipe in the Santa Ana dam. As a consequence of the stationarity of the fadings, the method proved not to accumulate errors, contrary to the case of wheel odometry systems. Furthermore, in the large-scale pipe, the transversal structure of the fadings could be exploited to improve the localization resolution (from one half of the period of the fading to one quarter) by adding two more triggers within one fading: where two 180 degree delayed signals cross each other. In addition, to extend our method to penstock pipes, we analyzed propagation in pipes with one closed end (where monomodal propagation yield a periodic stationary wave pattern, being the period shorter compared to the bimodal or trimodal

case), and in bent pipes (where the period of the fadings were not affected by the presence of elbows).

In order to adapt the methodology for tunnels, characterized for the presence of a near sector and a noisier received signal, we proposed using combinations of two or more signals (different frequencies and/or different transmitter positions) in order to obtain several fading structures with different periods and near-sector length.

Finally, large-scale spatial diversity schemes were proposed to facilitate the navigation while improving the localization and communications. Contrary to the usual small-scale spatial diversity schemes found in the literature, in tunnel scenarios the transversal structure of the large-scale fadings deserves special attention that cannot be ignored when designing such techniques. Moreover, we have highlighted the importance not only of the separation between antennas, but its cross-section position.

6.2 Ongoing and Future Work

Wireless propagation inside tunnels also depends on the antenna polarization. In this work, we only considered vertical polarization in the Somport tunnel, benefiting the excitation and detection of EH^y modes (**Chapter 3**). In that case, the fadings period is a function of the tunnel width (Eq. 3.9), and the fadings present a phase difference along the tunnel cross-section. On the other hand, horizontally polarized antennas enhance the excitation and detection of the EH^x modes. As a result, the fadings period becomes a function of the tunnel height. Hence, if the tunnel does not have a square-equivalent geometry, as it is the case of most tunnels, different period fadings can be obtained also by means of changing the antenna polarization.

As an extension of this work, we propose to perform a study of the fadings with different antenna polarizations, which can yield different period fadings for the same antenna position and operating frequency. This can provide more robustness to the localization method presented, extending the frequency and position multiplexing strategies, to polarization mutiplexing.

Also, as a consequence of using horizontal polarization, the transversal fading structure presented in **Chapter 3** is rotated 90 degrees, translating the latter to the vertical dimension, and viceversa. This opens a new research area, where aerial robots can be used to extend the navigation methodologies presented in **Chapter 4** for 1D and 2D spaces to the 3D domain.

The localization algorithm explored in **Chapter 5** represents a discrete solution to estimate the position of a robot inside tunnel-like environments. As the RF fadings maxima and minima can only be detected once the fadings are crossed, a delay is introduced, which depends on the RF receiver sampling rate, the filtering, and the robot speed. The algorithm works adequately on the premise that the signal is not noisy, as was the case of propagation inside pipes presented in this work. Nevertheless, noise in the received signal due to erratic behavior of the hardware, or reflections of the propagating signal due to irregularities in the pipe, can cause variations in the received RF power that can be erroneously interpreted as a fading maxima or minima.

To solve this problem, we are currently investigating more robust solutions. As a first approach, we are using a ground robot and we are implementing a particle filter that includes information about the propagation model and position estimation from the odometers. This makes the localization method continuous, while still correcting the accumulated odometric errors with the strictly periodic fadings model. In a near future, the goal is to implement the system on aerial robots for inspection and surveillance tasks. To do so, we are currently working in collaboration with the GRASP Laboratory at the University of Pennsylvania. We propose using information from an IMU to estimate the direction of movement and acceleration information to estimate the displacements. It is well known that IMU systems also accumulate errors over short periods of time and are traditionally reset with other sensors such as GPS. In our case, we propose using IMU, the RF sensors, and the propagation model together to accurate estimate the position of the robot inside the pipe. This method could also be adapted to correct the errors accumulated by visual odometry systems.

Since the signal is typically noisy in tunnel environments, the algorithm requires a more robust localization method that includes the propagation model, as previous discussed. In addition, the methodologies proposed in **Chapter 5** to deal with localization in the messy near sector still need further development and experimentation. These will also be explored in future work.

6.3 Conclusiones

En esta tesis hemos resuelto problemas relevantes para la robótica, con el fin de proporcionar herramientas necesarias para la exploración con robots en entornos tipo túnel, bajo restricciones de conectividad en términos de comunicaciones. A pesar de que los desvanecimientos o *fadings* de las señales RF en estos entornos confinados son inevitables, y son considerados un problema serio para las comunicaciones, hemos mostrado una forma interesante de abordar esta problemática, generando y detectando *fadings* periódicos de estructura conocida y predecible. También mostramos cómo navegar para lidiar con estos *fadings* mientras se mantiene la conectividad de la red formada por los robots y una estación base, y cómo beneficiarse de la periodicidad de los *fadings* para localizarse en estos entornos problemáticos. La tesis tienen un sólido soporte experimental, validando los algoritmos planteados en entornos reales.

Primeramente, realizamos un análisis teórico y experimental sobre la propagación en los dos entornos tipo túnel más comunes: túneles y tuberías. En el **Capítulo 2**, analizamos la propagación inalámbrica en tuberías cilíndricas metálicas, con énfasis en el fenómeno de los *fadings*. Tomando como base la teoría modal, se estudió que los *fadings* son causados por la interacción entre los *modos*, que se propagan por la guía con diferentes longitudes onda. Cada par de modos interactúa y es responsable de una estructura estrictamente periódica de *fadings*. A mayor número de modos, más compleja es la estructura espacial del campo electromagnético resultante. Por tanto, la mejor forma de generar *fadings* periódicos es facilitar la interacción entre dos modos. Analizando la distribución de campo eléctrico de los modos presentes, se optimizaron las posiciones y orientaciones de las antenas para mejorar la potencia acoplada a los modos de interés. En el caso de la tubería, se obtuvieron *fadings* periódicos propagando dos y tres modos (propagación bimodal y trimodal). La propagación bimodal genera *fadings* de mayor periodo que la propagación trimodal. En esta última, los *fadings* se producen por la interacción entre el primer y tercer modo. La configuración de las antenas nos permitió minimizar la influencia del segundo modo para obtener una señal limpia y estrictamente periódica. También se determinó la estructura de los *fadings* en la sección transversal de la tubería. Ésta se dividió virtualmente en dos mitades (horizontal y verticalmente), y dependiendo de la configuración de las antenas, los *fadings* de cada mitad presentan, o no, una diferencia de fase de 180 grados respecto a la otra mitad. Experimentalmente, los conceptos fueron probados en una tubería de pequeña escala en

el laboratorio, y en dos entornos reales: una tubería de la represa de Allatoona (Georgia, EUA), y la tubería de drenaje del Embalse Santa Ana (Castillonroy, España).

En el **Capítulo 3**, se realizó un análisis extenso de propagación inalámbrica en un túnel de sección transversal con forma de herradura. Se realizó un estudio clásico de propagación en túneles, destacando la presencia de los sectores cercano y lejano, y de *fadings* rápidos y lentos, como en la literatura. Para ello, se presentó el uso de las Wavelets como herramienta de análisis, que permitió observar las principales características de la propagación en túneles en un solo gráfico, constituyendo una herramienta poderosa para este tipo de estudios. Posteriormente, análogo al análisis en tuberías, se estudió la excitación modal en función de la distribución del campo eléctrico de los modos de interés, permitiendo obtener las posiciones de la antena transmisora para motivar la aparición de *fadings* periódicos y bien definidos. En la dimensión transversal, se determinó la estructura de los *fadings* utilizando, igualmente, la distribución de campo eléctrico de los modos presentes, permitiendo obtener *fadings* con diferencias de fase en función de la posición del receptor en la sección transversal. Se demostró que los *fadings* recibidos son repetibles en el dominio espacial y temporal, un resultado relevante para esta tesis. Para el análisis modal, se modeló el túnel como una guía rectangular dieléctrica, y sus dimensiones equivalentes se hallaron como aquellas que mejor reprodujeron los resultados experimentales, como se suele hacer en la literatura. La concordancia entre las predicciones y los resultados experimentales nos permitieron validar la utilidad de esta aproximación en un rango amplio de frecuencias. Sin embargo, la desventaja principal es que requiere de una campaña de mediciones para poder determinar las dimensiones equivalentes, cuestión que no siempre es posible. Posteriormente validamos el método de aproximación rectangular usando el método de elementos finitos, considerado hasta los momentos como exigente en términos de memoria y procesador. Sin embargo, demostramos que en túneles uniformes, las variables de interés (constante de fase y atenuación) se pueden obtener a través de un análisis en dos dimensiones en lugar de tres, lo que reduce el tiempo de análisis a pocos minutos con computadores convencionales de hoy en día. Comparando ambos métodos con nuestras campañas de medición y resultados de la literatura, demostramos que el método de elementos finitos produce resultados más precisos. Además, para este tipo de análisis sólo se requiere la sección transversal del túnel, que se puede obtener, como en nuestro caso, colocando un sensor láser en la entrada del mismo. Esto permite predecir el periodo de los *fadings* sin tener que adentrarse en el túnel, evitando también las extenuantes

campañas de mediciones que requiere la aproximación de guía rectangular.

Comparando la propagación en ambos escenarios, podemos destacar que en las guías metálicas hay una frecuencia de corte bien definida para cada modo de propagación, y se puede seleccionar una frecuencia de operación para propagar los modos de interés. En el caso de túneles dieléctricos, no hay una frecuencia de corte para cada modo. Para que se comporten como guías de onda y alcanzar un rango de comunicaciones en el orden de los Kilómetros, la longitud de onda de la señal debe ser mucho más pequeña que la sección transversal del túnel. Esto causa que se propaguen múltiples modos, produciendo el llamado sector-cercano, donde la señal esta caracterizada por fluctuaciones muy rápidas. Para apreciar los *fadings* periódicos, debemos esperar a que los modos de orden superior se atenúen.

Una vez definidas las configuraciones de emisión y recepción para obtener *fadings* periódicos, y su estructura en las tres dimensiones, en el **Capítulo 4** se presentó una técnica de navegación multi-robot, con el fin de explorar un túnel mientras se mantiene la conectividad de la red formada por los robots y la estación base, localizada en la entrada del túnel. El nivel de potencia recibida se debe mantener por encima de cierto umbral para garantizar una PDR del 100%. En el despliegue, los robots viajan en línea recta (1D), y se utilizan unos a otros para cruzar los *fadings*, permitiendo así mantener la conectividad entre ellos. El sistema se evaluó primeramente en simulaciones, y posteriormente se realizó un experimento en una sección de tres Kilómetros del túnel de Somport. Se comprobó que la conectividad se mantuvo en todo momento, garantizando la existencia de un camino seguro, en términos de comunicaciones, en todo momento. A pesar de que el algoritmo se sintonizó con los valores del túnel de Somport obtenido en los capítulos anteriores, la estrategia es general y se puede adaptar a cualquier entorno tipo túnel que presente estas características. Más aún, a pesar de la sintonización de parámetros, se utiliza el nivel de potencia recibida, en tiempo real, para el planeamiento del despliegue. Por otra parte, si únicamente se dispone de un solo robot con un receptor, se propuso un algoritmo de navegación 2D con el fin de mejorar las comunicaciones con la estación base, comparando con el caso de viajar en línea recta a lo largo del túnel. Tomando en cuenta la posición del transmisor, el robot debe navegar en forma de zig-zag, de los máximos de uno de los sectores definidos por la estructura transversal de los *fadings* a los máximos de los otros sectores.

La localización de los robots en los experimentos previos de navegación multi-robot fue posible debido a la identificación, a través de sensores láser, de refugios de emergencia en el

túnel de Somport, características estructurales periódicas muy específicas de este túnel. Sin embargo, si el túnel carece de éstas, como es el caso de la mayoría, los errores acumulados por la odometría no se hubiesen podido corregir. Mas aún, si se utiliza un robot aéreo, carente de odómetros, no existe un método de localización confiable que se pueda usar dentro del túnel: la falta de características estructurales, oscuridad, y la naturaleza del entorno, dificultan la posibilidad de usar algoritmos de localización basados en láseres, cámaras o sensores GPS. Para resolver esta problemática, en el **Capítulo 5** se desarrolló un método de localización para entornos tipo túnel, basado en la periodicidad predecible y comprobada de los *fadings* en las configuraciones estudiadas. El robot cuenta el número de *fadings* que atraviesa, y con un conocimiento teórico previo del valor del periodo, estima su posición respecto al emisor. La resolución del algoritmo es de medio periodo de los *fadings*, distancia entre dos disparadores o *triggers* consecutivos (máximo y mínimo del fading). Se realizaron varios experimentos para validar el algoritmo en dos escenarios: una tubería de pequeña escala en un laboratorio, y una tubería de gran escala en el Embalse Santa Ana. Por ser los *fadings* estacionarios, el método demostró no acumular errores, contrario al caso de la odometría. Mas aún, en la tubería a gran escala, se pudo aprovechar la estructura transversal de los *fadings* (específicamente, dos señales con diferencia de fase de 180 grados), para mejorar la resolución del algoritmo, de mitad del periodo de los *fadings*, a un cuarto de este, permitiendo añadir dos *triggers* más cuando las señales desfasadas 180 grados se cruzan. También se analizó la propagación en tuberías con un extremo cerrado (donde la propagación monomodal produjo *fadings* de menor periodo que la propagación bimodal y trimodal), y tuberías inclinadas (donde las uniones no afectaron el periodo de los *fadings*), con el fin de extender la validez del método a tuberías en represas.

Para adaptar la metodología a túneles, donde la señal es mas ruidosa y existe un sector-cercano caracterizado por rápidas fluctuaciones, se propuso utilizar combinaciones de varias frecuencias y/o posiciones de emisor, de forma de obtener varias estructuras de *fadings*, de diferente periodos, alcances, y longitud del sector cercano.

Por último, se propusieron esquemas de diversidad espacial a gran escala, con el objetivo de facilitar la navegación mientras se mejora la localización y comunicación. Contrario al caso de los esquemas a pequeña escala, la estructura transversal de gran escala de los *fadings* en los túneles merece especial atención, que no se puede ignorar cuando se diseñan esquemas de diversidad espacial. Mas aún, hemos destacado que lo relevante no es la separación entre

antenas, sino de su posición en la sección transversal.

6.4 Trabajo en curso y a futuro

La propagación inalámbrica en túneles también depende de la polarización de las antenas. En esta tesis, únicamente consideramos polarización vertical en el túnel de Somport, beneficiando la excitación y detección de modos EH^y (**Capítulo 3**). En ese caso, el periodo de los *fadings* es función del ancho del túnel (Eq. 3.9), y los *fadings* presentan una diferencia de fase en función de la posición del receptor en la sección transversal. Sin embargo, si se utiliza polarización horizontal, se beneficia la excitación de modos EH^x. Como consecuencia de esto, el periodo de los *fadings* es función de la altura del túnel, en lugar del ancho. Por lo tanto, si el túnel no tiene una geometría equivalente a un cuadrado, como es el caso de la mayoría de los túneles, se pueden obtener *fadings* de diferente periodo únicamente cambiando la polarización de la antena.

Como extensión de este trabajo, proponemos realizar un estudio de los *fadings* con diferentes polarizaciones, lo que puede llevar a obtener *fadings* de diversos periodos manteniendo la misma posición y frecuencia de operación. Esto puede proporcionar mayor robustez al método de localización, extendiendo las metodologías presentadas de multiplexación de posición y frecuencia, a multiplexación de polarización.

Como consecuencia de usar polarización horizontal, la interpretación de los *fadings* transversales presentadas en el **Capítulo 3** se debe rotar, trasladando esta estructura a la vertical, y viceversa. Esto abre una nueva línea de investigación, donde se pueden utilizar robots aéreos, extendiendo las técnicas de navegación presentadas en el **Capítulo 4**, de un espacio 1D y 2D, a uno 3D.

El algoritmo de localización presentado en el **Capítulo 5** representa una solución discreta para estimar la posición de un robot dentro de un entorno tipo túnel. Como los máximos y mínimos de los *fadings* se detectan una vez que éstos se cruzan, esto introduce un retardo, que depende de la frecuencia de muestreo del equipo receptor, el filtrado, y la velocidad del robot. El algoritmo funciona adecuadamente bajo la premisa de que la señal no es ruidosa, como fue el caso de la propagación en tuberías. Sin embargo, el ruido en la señal recibida debido a un comportamiento errático del hardware, o reflexiones debido a irregularidades en la tubería, puede producir variaciones en la potencia recibida que se pueden malinterpretar como el máximo

o mínimo de un fading.

Para solventar esta situación, actualmente estamos investigando soluciones más robustas. Como una primera aproximación, se está utilizando un robot terrestre e implementando un filtro de partículas, usando información del modelo de propagación de la señal y la posición estimada por odómetros. La idea es obtener una localización continua, corrigiendo los errores acumulados por la odometría, con el modelo de *fadings*. En un futuro cercano, el objetivo es implementar el sistema en robots aéreos. Para ello, estamos trabajando en colaboración con el GRASP Laboratory de la Universidad de Pensilvania. Se pretende utilizar información de una IMU para estimar la dirección del movimiento, y la aceleración para determinar los desplazamientos. Es sabido que las IMU acumulan errores en un corto instante de tiempo, que usualmente son corregidos con un GPS. En nuestro caso, la idea es utilizar la IMU con sensores RF y el modelo de propagación, para estimar la posición de un robot volador dentro de una tubería. También se quieren corregir los errores acumulados por sistemas odométricos visuales, con información de los *fadings* periódicos.

En el caso de los túneles, como la señal es más ruidosa en este tipo de entornos, el algoritmo de localización requiere de una mayor robustez, como se expuso anteriormente. Además, se debe trabajar para implementar las metodologías de localización propuestas en el **Capítulo 5**, tales como la multiplexación de frecuencia para resolver el problema de localización en el sector cercano. Esto también será explorado como un trabajo a futuro.

Appendix A

Tools for coverage mapping

In order to study RF propagation in the different scenarios, different tools were developed and improved.

A.1 Yellowjacket WLAN Analyzer

The first tool used consisted on a Berkeley Varitronics Systems Yellowjacket [Yellowjacket], which is a 802.11 b/a/n/g Wireless Local Area Network (WLAN) testing and measuring platform that includes both spectrum and packet analysis. It uses a Samsung tablet PC for its user interface (Fig. A.1).

The first propagation studies were performed by means of placing a computer broadcasting frames at the entrance of the tunnel (as the transmitter), and measuring the RSS at different points from the transmitter with the Yelowjacket (as receiver). The mean received power as a function of the distance from the transmitter were manually logged to a computer. It was discovered that at certain distances far from the transmitter, the received power was higher compared to the received power at closer distances, evidencing a different behavior in comparison to propagation in free-space.

Figure A.1: Berkeley Varitronics Systems Yellowjacket [Yellowjacket].

Figure A.2: Coverage mapping tool based on Pioneer 3-AT robot.

A.2 Pioneer 3-AT

In order to automate the coverage mapping process and associate the received power to spatial coordinates in a more effective manner, a tool was developed using a Pioneer 3-AT robot as the mobile platform [Pioneer]. It had two built-in odometers, and was instrumented with a SICK laser range sensor, three Dell D630 laptops (each with one Atheros chipset wireless network card with external antenna capability), and a structure to hold the receivers' antennas (see Fig. A.2). All the modules streamed data to ROS operating system. A network was established between the laptops, allowing to have the same timestamps and hence synchronize all the data.

To automate the navigation and travel in a straight line, an algorithm based on the Hough transform was developed. The classical Hough transform was concerned with the identification of lines in the image [Hough 60], and it was adapted to detect the tunnel walls from laser data.

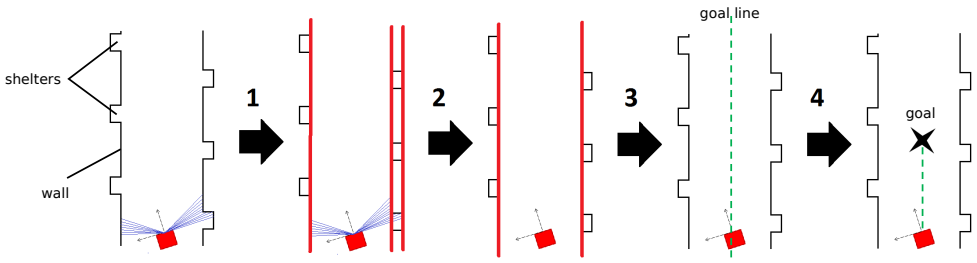

Figure A.3: Navigation algorithm based on the Hough transform.

The algorithm works in four steps, illustrated in Fig. A.3

1. **Walls and shelters detection:** based on the information from the laser range sensor, the Hough Transform detects the straight lines derived from the measurements. In the tunnel, these happen to be the tunnel walls, and emergency shelters.

2. **Emergency shelters filtering:** once the lines are detected, a filtering process is applied to eliminate the small emergency shelters and detect the left and right tunnel walls. This is done with information about the number of votes obtained by each line in the Hough Transform.

3. **Goal line:** after selecting which lines are the tunnel walls, a *goal line* is generated, maintaining a certain constant distance from the walls.

4. **Goal setting:** once the goal line is determined, a goal is placed over it, at a certain distance from the robot (in the longitudinal dimension).

Once the robot achieves the goal, the whole process is repeated.

A.3 All-terrain Vehicle

The main drawback of the Pioneer robot is its maximum speed (of about 1.5 m/s), making unfeasible to perform propagation studies covering several kilometers, multiple times. To solve this, an all-terrain vehicle was used as a substitute of the Pioneer as the mobile platform. This time, the navigation is carried out by a human operator.

(a) Laser sensor (b) IR odometer (c) Receivers' antennas

Figure A.4: Coverage mapping tool, ATv1.

A.3.1 All-terrain version 1 (ATv1)

The communication modules (laptops with network cards) and the laser range sensor were taken from the Pioneer robot, but the odometers had to be developed. As a first approach, two infrared light emitter-receiver (Infrared (IR) sensors) were used. A total of four pieces of reflective tape were placed over each rear wheel, yielding a resolution of 90 degrees (Fig. A.4(b)). Each time the reflective tape passes in front of the IR sensor, an electronic pulse is received, and with knowledge of the radius of the wheel, the traveled distance is determined. The setup is shown in Fig. A.4.

A.3.2 All-terrain version 2 (ATv2)

Due to the presence of fine dust inside the tunnel, the reflective tape sometimes gets covered with a layer of dust, making the odometer to perform erratically. To solve this situation, two 0.5 degree resolution wheel encoders were attached directly to the wheel axis (shown in Fig. A.5). A driver was developed to receive and process the data in ROS.

A.3.3 All-terrain version 3 (ATv3)

To extend the study to other frequencies, three portable spectrum analyzers (RF Explorer model 3G [RFExplorer]) were acquired. This time, the transmitter was a Continuous Wave Signal Generator (Agilent model E4432B), allowing perform measurements at 433, 868, 1800 and 2400 MHz. A driver was developed to streamed and synchronize the RF data with data from the

Figure A.5: 0.5 degree resolution wheel encoder from ATv2.

(a) Signal generator used as tx

(b) RF Explorer in a protective case

(c) RF Explorers on ATv3

Figure A.6: Different components of ATv3.

laser and odometers in ROS.

A.3.4 All-terrain version 4 (ATv4)

Finally, in order to study the transversal fadings in detail, a set of twelve TP-LINK tl-wn7200nd wireless adapters with Ralink chipset were acquired, as well as six RF Explorer model 3G. A moving stucture was constructed, allowing to mount the receivers rack and modify its height and orientation (Fig. A.7).

A.4 Lego Mindstroms

To study propagation inside the small-scale pipe, one RF Explorer was installed over a small mobile robot, built with a Lego Mindstroms NXT kit. One motor allowed the robot to run forward and backwards inside the pipe. It is shown in Fig. A.8.

(a) Horizontal receivers at a height of 2 m.

(b) Horizontal receivers at a height of 3 m.

(c) Vertical receivers

Figure A.7: Twelve TP-LINK on ATv4.

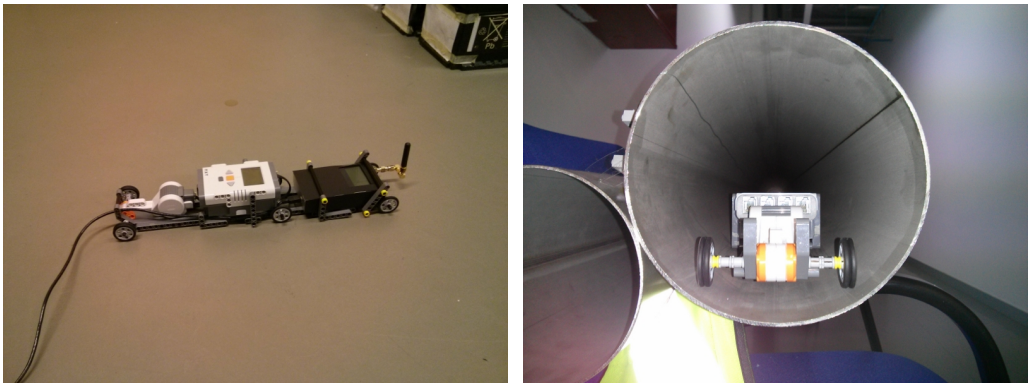

(a) Upper view

(b) Inside the pipe

Figure A.8: Lego robot for small-scale in-pipe studies.

In the large-scale pipe, the Pioneer robot was used instead (Section A.2), with the RF Explorers as RF receivers.

A.5 Hexrotor

Finally, to test the localization algorithm inside the tunnel, a DJI F550 Hexrotor was used as the mobile robot. It was equipped with white and red LEDs for piloting orientation purposes, a Raspberry Pi model B as the onboard computer, a Phidgets IMU, an RF explorer, and a network card for networking purposes (to remotely launch the programs on the Raspberry Pi). The hexrotor is piloted with a Futaba 6CH Radio Controller. With this setup, the robot is able to fly for a continuous twelve-minute period with a 5500 mAh 14.8 V LiPo battery. The setup is

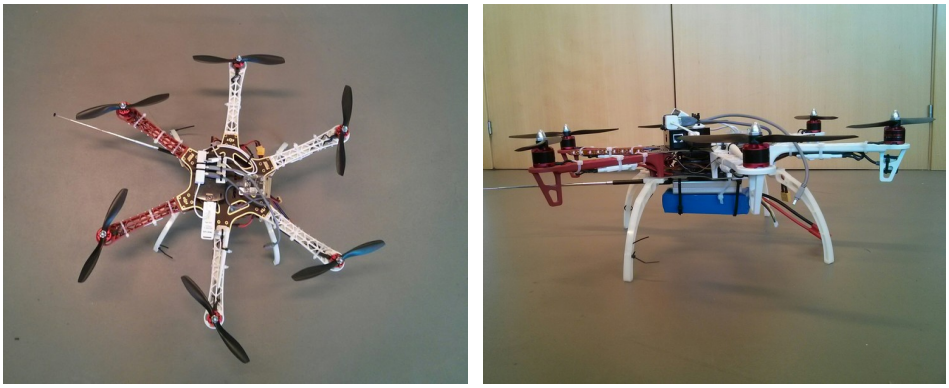

(a) (b)

Figure A.9: Instrumented DJI F550 hexrotor.

shown in Fig. A.9.

Appendix B

Experiments

Along this appendix we present the different experiments and scenarios used as testbed during the development of the thesis, mentioning the challenges addressed in each of them.

B.1 University of Zaragoza: the Robotics Lab and Surrounding Areas

The University of Zaragoza (Unizar), located in Zaragoza, Spain, was the test scenario for several indoor and outdoor experiments. Within the Robotics Lab (Cambus Rio Ebro, Edificio I+D+i), an area was specially destinated to perform propagation studies in different small-scale pipes (Fig. B.1(a)). In the outdoors, its surrounding areas free of obstacles were used as the test scenario to study the relation between the RSSI and PDR metrics (Section 4.2.3). By means of placing a set of receivers at different distances from the transmitter, the correlation between these two metrics could be established. Also, the outdoor areas served to test the robotics navigation for both ground and aerial robots (Fig. B.1(c)).

B.2 The Somport Tunnel

The Somport tunnel was selected as the tunnel scenario to carry out the experiments. It is located in Canfranc (Spain), at 170 km from the University campus. It is an old out-of-service railway tunnel representative of long straight tunnels common in transport or mine applications. The

(a) Small-scale pipe in the Robotics Lab

(b) PDR measurement setup

(c) Testing the hexrotor in dark conditions

Figure B.1: Different experiments at University of Zaragoza.

7.7 km long railway tunnel connects Spain with France through the central Pyrenees. It has a horseshoe-shape cross section, approximately 5 m high and 4.65 m wide. The tunnel is straight but suffers a change in slope at approximately 4 km from the Spanish entrance. The walls are limestone with short sections covered with a thin concrete layer. The tunnel also has small emergency shelters every 25 m, which are 1 m wide, 1.5 m high, and 0.6 m in depth; and 17 lateral galleries, each more than 100 m long and of the same height as the tunnel. As one section of the tunnel is within the Spanish border while the other is part of the French border, special permissions must be authorized to perform experiments inside the tunnel.

Tunnels can be considered hostile environments. In our specific case, most of the Somport tunnel lack any source of illumination. The temperature is low during the whole year, with a mean value of around 8 degrees Celsius, and the humidity and cold air streams from the Pyrenees traversing the tunnel turn the thermal sensation even lower. Also, the floor is covered with a fine layer of rock dust.

One of the challenges addressed in this scenario is the platform instrumentation, which has to take place in situ (national regulations does not allow the circulation of the instrumented vehicle in regional roads). Instrumenting the all-terrain vehicle inside the tunnel can take up to four people working during one hour. Even the simple case of tighten some screws, at low temperatures and with dusty air streams, becomes a difficult task.

In this scenario, we performed several measuring campaigns in order to determine the struc-

(a) Part of the team (b) Platform instrumentation (c) Sensor configuration and data logging

Figure B.2: Different experimental stages in the Somport tunnel.

(a) Propagation studies (b) Multirobot deployment (c) Hexrotor localization

Figure B.3: Experiments performed in the Somport tunnel.

ture of the fadings in a three-dimensional space (Chapter 3), as well as multirobot deployment experiments (Chapter 4), and localization with an hexrotor (Chapter 5). The experiments and details are summarized in Table B.1, where the displacement is the distance between the university campus and the experiments site. The total time invested is the time period between leaving and returning to university campus, while the experimental time is the time dedicated for testing.

B.3 The Santa Marta Mine

The Santa Marta mine is located in Villarubia de Santiago, Toledo (Spain), at around 360 km from the University campus. It is a sodium sulfate mine currently on duty. Although not mentioned during the work, several propagation studies were carried out in this environment in June

Table B.1: Summary of experiments

Date	Place	Displacement (km)	Time invested total/tests (hours)	Objective
2011-02-06	Somport tunnel	170 x 2	13 / 7	Propagation studies @ 2.4 GHz with Yellowjacket
2011-09-06	Somport tunnel	170 x 2	13 / 7	Propagation studies @ 2.4 GHz with Pioneer
2011-12-06	Somport tunnel	170 x 2	13 / 7	Propagation studies @ 2.4 GHz with ATv1
2012-01	Unizar	0	6 / 6	PDR measurements
2012-02-06	Somport tunnel	170 x 2	13 / 7	Multi-robot deployment
2012-06-08 to 2012-06-10	Santa Marta mine	360 x 2	52 / 16	Coverage mapping @ 433, 868 and 2400 MHz
2012-11-06	Somport tunnel	170 x 2	13 / 7	Longitudinal fadings @ 433, 868 and 2400 MHz
2013-04-19	Somport tunnel	170 x 2	13 / 7	Transversal fadings @ 2.4 GHz
2013-08-25 to 2013-08-27	Allatoona dam	> 7000 x 2	60 / 12	Propagation in pipes
2013-10-04	Somport tunnel	170 x 2	13 / 7	Transversal fadings @ 2.4 GHz
2013-10-28	Santa Ana dam	180 x 2	14 / 7	Longitudinal fadings in pipes
2013-12-11	Somport tunnel	170 x 2	13 / 7	Transversal fadings @ 2.4 GHz, influence of tx position
2014-01 to 2014-02	Unizar	0	24 / 24	Propagation in straight pipes
2014-03-21	Somport tunnel	170 x 2	13 / 7	Transversal fadings @ 433 and 868 MHz, influence of tx position
2014-04-06	Somport tunnel	170 x 2	13 / 7	Vertical fadings, and experiments with quadrotor
2014-05-06	Somport tunnel	170 x 2	13 / 7	Transversal fadings @ 433,868,1800,2400 MHz
2014-07 to 2014-08	Unizar	0	20 / 20	Propagation in bent pipes
2014-11-07	Santa Ana dam	180 x 2	14 / 7	Transversal fadings in pipes
2014-12-02	Santa Ana dam	180 x 2	14 / 7	Localization inside pipes with Pioneer robot

(a) The team (b) A Pioneer robot inside the mine (c) Instrumented all-terrain vehicle

Figure B.4: Different experimental stages in the Santa Marta mine.

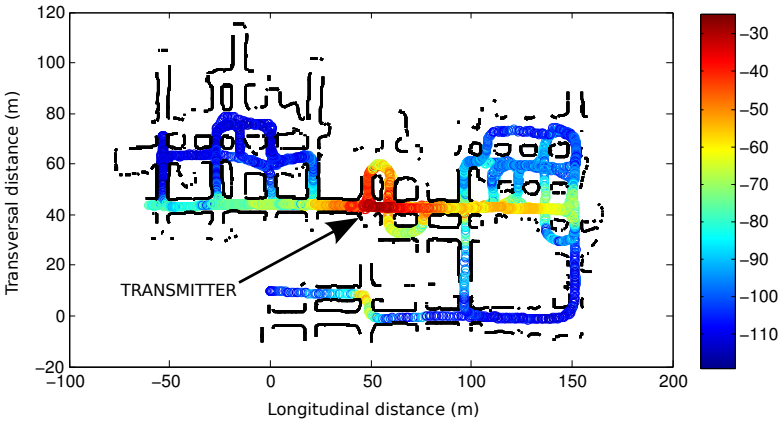

Figure B.5: Coverage map of a section of the Santa Marta mine, at 433 MHz.

2012 (see Table B.1), to provide a network deployment planning for the staff communication using RF devices. A map of one section of the mine was build with a Pioneer robot, and the all-terrain vehicle was used to study propagation at 433, 868 and 2400 MHz. As an example, Fig. B.5 shows a coverage map of a zone of the mine, at an operating frequency of 433 MHz.

B.4 The Allatoona Dam

The Allatoona dam is located in Cartersville, Georgia (United States of America), at more than 7000 km from the University campus. It is used for hydropower generation and water supply, and is under jurisdiction of the U.S. Army Corps of Engineers. The dam is a concrete gravity-type structure with curved axis convex upstream. It is composed of two 40,000 kW main units

and one 2,200 kW small unit. The large-units penstock-pipes are carbon steel with a diameter of 5.5 m. The first portion is on a horizontal plane and the second part slopes upwards, with an inclination of 23 degrees with respect to the horizontal part.

The University of Pennsylvania, under funding of the US Army Research Laboratory grant no. W911NF-08-2-0004, is developing a system to perform inspection tasks inside the penstock pipes with aerial vehicles (specifically, quadrotors). Motivated by problems using visual odometry to estimate the position of the quadrotor inside the pipe, and the appearance of periodic fadings in the Somport tunnel, we developed the idea of taking advantage of this periodicity to localize. The first propagation studies inside pipes were performed in one of the Allatoona dam penstock pipes.

As the hydropower station is on service, we had to wait for a maintenance outage to perform the experiments. The first opportunity was in August 2013 (see Table B.1). In order to access the facilities, a security-risk course was taken by the whole team accessing the dam, and a security-related written examination needed to be passed in order to be able to perform the experiments. As a curiosity, for security reasons, the key that activates the penstock (filling the pipe with water from the lake) is put inside a metallic box, locked with a number of locks equal to the number of persons inside the pipe. Each person has a different key, corresponding to his/her unique lock. Hence, the penstock can not be activated until every person has removed his/her lock. The box is shown in Fig B.6(b).

The first experiments showed the presence of fadings inside the pipe, and as exposed in this thesis, one of it uses may be to reset the cumulative errors caused by visual odometry. After the first tests, performed in August 2013, the next service outage was planned for October 2014. Unfortunately it was postponed for April 2015, and due to mechanical issues with the robots, the trip was canceled. As the time of writing this thesis, we are still waiting for the next service outage to test the concepts.

B.5 The Santa Ana Dam

The Santa Ana Dam is located in the vicinity of Castillonroy (Spain), at 170 km from the university campus. The Santa Ana dam drainpipe was selected as the test scenario to continue the experiments began at the Allatoona dam. The pipe is used to redirect the water from the dam,

(a) Allatoona dam and lake

(b) Locked box with the penstock activation key

(c) Sensor calibration inside the penstock pipe

(d) Propagation studies inside the penstock pipe

Figure B.6: Different experimental stages in the Allatoona dam.

over the N-230 highway, for agriculture purposes (Fig. B.7(a)). It is made from carbon steel, and has a diameter of 4 m. It is composed by three sectors, measuring a total length of 360 m: both extremes are inclined and open to air (no presence of penstocks). The central sector, in which the experiments were performed, is practically horizontal with a length of 200 m. All of them are soldered together, providing electrical continuity. As the pipe is on duty most of the year, we had to take advantage of some maintenance outage during the winter season to perform the experiments. The first experiments were performed in October 2013, and the next opportunity was November 2014 (see Table B.1).

The experiments performed consisted on propagation studies (Chapter 2), and localization with the Pioneer robot (Chapter 5). In order to move the equipment and access the horizontal part of the pipe, special climbing equipment needed to be used, as shown in Fig. B.7.

(a) The Santa Ana dam drainpipe from the outside

(b) Accessing the pipe with climbing equipment

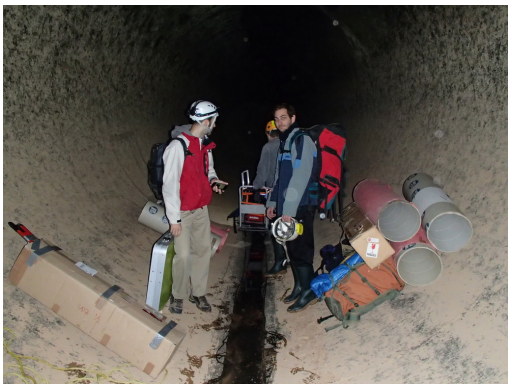

(c) Equipment needed to perform the experiments

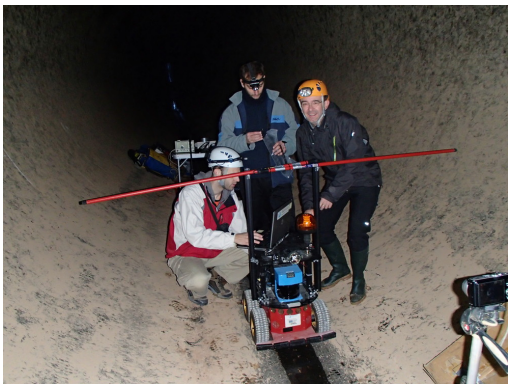

(d) Instrumenting the Pioneer robot

Figure B.7: Different experimental stages in the Santa Marta dam drainpipe.

Bibliography

[Balanis 89] C.A. Balanis. Advanced engineering electromagnetics. John Wiley & Sons, 1989. (Cited on pages 20 and 21.)

[Bernado 11] L. Bernado, A. Roma, A. Paier, T. Zemen, N. Czink, J. Karedal, A. Thiel, F. Tufvesson, A.F. Molisch & C.F. Mecklenbrauker. *In-Tunnel Vehicular Radio Channel Characterization*. In Vehicular Technology Conference (VTC Spring), 2011 IEEE 73rd, pages 1–5, may 2011. (Cited on pages 2 and 40.)

[Biswas 10] J. Biswas & M. Veloso. *WiFi localization and navigation for autonomous indoor mobile robots*. In Robotics and Automation (ICRA), 2010 IEEE International Conference on, pages 4379–4384, May 2010. (Cited on page 5.)

[Boksiner 12] J. Boksiner, C. Chrysanthos, J. Lee, M. Billah, T. Bocskor, D. Barton & J. Breakall. *Modeling of radiowave propagation in tunnels*. In MILITARY COMMUNICATIONS CONFERENCE, 2012 - MILCOM 2012, pages 1–6, Oct 2012. (Cited on pages 2 and 40.)

[Cerasoli 04] C. Cerasoli. *RF propagation in tunnel environments*. In Military Communications Conference, 2004. MILCOM 2004. 2004 IEEE, volume 1, pages 363–369 Vol. 1, Oct 2004. (Cited on pages 2 and 40.)

[Chen 96] Shin-Hon Chen & Shyh-Kang Jeng. *SBR image approach for radio wave propagation in tunnels with and without traffic*. Vehicular

Technology, IEEE Transactions on, vol. 45, no. 3, pages 570–578, Aug 1996. (Cited on pages 3 and 40.)

[Chiba 78] J. Chiba, T. Inaba, Y. Kuwamoto, O. Banno & R. Sato. *Radio Communication in Tunnels*. Microwave Theory and Techniques, IEEE Transactions on, vol. 26, no. 6, pages 439–443, Jun 1978. (Cited on pages 3 and 40.)

[Cocheril 09] Yann Cocheril, Marion Berbineau, Piere Combeau & Yannis Pousset. *On the Importance of the MIMO Channel Correlation in Underground Railway Tunnels*. Journal of Communications, vol. 4, no. 4, 2009. (Cited on page 123.)

[COMSOL] COMSOL. http://www.comsol.com/. (Cited on page 65.)

[Delogne 91] P. Delogne. *EM propagation in tunnels*. Antennas and Propagation, IEEE Transactions on, vol. 39, no. 3, pages 401 –406, mar 1991. (Cited on page 48.)

[Dudley 07] D.G. Dudley, M. Lienard, S.F. Mahmoud & P. Degauque. *Wireless propagation in tunnels*. Antennas and Propagation Magazine, IEEE, vol. 49, no. 2, pages 11–26, april 2007. (Cited on pages 3, 40, 41, 44, 49, 52, and 76.)

[Emslie 75] A. Emslie, R. Lagace & P. Strong. *Theory of the propagation of UHF radio waves in coal mine tunnels*. Antennas and Propagation, IEEE Transactions on, vol. 23, no. 2, pages 192–205, Mar 1975. (Cited on pages 3, 6, 40, 41, 43, and 60.)

[Fink 10] J. Fink & V. Kumar. *Online methods for radio signal mapping with mobile robots*. In IEEE International Conference on Robotics and Automation, pages 1940–1945, May Anchoragei,2010. (Cited on pages 4 and 74.)

[Gentile 12] Camillo Gentile, Fabien Valoit & Nader Moayeri. *A raytracing model for wireless propagation in tunnels with varying cross sec-*

tion. In Global Communications Conference (GLOBECOM), 2012 IEEE, pages 5027–5032, 2012. (Cited on page 41.)

[Gil 13] Stephanie Gil, Swarun Kumar, Dina Katabi & Daniela Rus. *Adaptive Communication in Multi-Robot Systems Using Directionality of Signal Strength*. In Proceedings of the International Symposium on Robotics Research, 2013. (Cited on page 4.)

[GlenDam] GlenDam. *Schematic of river outlets @ Glen Canyon Dam*. http://www.onthecolorado.com/resources.cfm?mode=section&id=Graphics. (Cited on pages xvii and 112.)

[GMapping] GMapping. https://www.openslam.org/gmapping.html. (Cited on page 109.)

[Grisetti 05] G. Grisetti, C. Stachniss & W. Burgard. *Improving Grid-based SLAM with Rao-Blackwellized Particle Filters by Adaptive Proposals and Selective Resampling*. In Robotics and Automation, 2005. ICRA 2005. Proceedings of the 2005 IEEE International Conference on, pages 2432–2437, April 2005. (Cited on page 109.)

[Grisetti 07] G. Grisetti, C. Stachniss & W. Burgard. *Improved Techniques for Grid Mapping With Rao-Blackwellized Particle Filters*. Robotics, IEEE Transactions on, vol. 23, no. 1, pages 34–46, Feb 2007. (Cited on page 109.)

[Grossmann 84] A. Grossmann & J. Morlet. *Decomposition of Hardy Functions into Square Integrable Wavelets of Constant Shape*. Siam Journal on Mathematical Analysis, vol. 15, 1984. (Cited on page 50.)

[Han 09] Dongsu Han, DavidG. Andersen, Michael Kaminsky, Konstantina Papagiannaki & Srinivasan Seshan. *Access Point Localization Using Local Signal Strength Gradient*. In Passive and Active Network Measurement, volume 5448, pages 99–108. Springer Berlin Heidelberg, 2009. (Cited on page 99.)

[Hansen 11] P. Hansen, H. Alismail, P. Rander & B. Browning. *Monocular visual odometry for robot localization in LNG pipes*. In Robotics and Automation (ICRA), 2011 IEEE International Conference on, pages 3111–3116, May 2011. (Cited on pages 5 and 104.)

[Holland 01] G. Holland, N. Vaidya & P. Bahl. *A rate-adaptive MAC protocol for multi-Hop wireless networks*. In Proceedings of the 7th annual international conference on Mobile computing and networking, MobiCom '01, pages 236–251, New York, NY, USA, 2001. ACM. (Cited on page 78.)

[Honcharenko 92] W. Honcharenko, Henry L. Bertoni, J.L. Dailing, J. Qian & H.D. Yee. *Mechanisms governing UHF propagation on single floors in modern office buildings*. Vehicular Technology, IEEE Transactions on, vol. 41, no. 4, pages 496–504, Nov 1992. (Cited on pages 3 and 40.)

[Hough 60] P.V.C. Hough & B.W. Powell. *A method for faster analysis of bubble chamber photographs*. Il Nuovo Cimento, vol. 18, no. 6, pages 1184–1191, 1960. (Cited on page 142.)

[Howard 03] Andrew Howard, Sajid Siddiqi & Gaurav S. Sukhatme. *An Experimental Study of Localization Using Wireless Ethernet*. In in 4th International Conference on Field and Service Robotics, 2003. (Cited on page 5.)

[Hrovat 14] A. Hrovat, G. Kandus & T. Javornik. *A Survey of Radio Propagation Modeling for Tunnels*. Communications Surveys Tutorials, IEEE, vol. 16, no. 2, pages 658–669, Second 2014. (Cited on pages 40 and 64.)

[Hsieh 08] M. Ani Hsieh, Anthony Cowley, Vijay Kumar & Camillo J. Taylor. *Maintaining network connectivity and performance in robot teams*. Journal of Field Robotics, vol. 25, no. 1-2, pages 111–131, 2008. (Cited on pages 3 and 74.)

[Kjeldsen 06] E. Kjeldsen & M. Hopkins. *An Experimental Look at RF Propagation in Narrow Tunnels*. In Military Communications Conference, 2006. MILCOM 2006. IEEE, pages 1–7, Oct 2006. (Cited on pages 2 and 40.)

[Kyritsi 02] P. Kyritsi & D.C. Cox. *Expression of MIMO capacity in terms of waveguide modes*. Electronics Letters, vol. 38, no. 18, pages 1057–1058, Aug 2002. (Cited on page 41.)

[Laakmann 76] Katherine D. Laakmann & William H. Steier. *Waveguides: characteristic modes of hollow rectangular dielectric waveguides*. Appl. Opt., vol. 15, no. 5, pages 1334–1340, May 1976. (Cited on pages 41, 42, 44, 45, and 66.)

[Ladd 02] Andrew M. Ladd, Kostas E. Bekris, Algis Rudys, Guillaume Marceau, Lydia E. Kavraki & Dan S. Wallach. *Robotics-based Location Sensing Using Wireless Ethernet*. In Proceedings of the 8th Annual International Conference on Mobile Computing and Networking, MobiCom '02, pages 227–238, New York, NY, USA, 2002. ACM. (Cited on page 5.)

[Lazaro 10] M.T. Lazaro & J.A. Castellanos. *Localization of probabilistic robot formations in SLAM*. In Robotics and Automation (ICRA), 2010 IEEE International Conference on, pages 3179–3184, May 2010. (Cited on pages 46, 87, 110, and 114.)

[Lee 85] C. S. Lee, S. W. Lee & S. L. Chuang. *Plot of Modal Field Distribution in Rectangular and Circular Waveguides*. Microwave Theory and Techniques, IEEE Transactions on, vol. 33, no. 3, pages 271–274, Mar 1985. (Cited on page 20.)

[Lee 07] Dik Lun Lee & Qiuxia Chen. *A Model-based WiFi Localization Method*. In Proceedings of the 2Nd International Conference on Scalable Information Systems, InfoScale '07, pages 40:1–40:7,

ICST, Brussels, Belgium, Belgium, 2007. ICST (Institute for Computer Sciences, Social-Informatics and Telecommunications Engineering). (Cited on page 5.)

[Lee 09] Jung-Sub Lee, Se gon Roh, Do Wan Kim, Hyungpil Moon & Hyouk Ryeol Choi. *In-pipe robot navigation based on the landmark recognition system using shadow images*. In Robotics and Automation, 2009. ICRA '09. IEEE International Conference on, pages 1857–1862, May 2009. (Cited on pages 5 and 104.)

[Lee 11] Dong-Hyuk Lee, Hyungpil Moon & Hyouk Ryeol Choi. *Autonomous navigation of in-pipe working robot in unknown pipeline environment*. In Robotics and Automation (ICRA), 2011 IEEE International Conference on, pages 1559–1564, May 2011. (Cited on pages 5 and 104.)

[Lienard 98] M. Lienard & P. Degauque. *Propagation in wide tunnels at 2 GHz: a statistical analysis*. Vehicular Technology, IEEE Transactions on, vol. 47, no. 4, pages 1322–1328, nov 1998. (Cited on pages 3, 40, 48, and 53.)

[Lienard 03] M. Lienard, P. Degauque, J. Baudet & D. Degardin. *Investigation on MIMO channels in subway tunnels*. Selected Areas in Communications, IEEE Journal on, vol. 21, no. 3, pages 332–339, Apr 2003. (Cited on page 123.)

[Lienard 06] Martine Lienard, Pierre Degauque & Jose Maria Molina-Garcia-Pardo. *Wave propagation in tunnels in a MIMO context-a theoretical and experimental study*. Comptes Rendus Physique, vol. 7, no. 7, pages 726 – 734, 2006. Towards reconfigurable and cognitive communications Vers des communications reconfigurables et cognitives. (Cited on pages 41 and 122.)

[Lienard 14] M. Lienard, C. Sanchis-Borras, J.-M. Molina-Garcia-Pardo, D.P. Gaillot, P. Laly & P. Degauque. *Performance Analysis of Antenna*

Arrays in Tunnel Environment. Antennas and Wireless Propagation Letters, IEEE, vol. 13, pages 122–125, 2014. (Cited on page 41.)

[Mahmoud 74a] Samir F. Mahmoud & James R. Wait. *Geometrical optical approach for electromagnetic wave propagation in rectangular mine tunnels*. Radio Science, vol. 9, pages 1147–1158, 1974. (Cited on pages 3 and 40.)

[Mahmoud 74b] Samir F. Mahmoud & James R. Wait. *Guided electromagnetic waves in a curved rectangular mine tunnel*. Radio Science, vol. 9, no. 5, pages 567–572, 1974. (Cited on pages 3 and 40.)

[Mallat 99] Stéphane Mallat. A wavelet tour of signal processing (2. ed.). Academic Press, 1999. (Cited on page 50.)

[Mariage 94] P. Mariage, M. Lienard & P. Degauque. *Theoretical and experimental approach of the propagation of high frequency waves in road tunnels*. Antennas and Propagation, IEEE Transactions on, vol. 42, no. 1, pages 75–81, jan 1994. (Cited on pages 49 and 76.)

[Masson 09a] E. Masson, P. Combeau, M. Berbineau & R. Vauzelle. *Measurements and simulations comparisons of radio wave propagation in arch-shaped tunnels for mass transit applications*. In Intelligent Transport Systems Telecommunications,(ITST),2009 9th International Conference on, pages 37–41, 2009. (Cited on pages 48 and 53.)

[Masson 09b] Emilie Masson, Pierre Combeau, Marion Berbineau, Rodolphe Vauzelle & Yannis Pousset. *Radio Wave Propagation in Arched Cross Section Tunnels – Simulations and Measurements*. Journal of Communications, vol. 4, no. 4, 2009. (Cited on page 41.)

[Masson 11] E. Masson, Y. Cocheril, P. Combeau, L. Aveneau, M. Berbineau, R. Vauzelle & E. Fayt. *Radio wave propagation in curved rectangular tunnels at 5.8 GHz for metro applications*. In ITS Telecom-

munications (ITST), 2011 11th International Conference on, pages 81–85, 2011. (Cited on pages 2 and 40.)

[Masson 12] E. Masson, Y. Cocheril, M. Berbineau, J. Ghys, J. Kyrolainen & V. Hovinen. *4x4 MIMO channel sounding in tunnels for train-to-wayside communications*. In Wireless Communications in Unusual and Confined Areas (ICWCUCA), 2012 International Conference on, pages 1–5, Aug 2012. (Cited on page 41.)

[Michael 12] Nathan Michael, Shaojie Shen, Kartik Mohta, Yash Mulgaonkar, Vijay Kumar, Keiji Nagatani, Yoshito Okada, Seiga Kiribayashi, Kazuki Otake, Kazuya Yoshida, Kazunori Ohno, Eijiro Takeuchi & Satoshi Tadokoro. *Collaborative mapping of an earthquake-damaged building via ground and aerial robots*. Journal of Field Robotics, vol. 29, no. 5, pages 832–841, 2012. (Cited on page 1.)

[Minguez 01] J. Minguez, L. Montano, T. Siméon & R. Alami. *Global Nearness Diagram Navigation (GND).* In IEEE Int. Conf. on Robotics and Automation (ICRA'01), pages 33–39, 2001. (Cited on page 88.)

[Minguez 04] J. Minguez & L. Montano. *Nearness diagram (ND) navigation: Collision avoidance in troublesome scenarios*. IEEE Transactions on Robotics and Automation, vol. 20, no. 1, pages 45–59, 2004. (Cited on page 88.)

[Minguez 05] J. Minguez. *The Obstacle-Restriction Method (ORM) for Robot Obstacle Avoidance in Difficult Environments*. In Proc. of the IEEE Int. Conf. on Intelligent Robots and Systems, page 37063712, 2005. (Cited on page 88.)

[Molina-Garcia-Pardo 08a] J.-M. Molina-Garcia-Pardo, M. Lienard, A. Nasr & P. Degauque. *Wideband analysis of large scale and small scale fading in tunnels*. In ITS Telecommunications, 2008. ITST 2008. 8th International Conference on, pages 270–273, Oct 2008. (Cited on page 41.)

[Molina-Garcia-Pardo 08b] J.M. Molina-Garcia-Pardo, M. Lienard & P. Degauque. *Propagation channel and MIMO capacity in arched tunnels*. In Devices, Circuits and Systems, 2008. ICCDCS 2008. 7th International Caribbean Conference on, pages 1–4, April 2008. (Cited on page 41.)

[Molina-Garcia-Pardo 08c] J.M. Molina-Garcia-Pardo, M. Lienard, P. Degauque, D.G. Dudley & L. Juan-Llacer. *Interpretation of MIMO Channel Characteristics in Rectangular Tunnels From Modal Theory*. Vehicular Technology, IEEE Transactions on, vol. 57, no. 3, pages 1974–1979, May 2008. (Cited on pages 41 and 123.)

[Molina-Garcia-Pardo 08d] J.M. Molina-Garcia-Pardo, M. Lienard, A. Nasr & P. Degauque. *On the Possibility of Interpreting Field Variations and Polarization in Arched Tunnels Using a Model for Propagation in Rectangular or Circular Tunnels*. Antennas and Propagation, IEEE Transactions on, vol. 56, no. 4, pages 1206–1211, April 2008. (Cited on pages 52, 65, 67, and 70.)

[Molina-Garcia-Pardo 09a] J. Molina-Garcia-Pardo, M. Lienard, P. Degauque, E. Simon & L. Juan-Llacer. *On MIMO Channel Capacity in Tunnels*. Antennas and Propagation, IEEE Transactions on, vol. 57, no. 11, pages 3697–3701, Nov 2009. (Cited on page 46.)

[Molina-Garcia-Pardo 09b] J-M Molina-Garcia-Pardo, M Lienard & P Degauque. *Propagation in Tunnels: Experimental Investigations and Channel Modeling in a Wide Frequency Band for MIMO Applications*. EURASIP Journal on Wireless Communications and Networking, vol. 2009, no. 1, page 560571, 2009. (Cited on page 41.)

[Nasr 06] A. Nasr, J.M. Molina, M. Lienard & P. Degauque. *Optimisation of Antenna Arrays for Communication in Tunnels*. In Wireless Communication Systems, 2006. ISWCS '06. 3rd International Symposium on, pages 522–524, Sept 2006. (Cited on page 41.)

[Ocaña 07] Manuel Ocaña, LuisMiguel Bergasa, MiguelÁngel Sotelo, Ramón Flores, Elena López & Rafael Barea. *Comparison of WiFi Map Construction Methods for WiFi POMDP Navigation Systems*. In Roberto Moreno Díaz, Franz Pichler & Alexis Quesada Arencibia, editeurs, Computer Aided Systems Theory – EUROCAST 2007, volume 4739 of *Lecture Notes in Computer Science*, pages 1216–1222. Springer Berlin Heidelberg, 2007. (Cited on page 5.)

[Orfanidis 14] Sophocles J. Orfanidis. Electromagnetic waves and antennas. Rutgers University, 2014. (Cited on page 15.)

[Owen-Hill 13] A. Owen-Hill, R. Parasuraman & M. Ferre. *Haptic teleoperation of mobile robots for augmentation of operator perception in environments with low-wireless signal*. In Safety, Security, and Rescue Robotics (SSRR), 2013 IEEE International Symposium on, pages 1–7, Oct 2013. (Cited on page 75.)

[Ozaslan 13] Tolga Ozaslan, Shaojie Shen, Yash Mulgaonkar, Nathan Michael & Vijay Kumar. *Inspection of Penstocks and Featureless Tunnel-like Environments using Micro UAVs*. In Field and Service Robotics (FSR), International Conference On, 2013. (Cited on pages 105 and 110.)

[Parasuraman 14a] Ramviyas Parasuraman, Thomas Fabry, Luca Molinari, Keith Kershaw, Mario Di Castro, Alessandro Masi & Manuel Ferre. *A Multi-Sensor RSS Spatial Sensing-Based Robust Stochastic Optimization Algorithm for Enhanced Wireless Tethering*. Sensors, vol. 14, no. 12, pages 23970–24003, 2014. (Cited on page 75.)

[Parasuraman 14b] Ramviyas Parasuraman, Alessandro Masi & Manuel Ferre. *Wireless Communication Enhancement Methods for Mobile Robots in Radiation Environments. Radio communication for robotic application at CERN*. PhD thesis, Madrid, Polytechnic U., Sep 2014. Presented 17 Oct 2014. (Cited on page 75.)

[Peasgood 06] M. Peasgood, J. McPhee & C. Clark. *Complete and Scalable Multi-robot Planning in Tunnel Environments*. In 1st IFAC Workshop on Multivehicle Systems, October 2006. (Cited on pages 4 and 75.)

[Pioneer] Pioneer. *Adept Technology, Inc.* http://www.mobilerobots.com/. (Cited on page 142.)

[Pozar 05] D.M. Pozar. Microwave engineering. John Wiley & Sons, 3rd edition, 2005. (Cited on pages 19 and 43.)

[Quigley 09] Morgan Quigley, Ken Conley, Brian P. Gerkey, Josh Faust, Tully Foote, Jeremy Leibs, Rob Wheeler & Andrew Y. Ng. *ROS: an open-source Robot Operating System*. In ICRA Workshop on Open Source Software, 2009. (Cited on pages 23, 46, and 87.)

[RFExplorer] RFExplorer. http://www.rfexplorer.com/. (Cited on page 144.)

[Rizzo 12] Carlos Rizzo, Jose Luis Villarroel & Danilo Tardioli. *Spatial diversity based coverage map building in complex tunnel environments*. In Wireless Communications in Unusual and Confined Areas (ICWCUCA), 2012 International Conference on, pages 1 –7, aug. 2012. (Cited on pages 9 and 12.)

[Rizzo 13a] C. Rizzo, D. Tardioli, D. Sicignano, L. Riazuelo, J. L. Villarroel & L. Montano. *Signal-based deployment planning for robot teams in tunnel-like fading environments*. The International Journal of Robotics Research, vol. 32, no. 12, pages 1381–1397, 2013. (Cited on pages 10 and 12.)

[Rizzo 13b] Carlos Rizzo, Francisco Lera & Jose Luis Villarroel. *Transversal fading analysis in straight tunnels at 2.4 GHz*. In ITS Telecommunications (ITST), 2013 13th International Conference on, pages 313–318, Nov 2013. (Cited on pages 9 and 12.)

[Rizzo 13c] Carlos Rizzo, Francisco Lera & Jose Luis Villarroel. *UHF and SHF Fading Analysis Using Wavelets in Tunnel Environments*. In Vehicular Technology Conference (VTC Fall), 2013 IEEE 78th, pages 1–6, Sep 2013. (Cited on pages 9, 12, and 51.)

[Rizzo 14a] C. Rizzo, V. Kumar, F. Lera & J. Villarroel. *RF Odometry for Localization in Pipes Based on Periodic Signal Fadings*. In Intelligent Robots and Systems (IROS), 2014 IEEE/RSJ International Conference on, Sep 2014. (Cited on pages 9, 10, and 12.)

[Rizzo 14b] C. Rizzo, F. Lera & J.L. Villarroel. *A Methodology for Localization in Tunnels Based on Periodic RF Signal Fadings*. In Military Communications Conference (MILCOM), 2014 IEEE, pages 317–324, Oct 2014. (Cited on pages 11 and 12.)

[Rizzo 14c] C. Rizzo, D. Sicignano, D. Tardioli, F. Lera & J.L. Villarroel. *Promoting RF signal fadings: a solution for localization and navigation in tunnel-like featureless environments*. In Robotics: Science and Systems. Workshop on Communication-aware Robotics: New Tools for MultiRobot Networks, Autonomous Vehicles, and Localization., Jul 2014. (Cited on pages 10 and 12.)

[Rizzo 15a] Carlos Rizzo, Francisco Lera & Jose Luis Villarroel. *Fadings structure analysis inside Pipes towards Localization*. IEEE Transactions on Vehicular Technology. Under Review, 2015. (Cited on page 11.)

[Rizzo 15b] Carlos Rizzo, Francisco Lera & Jose Luis Villarroel. *On the validation and limitations of the Rectangular Waveguide Approximation using the Finite Element Method towards Localization inside Tunnels*. In IEEE Vehicular Technology Conference. Under Review, 2015. (Cited on page 11.)

[Rizzo 15c] Carlos Rizzo, Francisco Lera & Jose Luis Villarroel. *Three-dimensional Fadings Structure Analysis in Straight Tunnels to-*

wards Localization and Navigation. IEEE Transactions on Vehicular Technology. Under Review, 2015. (Cited on page 12.)

[Rolfe 07] B.F. Rolfe, S.W. Ekanayake, P.N. Pathirana & M. Palaniswami. *Localization with orientation using RSSI measurements: RF map based approach*. In Intelligent Sensors, Sensor Networks and Information, 2007. ISSNIP 2007. 3rd International Conference on, pages 311–316, Dec 2007. (Cited on page 5.)

[Sadiku 89] M.N.O. Sadiku. *A simple introduction to finite element analysis of electromagnetic problems*. Education, IEEE Transactions on, vol. 32, no. 2, pages 85–93, May 1989. (Cited on page 64.)

[Schaubach 92] K.R. Schaubach, IV Davis N.J. & T.S. Rappaport. *A ray tracing method for predicting path loss and delay spread in microcellular environments*. In Vehicular Technology Conference, 1992, IEEE 42nd, pages 932–935 vol.2, May 1992. (Cited on pages 3 and 40.)

[Seidel 92] S.Y. Seidel & T.S. Rappaport. *A ray tracing technique to predict path loss and delay spread inside buildings*. In Global Telecommunications Conference, 1992. Conference Record., GLOBECOM '92. Communication for Global Users., IEEE, pages 649–653 vol.2, Dec 1992. (Cited on pages 3 and 40.)

[Serrano 04] Oscar Serrano, Jose Maria Canas, Vicente Matellan, José María, Cañas Vicente Matellán & Luis Rodero. *Robot localization using WiFi signal without intensity map*, 2004. (Cited on page 5.)

[Souryal 06] M. R. Souryal, L. Klein-Berndt, L.E. Miller & N. Moayeri. *Link Assessment in an Indoor 802.11 Network*. In the 2006 IEEE Wireless Communications & Networking Conference, 2006. (Cited on page 78.)

[Srinivasan 06] K. Srinivasan & P. Levis. *RSSI is Under Appreciated*. In Proceedings of the Third Workshop on Embedded Networked Sensors (EmNets), 2006. (Cited on page 78.)

[Sun 08] Yi Sun, Jizhong Xiao, Xiaohai Li & F. Cabrera-Mora. *Adaptive Source Localization by a Mobile Robot Using Signal Power Gradient in Sensor Networks*. In Global Telecommunications Conference, 2008. IEEE GLOBECOM 2008. IEEE, pages 1–5, Nov 2008. (Cited on page 99.)

[Sun 10] Z. Sun & I.F. Akyildiz. *Channel modeling and analysis for wireless networks in underground mines and road tunnels*. IEEE Transactions on Communications, vol. 58, no. 6, pages 1758–1768, june 2010. (Cited on pages 41, 49, and 76.)

[Tardioli 07] D. Tardioli & J. L. Villarroel. *Real Time Communications over 802.11: RT-WMP*. In the 4th IEEE International Conference on Mobile Ad-hoc and Sensor Systems, pages 1–11, 2007. (Cited on page 90.)

[Tardioli 10] D. Tardioli, A.R. Mosteo, L. Riazuelo, J.L. Villarroel & L. Montano. *Enforcing Network Connectivity in Robot Team Missions*. The International Journal of Robotics Research, vol. 29, no. 4, pages 460–480, 2010. (Cited on pages 74 and 90.)

[Tardioli 12] Danilo Tardioli. *ros-rt-wmp*. http://www.ros.org/wiki/ros-rt-wmp, 2012. (Cited on page 87.)

[Twigg 12] J.N. Twigg, J.R. Fink, P.L. Yu & B.M. Sadler. *RSS gradient-assisted frontier exploration and radio source localization*. In Robotics and Automation (ICRA), 2012 IEEE International Conference on, pages 889–895, May 2012. (Cited on page 99.)

[Valdesueiro 10] J.A. Valdesueiro, B. Izquierdo & J. Romeu. *MIMO channel measurement campaign in subway tunnels*. In Antennas and Propaga-

tion (EuCAP), 2010 Proceedings of the Fourth European Conference on, pages 1–4, April 2010. (Cited on page 41.)

[Vlavianos 08] A. Vlavianos, L.K. Law, I. Broustis, S.V. Krishnamurthy & M. Faloutsos. *Assessing link quality in IEEE 802.11 Wireless Networks: Which is the right metric?* In Personal, Indoor and Mobile Radio Communications, 2008. PIMRC 2008. IEEE 19th International Symposium on, pages 1–6, sept. 2008. (Cited on page 78.)

[Wadhwa 11a] A. Wadhwa, U. Madhow, J. Hespanha & B.M. Sadler. *Following an RF trail to its source*. In Communication, Control, and Computing (Allerton), 2011 49th Annual Allerton Conference on, pages 580–587, sept. 2011. (Cited on pages 4 and 74.)

[Wadhwa 11b] A. Wadhwa, U. Madhow, J. Hespanha & B.M. Sadler. *Following an RF trail to its source*. In Communication, Control, and Computing (Allerton), 2011 49th Annual Allerton Conference on, pages 580–587, Sept 2011. (Cited on page 99.)

[Walker 09] V. Walker. *Idaho National Laboratory*. In INL Communications & Public Affairs, 2009. (Cited on pages 1, 4, and 74.)

[White 10] C. White, D. Hiranandani, C. S. Olstad, K. Buhagiar, T. Gambin & C. M. Clark. *The Malta cistern mapping project: Underwater robot mapping and localization within ancient tunnel systems*. J. Field Robot., vol. 27, no. 4, pages 399–411, July 2010. (Cited on page 75.)

[Yan 12] Y. Yan & Y. Mostofi. *Robotic Router Formation in Realistic Communication Environments - A Bit Error Rate Approach*. IEEE Transactions on Robotics, 2012. (Cited on page 74.)

[Yellowjacket] Yellowjacket. *Berkeley Varitronics Systems*. http://www.bvsystems.com/. (Cited on pages 141 and 142.)

[Yu 11] Paul L. Yu, Jeffrey N. Twigg & Brian M. Sadler. *Radio signal strength tracking and control for robotic networks*. volume 8031, pages 803116–803116–12, 2011. (Cited on page 99.)

[Zhuang 08] F. Zhuang, C. Zupan, Z. Chao & Z. Yanzheng. *A cable-tunnel inspecting robot for dangerous environment*. vol. 5, no. 3, pages 243–248, 2008. (Cited on pages 4 and 75.)